THESIS

ECONOMIC IMPACT OF THERMAL ENERGY STORAGE ON NATURAL GAS POWER WITH CARBON CAPTURE IN FUTURE ELECTRICITY MARKETS

Submitted by

Ethan James Markey

Department of Mechanical Engineering

In partial fulfillment of the requirements

For the Degree of Master of Science

Colorado State University

Fort Collins, Colorado

Summer 2022

Master's Committee:

Advisor: Todd M. Bandhauer

Jason C. Quinn

Daniel R. Herber

ABSTRACT

ECONOMIC IMPACT OF THERMAL ENERGY STORAGE ON NATURAL GAS POWER WITH CARBON CAPTURE IN FUTURE ELECTRICITY MARKETS

As policies evolve to reflect climate change goals, the use of fossil fuel power plants in expected to change. Specifically, these power plants will need to incorporate carbon capture and storage (CCS) technologies to significantly reduce their carbon emissions, and they will be operated flexibly to accommodate the growing concentration of renewable energy generators. Unfortunately, most CCS technologies are very expensive, and they impose a parasitic heat load on the power plant, thereby decreasing net power output and the ability to operate flexibly. This research evaluated the economic potential of using hot and cold thermal energy storages (TES) to boost the net power output and flexibility of a natural gas combined cycle (NGCC) power plant with CCS capabilities. Resistively heated hot TES was used to offset the parasitic heat load imposed on the NGCC by the CCS unit while vapor compression cooled cold TES was used to chill the inlet air to the power plant. Thermodynamic models were created for the base NGCC + CCS power plant, the hot TES equipment, and the cold TES equipment, to determine key performance and cost parameters such as net power output, fuel consumption, emissions captured, capital costs, and operational costs. These parameters were then used to simulate the operation of the power plant with and without the TES technologies in accordance with fourteen electricity pricing structures predicted for different future electricity market scenarios. The difference in net present value (NPV) between the base NGCC + CCS power plant and power plant with the TES technologies was used as the primary economic metric in this analysis. The NPV benefit from increased revenue due to TES utilization was found to outweigh the NPV penalty from the additional capital costs. This positive economic result was attributed to the low cost of the TES

equipment and the ability to charge the storages using cheap electricity from high levels of renewable output. The results have shown that hot TES increased NPV in 12 of 14 market scenarios while the cold TES increased NPV in 14 of 14 market scenarios. A combination of both hot and cold TES yielded the largest increases in NPV.

ACKNOWLEDGEMENTS

As my journey as a graduate student at CSU comes to a close, I would like to acknowledge that I would not be where I am today without the support of so many amazing people in my life. I would first like to thank my advisor, Dr. Bandhauer, for providing me with the opportunity to pursue research in a field that I am truly passionate about and guiding me throughout my journey at CSU. Dr. Bandhauer was the instructor of my undergraduate heat and mass transfer course, in which his knowledge and passion for thermal sciences and engineering helped ignite my own passion for energy related engineering. I was thrilled to assist him instruct that class the following year as an undergraduate learning assistant, and equally excited to join his research team, REACH CoLab as a graduate research assistant.

I would also like to acknowledge that the research presented in this thesis was largely the result of the collaboration of my project team. I would like to thank my coworkers, and dear friends Braden Limb, Roberto Vercellino, Maxwell Pisciotta, Joe Huyett, and Shane Garland in addition to my co-advisors Dr. Herber and Dr. Quinn. Throughout the two years that we have worked on this project together, we have developed very effective collaboration and have learned to rely on each other. Also, I really feel like we have maintained a very positive, friendly, and productive work environment throughout the entirety of the project duration.

Lastly, I would like to thank my friends and family for their unwavering love and support. A huge thank you to my parents, Rich and Sheri, who have cared for, and been here for me since day one. They have been my biggest role models and have shaped me into the person I am today. I would also like to thank my parents-in-law, Mike and Jeanie, who have also provided me with extensive love and support throughout the entire time I have known them. I would like to thank

my brother, Ellis, who I know I can count on to be here for me always, and is consistently very fun, funny, and enjoyable to be around. Finally, thank you Jocelyn for being my dear companion, best friend, and adventure buddy for life. I feel so lucky that you have got my back through thick and thin. I love you!

TABLE OF CONTENTS

LIST OF TABLES

LIST OF FIGURES

NOMENCLATURE

Variable	Description	Units
a	Compressor Cost Correlation Constant	-
AECI	Annual Electricity Cost Increase	$ yr^{-1}
AFCI	Annual Fuel Cost Increase	$ yr^{-1}
AFOMC	Annual Fixed Operating and Maintenance Cost	$ yr^{-1}
b	Pump Cost Correlation Constant	-
B31A	NGCC power plant specified by NETL	-
B31B	NGCC + CCS power plant specified by NETL	-
BECCS	Bio-Energy with Carbon Capture and Storage	-
BHP	Brake Horsepower	HP
CAES	Compressed Air Energy Storage	-
CAISO	California Independent System Operator	-
C	Cost	$
CAP	Capital Investment	$
CBR	Construction Build Rate	% yr^{-1}
CC	Capital Cost	$
CCS	Carbon Capture and Storage	-
CF	Capacity Factor	%
CIR	Construction Interest Rate	%
CLP	Cold Limitation Parameter	MW
CPD	Charging Power Decrease	MW
DAC	Direct Air Capture	-
DF	Discount Factor	-
DFI	Discharging Fuel Increase	kg s^{-1}
DPI	Discharging Power Increase	MW
E	Emissions	tonnes hr^{-1}
EC	Emissions Cost	$
ECC	Capital Cost All Equipment Other than Storage Mediums	$
ECP	Emissions Capture Percent	%
EES	Engineering Equation Solver	-
EF	Percent of Total Capital Paid in Equity	%
EP	Electricity Price	$ MWh^{-1}
EQ	Equity	$
ERCOT	Electricity Reliability Council of Texas	
ET	Emissions Tax	$ $tonne^{-1}$
F	Pump Cost Correlation Factor	-
FC	Fuel Consumption	kg s^{-1}
FP	Fuel Price	$ kg^{-1}
FOM	Fixed Operating and Maintenance	-
FOMC	Fixed Operating and Maintenance Costs	$ yr^{-1}
FTE	Fuel to Emissions Conversion Factor	tonnes kg^{-1}
g	Gravitational Constant	m s^{-2}

h	Enthalpy	kJ kg^{-1}
H	Pump Head	ft
HRSG	Heat Recovery Steam Generator	-
HP	High Pressure	-
HPHX	High Pressure Heat Exchanger	-
HV	Heating Value	kJ kg^{-1}
IF	Inflation Factor	-
IGCC	Integrated Gasification Combined Cycle	-
INT	Interest	$
IP	Intermediate Pressure	-
IPHX	Intermediate Pressure Heat Exchanger	-
IPR	Intermediate Pressure Reheater	-
IPCC	Intergovernmental Panel on Climate Change	-
LCOE	Levelized Cost of Electricity	$ MWh^{-1}
LCOS	Levelized Cost of Storage	$ MWh^{-1}
LF	Percent of Capital Paid by Loan	%
LIR	Loan Interest Rate	%
LP	Low Pressure	-
LPEC	Low Pressure Economizer	-
LPHX	Low Pressure Heat Exchanger	-
LPCP	Loan Principle	$
LPMT	Loan Payment	$ yr^{-1}
$\dot{m}$	Mass Flowrate	kg s^{-1}
MACRS	Modified Accelerated Cost Recovery System	-
MDR	MACRS Depreciation Rate	% yr^{-1}
MISO	Midcontinent Independent System Operator	
NETL	National Energy Technology Laboratory	-
NGCC	Natural Gas Combined Cycle	-
NPV	Net Present Value	$
NYISO	New York Independent System Operator	
P	Pressure	kPa
PO	Power Output	MW
PHES	Pumped Heat Energy Storage	-
PHS	Pumped Hydro Storage	-
PJM	Pennsylvania, New Jersey, and Maryland	-
Pr	Pressure Ratio	-
$\dot{Q}$	Heat Transfer/Heat Duty	kW
REV	Revenue	$
s	Entropy	kJ kg^{-1} K^{-1}
SCC	Storage Medium Capital Cost	$ hr^{-1}
SD	Storage Duration	hr
SSF	Storworks Scaling Factor	-
T	Temperature	°C
TAE	Total Annual Emissions	tonnes
TAEC	Total Annual Emissions Cost	$ yr^{-1}

TAF	Total Annual Fuel Consumed	kg
TAFC	Total Annual Fuel Cost	$ yr^{-1}
TAP	Total Annual Power	MW
TAR	Total Annual Revenue	$ yr^{-1}
TAVOMC	Total Annual Variable Operating and Maintenance Cost	$ yr^{-1}
TAX	Tax Amount Paid	$
TCC	Total Capital Cost	$
TES	Thermal Energy Storage	-
TI	Taxable Income	$
TR	Tax Rate	%
VOM	Variable Operating and Maintenance	-
VOMC	Variable Operating and Maintenance Costs	$ MWh^{-1}
$\dot{V}$	Volumetric Flowrate	kg s^{-1}
$\dot{W}$	Mechanical Power	kW
Greek Symbols		
Δ	Change	-
η	Efficiency	%
ρ	Density	kg m^{-3}
Subscripts		
a	Air	
amb	Ambient	
AUX	Auxiliary	
B	Blower	
BC	Blower Operated to Charge TES	
BD	Blower Operated to Discharge TES	
BDR	Blower Driver	
BP	Base Plant	
C	Compressor	
CC	Carbon Capture	
CCS	Carbon Capture and Storage	
CCP	Carbon Capture Pump	
CDR	Compressor Driver	
CMB	Combustor	
CMV	Condensate Mixing Valve	
CND	Condenser	
CP	Condensate Pump	
CPE	Chemical Process Equipment	
CS	Cold Storage	
CSC	Cold Storage Charging	
CSD	Cold Storage Discharging	
CST	Cold Storage Technology	
CT	Cooling Tower	
CTW	Cooling Tower Water	
DP	Design Point	

EV	Expansion Valve	
f	Fuel	
g	Flue Gas	
GC	Gas Compressor	
GT	Gas Turbine	
HP	High Pressure	
HPHX	High Pressure Heat Exchanger	
HPP	High Pressure Pump	
HPT	High Pressure Turbine	
HRSG	Heat Recovery Steam Generator	
HS	Hot Storage	
HSC	Hot Storage Charging	
HSD	Hot Storage Discharging	
HSSG	Hot Storage Steam Generator	
HST	Hot Storage Technology	
i	Isentropic	
I	Inlet	
IP	Intermediate Pressure	
IPHX	Intermediate Pressure Heat Exchanger	
IPP	Intermediate Pressure Pump	
IPR	Intermediate Pressure Reheater	
IPT	Intermediate Pressure Turbine	
j	Designates a Given Hour	
k	Designates a Given Year	
LP	Low Pressure	
LPEC	Low Pressure Economizer	
LPHX	Low Pressure Heat Exchanger	
LPT	Low Pressure Turbine	
N	Neutral Operation Mode	
net	Net	
NGCC	Natural Gas Combined Cycle	
NPV	Designates a Component of the Net Present Value	
O	Outlet	
P	Pump	
PH	Preheater	
r	Refrigerant	
RH	Resistance Heater	
RC	Refrigerant Compressor	
s	Steam or Water in the Base Plant Steam Cycle	
SCP	Condensate Pump in the Base Plant Steam Cycle	
ST	Steam Turbine	
w	Water	

CHAPTER 1 Introduction

1.1 Motivation

The necessity to transition away from CO_2 emitting energy sources has become increasingly clear to mediate global climate change. Where the atmospheric carbon dioxide count did not exceed 310 ppm until the year 1950, the concentration is now greater than 410 ppm [1]. The intergovernmental panel on climate change (IPCC) states that the increase in global average temperature needs to be limited to 1.5°C by 2100 [2]. To meet this goal, global CO_2 emissions need to be reduced to zero by the middle of the century [2]. Electricity production is responsible 42% of all CO_2 emissions [3], and therefore reducing CO2 emissions from power generators is key to achieve climate change goals.

The immediate solution to reducing emissions in the electricity grid is to replace fossil fuel generation with renewable resources. As their technologies have matured, wind and solar generators have become financially superior to their fossil fuel competitors [4]. Table 1- 1, extracted from LAZARD's "Levelized cost of energy, levelized cost of storage, and levelized cost of hydrogen" [4] shows that the levelized cost of solar and wind technologies are significantly lower than gas and coal power plants.

As a result, the concentration of renewables in the electricity grid is increasing rapidly. Figure 1- 1, taken from the Energy Information Administration [5] shows that 63% of the planned new generation capacity for 2022 will come from wind and solar generators, and in coming years, renewables are expected to stand for a major share of all global electricity production [6]. However, wind and solar generators are dependent on the availability of their corresponding resource, so the electricity that they produce is intermittent and unreliable. Therefore, technologies

that can supplement the generation of renewable resources are of extreme importance to the electricity grid. Two such technologies are batteries and natural gas power plants. Figure 1- 1 shows significant expected deployment of both batteries and natural gas plants and significant retirement of coal plants, which are more expensive and less compatible with renewables.

Table 1- 1: Levelized cost of electricity of different generators [4]

Generation Type	**LCOE ($/MWh)**
Utility Scale Solar	28-41
Utility Scale Wind	26-50
Natural Gas Combined Cycle	45-74
Coal	65-152
Natural Gas Peaking	151-196

Batteries are now considered to be a major player in the electricity grid because large, rechargeable batteries have become a mature technology with very high round trip efficiencies [7], [8]. However, batteries are still very expensive with a levelized cost of storage (LCOS) ranging from $131 per MWh to $279 per MWh [4], which is $145.5 per MWh larger than the average LCOE of natural gas combined cycles (NGCCs). In addition, 43% of the current electricity market infrastructure is made up of natural gas power plants with a total capacity of 483 GW while the concentration of batteries is largely insignificant [9]. Therefore, natural gas is expected to continue to play a major role in the electricity grid for the foreseeable future.

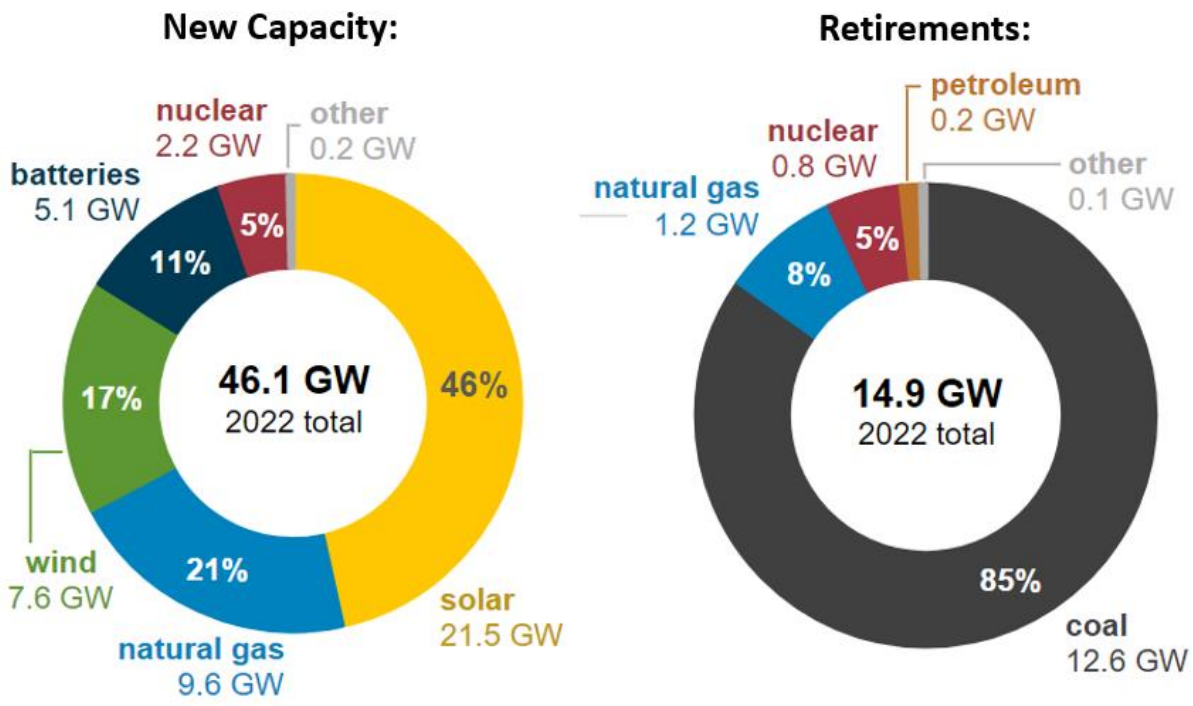

Figure 1- 1: Planned new capacity and retirements for the U.S. in 2022 [5,10]

NGCCs are the current state of the art natural gas power plants. They use both gas turbines and steam turbines to maximize the energy created from burning natural gas, in which the exhaust exiting the gas turbines is used to generate the steam for the steam turbines. NGCCs are very effective in precisely following electricity load. They can start up completely from cold conditions (IE the plant has been off for long periods of time) in 2.5-4.5 hours [11–13] but can start up much more rapidly if the plant if the plant is warm (IE the plant has been off for less than 70 hours) [11]. In addition, the ramp rate of NGCCs is 2-11% plant capacity per minute and the minimum load is 25-45% [11–13]. The potential of NGCCs to operate flexibly allows them to integrate successfully into electricity markets with high renewable penetration.

NGCCs typically run very fuel lean, and as a result they have lower emissions than fossil fuel competitors. NGCC plants have estimated specific CO_2 emissions of 370 (g/kWh) while coal

plants have specific emissions of 820 (g/kWh) [14]. However, NGCC emissions still need to be significantly reduced to meet climate change goals. This can be achieved by incorporating carbon capture and storage (CCS) technologies, which use a chemical or physical scrubbing process to remove up to 98% carbon dioxide emissions [15].

Unfortunately, the ability to capture CO_2 decreases both the performance and the economics of NGCC power plants. The CCS technology imposes a parasitic load on NGCCs which decrease the maximum power output and can cause up to a 30% decrease in efficiency [15,16]. Second, the capital costs of CCS technology are usually more than the rest of the power plant combined [16]. Therefore, it is highly desirable to recover the efficiency penalty and improve the economics of NGCC+CCS power plants.

1.2 Current and Future Electricity Grids

The necessity to reduce CO_2 emissions coupled with the increasing concentration of renewable recourses are changing the nature of the electricity grid. First, various policies such as emissions taxes and tax benefits have been already implemented which seek to financially motivate carbon capture [17–20], and the severity of these policies are expected to increase in coming years [21,22]. Second, natural gas power plants are being forced to operate variably to satisfy the electricity demand that is unable to be met by intermittent renewables. The result is that electricity prices are becoming highly variable. At times of high renewable generation, prices must be low to prevent an excess of electricity dispatch to the grid. Similarly, at times of low renewable generation, electricity prices must be high enough to motivate the operation of fossil fuel power plants.

To demonstrate recent variability in electricity prices, location marginal pricing data was examined in individual regions in the New York Independent System Operator (NYISO) electricity market [23] and the Electricity Reliability Council of Texas (ERCOT) electricity market [24] for each hour throughout 2019. The average, median, minimum, maximum, and standard deviation of the prices in these two regions are presented in Table 1- 2. It can be seen from the figure that the maximum price is 58 and 127 times higher than the mean price for the New York and Texas profiles respectively. This indicates that a very large spread of electricity prices can occur. Additionally, the standard deviation of both profiles is higher than their corresponding mean and median prices. This indicates that variability in electricity pricing is very frequent.

Table 1- 2: Electricity price metrics for regions in New York and Texas throughout 2019

	Average	**Median**	**Minimum**	**Maximum**	**Standard Deviation**
New York	27.32	23.19	-19.76	1584.57	29.31
Texas	39.42	22.37	4.48	5010.22	164.17

As solar and wind become some of the main contributors to the electricity grid, further variability in electricity prices is expected. Wind generation is volatile, meaning the generation amounts increase and decrease dramatically over short time periods. This volatility carries over into pricing structures and can result in dramatic spikes [25]. On the other hand, solar generation is less volatile but causes price variability over longer time periods [25]. Meanwhile, severe emissions policies with force fossil fuel generators to either pay high emissions taxes during operation or operate with carbon capture technology. This will increase the electricity price necessary to financially motivate the operation of the fossil fuel plants [22].

1.3 Research Objectives

The economics of power plants with carbon capture can be improved by taking advantage of the variations in electricity price. When the price is very high, it is desirable to generate and sell as much electricity as possible, and when the price is very low, it can be desirable to reduce power output, or even to remove excess electricity from the grid. Various technologies have been proposed that temporarily increase power plant electricity output and to counteract the parasitic draw of the carbon capture unit, often at the expense of further reducing power at of peak time periods. These technologies are referred to in this this thesis as “flexible carbon capture”. The present research proposes electrically charged thermal energy storage (TES) to be used as a mechanism for flexible carbon capture. Both hot TES and cold TES are evaluated in this research. Thermal energy can be generated and stored using cheap electricity from the grid during times of low prices. Then, the thermal energy can be released to increase power output and efficiency of the power plant during times of high electricity prices. This research uses electricity profiles predicted for future electricity markets with high concentrations of renewables and emissions tax policies to evaluate the economic potential of electrically charged TES for flexible carbon capture.

The primary goal of this thesis is to determine the economic impact that electrically charged hot and cold TES technologies have on NGCCs with CCS. Ultimately, it is desired to determine if the proposed storage technologies are worth the investment in grid scenarios in which it is desirable to use carbon capture technologies. To meet this goal, the following objectives were met:

1. Develop thermodynamic models of an NGCC power plant, a carbon capture unit, and the proposed hot and cold TES to accurately represent the effect that TES has on power plant electricity generation, fuel consumption, emissions, and costs.

2. Simulate the operation of the NGCC, CCS, and TES technologies in accordance with one year of data from a variety of predicted future electricity market scenarios to determine annual revenue and operating costs.
3. Calculate the net present value (NPV) of the power plant with and without thermal energy storage for a 30-year plant lifetime.
4. Compare the NPVs of the base power plant to the NPV of the power plant with the storage technologies to quantify the economic impact of TES. Speculate the technological reasons and market characteristics that can enable the TES technologies to be a financially viable option.

1.4 Thesis Organization

The following chapters outline the steps taken to evaluate the economic feasibility of electrically charged TES for flexible carbon capture. Chapter 2 provides a literature review covering the existing carbon capture technologies, the mechanisms currently proposed for flexible carbon capture, and the applications of thermal energy storage to the electricity grid that have been examined thus far. Chapter 3 details the process used to model the NGCC, CCS, and TES technologies, specifies the methodology used to simulate the operation in accordance with the electricity market data, and outlines the process used to calculate NPV. Chapter 4 presents the results of the study, including important technology performance and cost parameters, and NPV comparisons between the NGCC power plant with and without CCS and TES technologies. Chapter 5 describes the conclusions and recommendations for future work. Chapter 6 lists citations used in the research. Finally, the Appendix shows detailed process flow diagrams and power/heat flows for all technology modeled in this thesis and includes the NPV breakdown for all future electricity market scenarios analyzed.

CHAPTER 2 Literature Review

Fossil fuel power plants utilizing CCS technologies are a promising electricity generation resource for the evolving electricity grid. The following chapter details the existing methods used to increase the variability and economics of existing carbon capture technologies. First, an overview of current state of the art CCS technologies is discussed. Then, the methods proposed to increase variability, performance, and economics of these technologies are presented including CCS unit bypass and venting, solvent storage, hydrogen storage, and liquid oxygen storage. The significant findings of the studies using these methods are discussed. Next, the prospect of TES utilization for power generation is introduced including uses for both hot and cold storage mediums. While TES has not been directly integrated into existing carbon capture technologies in previous research, it has been examined in the context of fossil power plants without CCS as well as other thermal generators like concentrated solar plants. Many of the TES principles used for these power plants can be applied to fossil generation utilizing CCS. Finally, the needs for future research are identified.

2.1 Overview of Carbon Capture Technology

Carbon dioxide separation technologies have existed for 95 years for various purposes. CO_2 is separated from natural gas to purify it, separated from reagents in the production of ammonia, alcohols, and iron, and more recently separated from various fluid streams in fossil fuel power plants for sequestration and storage [26]. As of October 2019, 51 CCS plants existed globally. Of which, 19 were in operation, 4 were under construction, and 28 were in various stages of development [27]. Carbon capture can be split into three categories: oxy-fuel combustion, pre-combustion, and post-combustion. Oxy-fuel combustion is incorporated in power plants that use pure oxygen as the fuel oxidizer instead of air. This results in higher efficiency combustion with

lower exhaust volumes and higher concentrations of CO_2. These plants often utilize exhaust gas recirculation (EGR) to keep combustion flame temperatures and radiative profiles close to the conditions of conventional combustors [15]. Large concentrations of CO_2 combined with low exhaust flow rates make oxy-fuel combustion plants an ideal target for CCS. Oxy-fuel combustion approaches require an air separation unit to generate the source of oxygen from ambient air. Air separation usually utilizes cryogenic separation or pressure swing absorption technologies which are highly energy intensive and impose a large parasitic load on the power plant [3].

Pre-combustion CO_2 capture is possible in integrated gasification combined cycle (IGCC) power plants. These plants turn carbon-based fossil fuels into a hydrogen and carbon monoxide rich synthesis gas which is combusted to produce power in a combined cycle plant. The synthesis gas can undergo a rection called the water-gas shift in which CO and H_2O are reacted to form more H_2 and high concentrations of CO_2. It's high CO_2 content makes the synthesis gas an easy target for carbon removal. The result is hydrogen dominated combustion with minimal greenhouse emissions.

Post-combustion capture separates CO_2 from the exhaust streams of standard power plants. Currently post-combustion capture involves removal of CO2 from flue gas via a solvent scrubbing process, membrane CO2 capture, or cryogenic CO2 capture [3]. Most commercial products use a liquid solvent to absorb CO_2 from the flue gas, then apply heat to strip the CO_2 from the solvent for transportation and storage. This process is illustrated in Figure 2- 1 and summarized as follows. Exhaust from the power plant is driven by a fan and cooled before entering the absorber column. Inside the absorber, the solvent absorbs the CO_2, separating it from the rest of the exhaust stream. Solvents typically consist of amine based, carbonated based, or aqueous ammonia-based solutions.

The absorption process utilizes a chemical reaction mechanism such as equation 2.1, where the left side chemicals are the reactants and the right side chemicals are the products.

$$CO_2 + 2HOCH_2NH_2 \leftrightarrow HOCH_2CH_2NH_3^+ + HOCH_2CH_2NHCO_2^- \quad (2.1)$$

The clean flue gas is then exhausted from the absorber column. After the absorption process, the CO_2 rich solvent exits the absorber column, is pumped, and is heated by the CO_2 lean solvent entering the absorber. The CO_2 rich solvent then enters the stripper column which uses heat from condensing steam to strip the CO_2 from the solvent in a highly endothermic process.

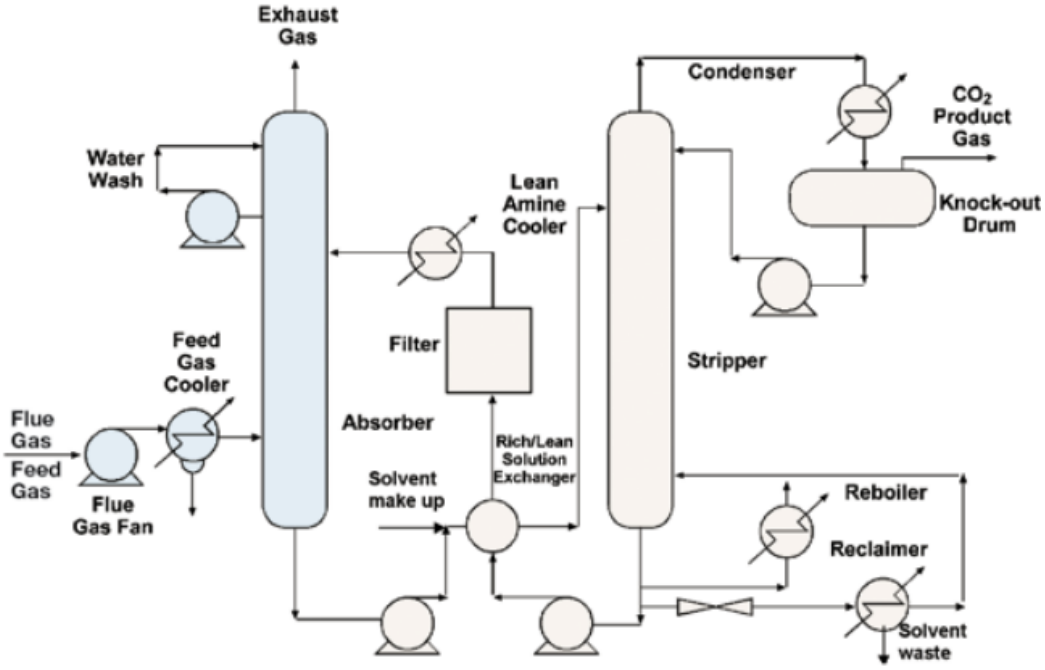

Figure 2- 1: Absorption carbon capture diagram [26]

The mechanism is described by the reverse of equation 2.1 where the chemicals on the right side are the reactants and the chemicals on the left side are the products. The steam is created in the reboiler. After the removal of CO_2, the lean solvent is pumped, transfers heat to the rich solvent entering the stripper, filtered, cooled, and then reintroduced to the absorber. The stripped

CO_2 exits the stripper column and passes through a condenser where any water is removed from the stream. The CO_2 then exits the capture unit and can be compressed and transported to a storage site.

2.2 Flexible Carbon Capture

All the current methods utilized to capture CO_2 impose a parasitic electricity load on the base fossil fuel plant. This load both decreases the peak power output of the plant and reduces its ability to operate variably, therefore impacting its effectiveness to balance the grid instabilities created by renewables. Previous research has presented methods that can temporarily remove most of the parasitic electricity load, recovering a large amount of the lost peak power output. These methods can also decrease power output to levels lower than the minimum capacity of the base fossil fuel + CCS plant. By increasing variability, the power plant is better suited to follow the changing electricity load. In addition, carbon capture plants with flexible technologies can operate more economically than those without flexible technologies because they can sell more power at times when the electricity prices are high, consequently increasing total plant revenue. The existing flexible carbon capture techniques are described in the following sections.

2.2.1 Bypass and Venting

One method used in a multitude of studies [28–33] to eliminate the parasitic load imposed by carbon capture technology is to bypass the CCS unit when desirable. This way plant operators have the option to use the CCS unit during regular operation of the plant but are still able to increase power output to its plant maximum capacity achievable without CCS. Ideally, bypass would happen at times of peak electricity demand and prices. Bypass can be accomplished in two ways. The first way is to vent the flue gas instead of feeding it through the absorber as described in a

method proposed by Oates et. al. [30], illustrated in Figure 2- 2 left. This is a very simple concept as the only additional equipment necessary would include the valves and ducting used to redirect the flue gas to the stack instead of routing it through the absorber column. The second method is to incorporate a bypass steam for the rich solvent to be reintroduced to the absorber instead of routed through the stripper as illustrated in Figure 2- 2 right in a method proposed by Cohen et. al. [31]. This method offers more precise control of power output as the carbon capture unit can be turned down more easily to capture a lower percentage of CO_2 in the exhaust. Both the bypass stream and the steam amount can be varied between 0 and 100% flow. This method also requires minimal extra equipment to be installed with the capture facility.

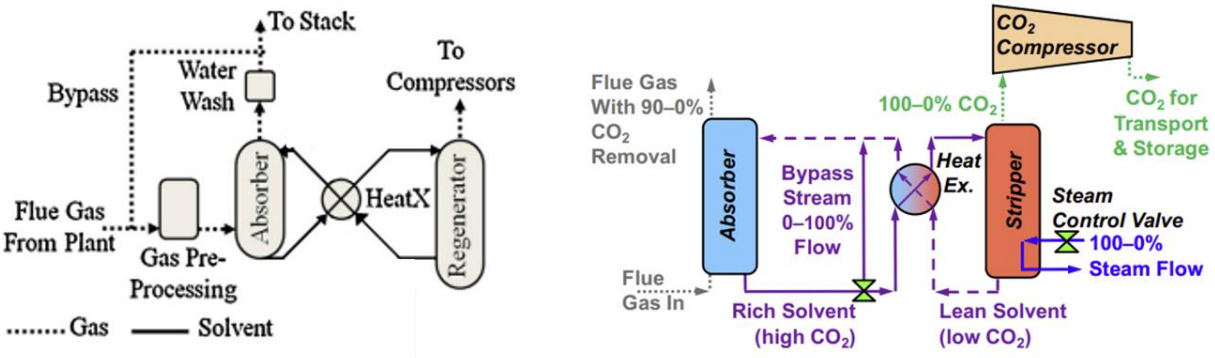

Figure 2- 2: Bypass diagrams from [30] and [31]

Tait et. al. [28] analyzed bypass as one of five options to enhance flexibility in post combustion carbon capture systems. The goal of the study was to determine the barriers imposed by carbon capture on flexible operation. They concluded that while no significant barriers to flexible operation were found, capture rate and lag times were highly dependent on the solvent inventory and circulation times. Chen et. al. [29] formulated a profit model for flexible carbon capture including venting as solution and concluded that operating profits could be increased up

to 20% when flexibility is employed. Oates et. al. [30] and Cohen et. al. [31] calculated the profits and speculated the economic success of a couple flexibility methods including bypass under different electricity grid conditions.

When policies like CO_2 taxes are enacted, bypass technologies enable power plant operators to decide whether it is more economical to maximize the percent of emissions captured, thereby suffering a decrease in revenue due to the parasitic load, or to pay the emissions cost associated with lower CO_2 capture percentages to increase power output and revenue. This ability has a few implications for CCS dispatch in electricity market conditions with different policies. First, for high CO_2 taxes (>$70/ton), it is typically more profitable to run the CCS unit at full capacity to maximize the total emissions captured and avoid paying large amounts in emissions taxes [31]. Conversely, at very low CO_2 tax amounts (<$20 per tonne), the bypass technologies will be in frequent operation as it is more economical to pay the emissions tax than to suffer a decrease in plant revenue due to the parasitic load imposed by running the capture unit. Therefore, bypass makes the most sense at mid-range CO_2 taxes. Cohen et. al. [31] determined that CCS with bypass technologies yielded profits up to 10% higher than technologies without bypass at carbon taxes of $20-$70 per ton.

In theory, the use of bypass could be used to decreases the minimum CO_2 tax required to financially motivate the installation of CCS technologies since it has the potential to increase profits without adding additional electricity cost. However, Oates et. al. [30] determined that the profitability of bypass only occurred in grid conditions where NPVs were negative. Therefore, the predicted grid situations that make sense for carbon capture will have minimal use of the bypass technologies.

2.2.2 Solvent Storage

The previous studies that examined the use of bypass for flexibility [28–33] also considered solvent storage to be a viable option. Solvent storage allows a high degree of CCS flexibility while maintaining low emissions during times of high plant power output. The solvent storage technique is illustrated in Figure 2- 3 and explained as follows. The CCS interaction with flue gas remains unchanged from inflexible operation, in which the CO_2 is continuously removed from the stream in the absorber column. However, the lean solvent used in the absorber can either be supplied directly from the stripper, or from a lean storage tank. Likewise, the rich solvent exiting the absorber can be stored in a rich storage tank.

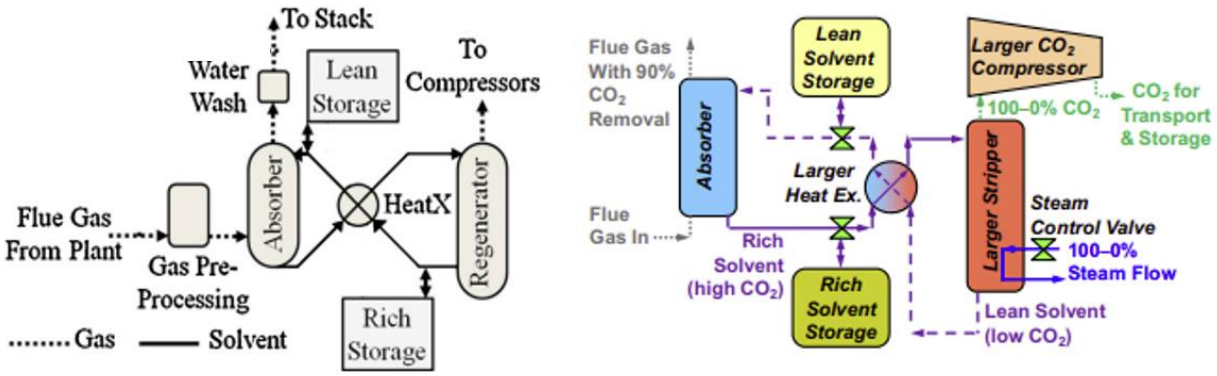

Figure 2- 3: Solvent storage diagrams from [30] and [31]

The tanks operate simultaneously in a charge – discharge process. When charging, the stripper receives solvent both from the absorber and from the rich storage tank and provides solvent to both the absorber and the lean storage tank. When discharging, the lean storage feeds solvent to the absorber and the absorber feeds solvent to the rich storage. During discharge, the absorption process can continue without the energy intensive steam source required to run the stripper, which results in avoidance of the parasitic energy penalty.

When low quantities of emissions tax (~$20 per tonne) are applied in economic analysis, the profits associated with solvent storage are comparable to those associated with bypass technologies [29–31]. However, as CO_2 taxes are increased, solvent storage technologies yield higher profits than bypass technologies. Cohen et. al. [31] found that CCS technologies with solvent storage were 9-29% more profitable than those without solvent storage even at high CCS taxes. However, unlike bypass technologies, solvent storage requires a significant amount of additional equipment to function. Additionally, the capacities of the stripper column and the compressor must be increased so that the storage can be charged at full load. The result is higher capital costs for solvent storage compared to inflexible carbon capture and bypass technologies.

Domenichini et. al. [12] reported four flexible carbon capture scenarios utilizing solvent storage. Two out of the four scenarios yielded higher percent increases in peak power output than percent increases in capital cost. Oates et. al. [30] have determined that solvent storage offers increases in net present value when the applied emissions tax is low or mid-range but is not economically viable in market conditions where the net present value of carbon capturing power plants is positive. Therefore, Oates et. al. have concluded that solvent storage is not a profitable option in market scenarios with CO_2 taxes high enough to financially motivate the operation of carbon capture technologies.

For optimal flexible post carbon capture performance, solvent storage can be combined with bypass techniques. Configurations including solvent storage with optimal component sizes and bypass techniques yielded a net present value difference from non-flexible carbon capture that was 3.9 times larger than the net present value difference between solvent storage technologies without bypass and non-flexible carbon capture in the absence of CO_2 taxes [30]. The optimal storage durations used for solvent storage varies from study to study. Oates et. al. [30] have

concluded that larger storage sizes (greater than 2 hours) are more profitable if the cost of increasing the size of the stripper is avoided while Cohen et. al. [31] have concluded that short storage durations ranging from 15-30 minutes per day make the most sense. However, even when solvent storage is combined with bypass technologies, it is not a profitable option when the CO_2 tax is high enough to financially justify the inclusion of carbon capture in power plants [30]. This is because the cost of emitting is too high to justify bypass while the increased costs of solvent storage outweigh the revenue increase due to flexibility.

2.2.3 Hydrogen Storage

Pre combustion carbon capture can also be made to operate more flexibly and economically by integrating the co-production of hydrogen and the use of hydrogen storage. This concept is utilized in various studies by Szima et. al. [34], Ajiwobowo et al. [35], and Davison et al. [36]. An example process is illustrated in Figure 2- 4 and described as follows. Fossil fuels such as methane are converted to a synthesis gas consisting mainly of H_2 and CO in the reactor unit. The synthesis gas then undergoes water-gas shift reactions via a steam input to convert CO and H_2O to H_2 and CO_2 in the shift reactors. The CO_2 is then removed in the carbon capture unit. At this point the option exists to separate some hydrogen from the synthesis gas. The separated hydrogen can be transported and sold or stored. The remaining synthesis gas is combusted to create power in a combined cycle gas turbine. It is desirable to store hydrogen because it can either be sold for a premium at times of high H_2 demand [36] or used in the combined cycle gas turbine at times of high electricity prices.

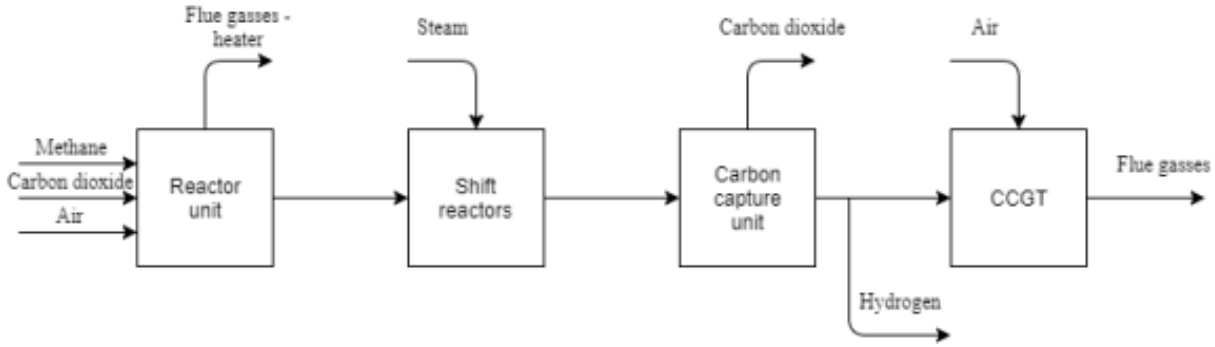

Figure 2- 4: Hydrogen co production and storage diagram from [34]

Co-production of hydrogen and the use of hydrogen storage add a couple degrees of variability to the electricity generation process. First, at times of low electricity demand and prices, plant operators can opt to sell the hydrogen in another market rather than use it for electricity generation. Conversely, at times of high electricity demand and prices, the hydrogen can be used for power generation. Second, hydrogen storage can be used to match hydrogen sales with demand, which allows more hydrogen to be sold at a higher price. Third, when stored hydrogen is used for power generation, the fossil fuel consumption can be decreased, which allows the carbon capture unit to be operated at lower loads and the electricity output to be increased without increasing emissions.

Szima et al. [34] examined 4 cases of hydrogen and electricity co production utilizing different ratios of hydrogen production to electricity generation. They found that most of the total efficiency penalty imposed by the carbon capture unit could be recovered by the co-generation of hydrogen. Szima et al. also found that the specific natural gas consumption of generating co-generating hydrogen was less than that of conventional steam methane reforming technologies. Ajiwibowo et al. [35] determined that a maximum energy efficiency of up to 56% could be achieved using methane to co-produce electricity and hydrogen. Davison et al. [36] found that co-

production plants with hydrogen storage yielded a cost of electricity generation 20% lower that of electricity or hydrogen only plants. Hydrogen can be stored as a refrigerated liquid, in metal hydrides, as a HP gas, or underground in salt caverns, aquifers, etc. Salt cavern storage is the most economical storage option.

While hydrogen storage has been shown to be a promising option for flexible carbon capture, it requires the existence of an IGCC power plant. There are only 113 gasifier facilities documented word wide and only a fraction of those facilities are used for power generation [37]. In addition, most existing gasifiers use a solid fuel such as petroleum residuals, petroleum coke, refinery wastes, and coal [37]. It is unlikely that IGCC power plants with CCS will be a widely adopted solution in future electricity grids because they are not compatible with the 2000+ existing state-of-the-art natural gas facilities.

2.2.4 Oxygen Storage

Oxygen storage techniques can be used in combination with oxy-fuel combustion carbon capture technologies. Oxygen storage can help offset the power output required to run the air separation unit in these plants. The air separation unit is used to generate oxygen storage at times of low demand and electricity prices, and the oxygen from the storage is used in the plant in lieu of running the air separation unit when the demand and electricity prices are high [12]. The most promising oxy-combustion configuration that is used in combination with oxygen storage in various studies [38,39] is called the Allam Cycle, and is illustrated in Figure 2- 5 and described as follows.

Oxygen either from the air separation unit or from the oxygen storage and a fuel are combined with a CO_2 steam and combusted. The flue gas is then expanded in a turbine and cooled

down first in a recuperator and then a gas cooler. The water is removed from the flue gas stream, leaving only CO_2 remaining in the cycle. A fraction of the CO_2 is heated by the recuperator and re-enters the combustor. The remaining CO_2 is transported and sequestered.

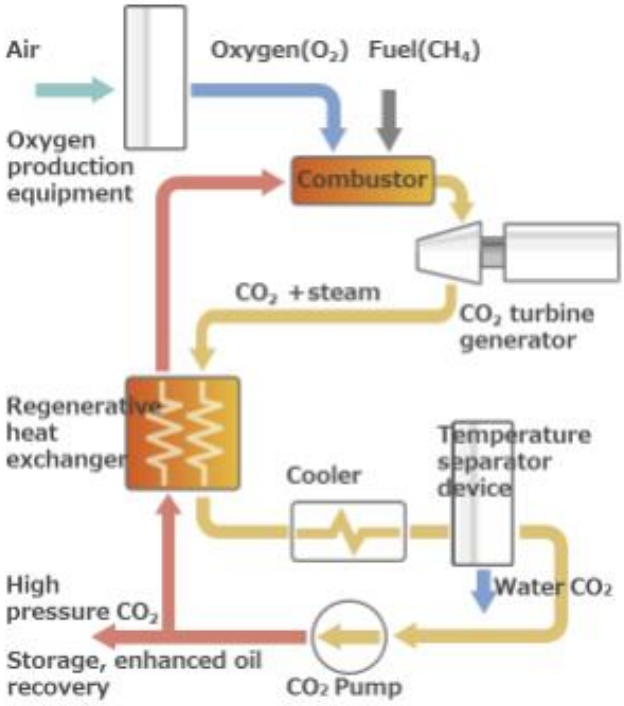

Figure 2- 5: Allam Cycle block diagram from [40]

Mitchel et al. [38] proposed a process model of an Allam cycle combined with liquid oxygen storage. They determined that the use of the storage increases Allam Cycle lower heating value efficiency by 8.1% and increases net electricity output by 17.6% during storage discharge. Hu et al. [39] studied the effect of peak and off-peak operation of the air separation unit with liquid oxygen storage based on a 530 MW coal fired plant. They found that there is a difference of 8.2% efficiency between peak and off-peak periods. In addition, the payback period of the investment was 13 years, and the lifecycle net present value was $23.3 M when examined with variable electricity costs. Higginbotham et al. [41] examined the air separation unit's ability to operate

flexibly. They determined that the ramp rate is 5% per minute and it is possible to turn down to 50% capacity. The study also realized a method to store and release liquid oxygen by simultaneously storing and discharging liquid air.

Although oxy-fuel combustion plants often use natural gas and have shown promising economic results, oxygen storage not compatible with the existing natural gas facilities. Oxy-fuel combustion and Allam cycles are still in the pilot stage with only a handful of plants existing worldwide [42,43]. It is unlikely that new fossil fuel power plants will be built because the reuse of the current infrastructure is a more favorable option.

2.2.5 Significance of Current Flexible Carbon Capture Techniques

A power plant with the ability to capture CO_2 can be more profitable if it can maximize power output when electricity prices are high, even if there is an efficiency penalty when prices are low. Previous research has suggested multiple ways of increasing the flexibility in a variety carbon capture power plants to accomplish this, and as a result the researchers have provided valuable insight for future studies. It has been concluded that flexibility has the potential to increase profitability by up to 35% depending on CO_2 prices. However, previous flexible post combustion carbon capture techniques have been shown not to be profitable under CO_2 policies severe enough to motivate carbon capture. This is because the plants either have to emit high concentrations of CO_2 or invest in more expensive equipment to achieve flexibility. Flexible pre-combustion and oxy-fuel combustion techniques are financially feasible, but they require the deployment of new fossil fuel infrastructure instead of making use of the current state-of-the-art.

2.3 Thermal Energy Storage and the Electricity Grid

While the interconnection between TES and CCS technology has not yet been studied extensively, TES has been explored in previous research as a method to stabilize the electricity grid. The following sections detail the current uses of both hot and cold storages in the context of their application to the electricity grid.

2.3.1 Hot Thermal Storage

Hot TES has proved to be a useful asset to the electricity grid both when it is integrated into certain types of existing power plants, and when it is used as a standalone storage technology. Its most common power plant application is integration with concentrated solar using both direct and indirect mechanisms. Direct storage concentrated solar plants use concentrated solar rays to create steam for power generation in steam turbines. The steam can either be immediately used in the turbine, or it can be stored in a tank for later use [44]. Indirect storage concentrated solar plants with thermal storage use concentrated solar rays to heat molten salts to temperatures close to 600°C. The hot molten salt can be used directly to generate steam for use in a steam turbine or it can be stored in tanks for use at a different time. TES is a particularly interesting prospect for concentrated solar because the storages can be charged when the sun is shining but electricity demand is low, and can be discharged when the electricity demand is high but the sun is not shining.

Hot TES has also been proposed for use gas combined cycle power plants. This can be accomplished by either using the flue gas from the gas turbine exit, or steam from the HRSG to heat the TES [45,46]. In both methods, the power output from the steam turbines is decreased to charge the TES because the plant heat is used instead to generate the storage. Conversely, steam

turbine power output is increased to levels higher than the nominal capacity when the TES is discharged. One TES design using HRSG steam, proposed by Chang et al. [46], is illustrated in Figure 2- 6 and described as follows. To charge the TES, high pressure (HP) steam is extracted from the HP HRSG outlet. This steam is then used to heat up the molten salts exiting the cold storage tank before it is mixed with the low pressure (LP) steam streams for use in the LP turbine. The molten salts that are heated up by the steam are then stored in the hot storage tank. To discharge the TES, the LP steam from the LP HRSG outlet and the LP steam from the intermediate pressure (IP) turbine outlet are mixed. The mixed LP steam absorbs heat from the molten salts exiting the hot tank before entering the LP turbine. The result of discharge is a higher energy content in the LP steam entering the turbine and a therefore higher power outputs from the LP turbine. Once the hot molten salts have exchanged heat with the steam, they are stored in the cold tank.

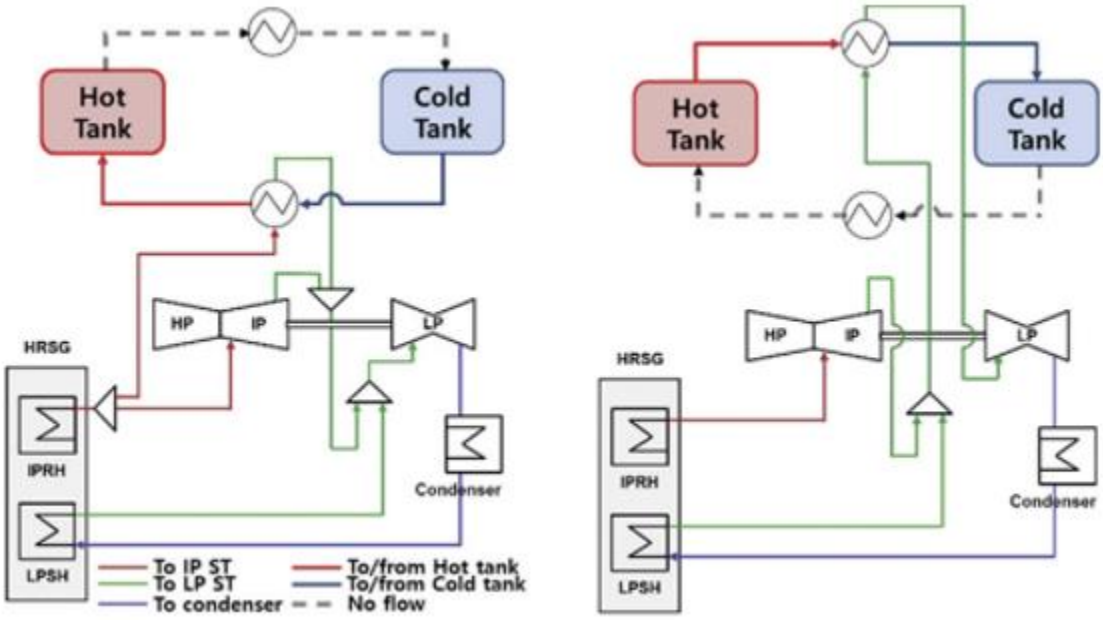

Figure 2- 6: TES integration with combined cycles charging (left) and discharging (right) [46]

Li et al. [45] used aspen plus to develop a dynamic model of a combined cycle gas turbine with TES generated from the gas turbine exhaust. They determined that it is realistically feasible to extract flue gas for TES generation and use the TES to generate high temperature & pressure steam for power generation. Chang et al. [46] used gPROMS and SimCentral to create a multiscale model of their proposed combined cycle with TES technology which decreased power output by 8.42% during a 3 hour TES charging period and increased power output by 1.56% during a 4 hour TES discharging period.

TES can also be used for grid storage and electricity load leveling in the form of pumped heat energy storage (PHES). To charge TES, PHES technologies act as mechanical heat pumps, using grid electricity to create and store heat. To discharge TES, PHES technologies act as mechanical heat engines, using the stored heat to create electricity. Some PHES technologies have been commercialized by companies such as Malta Inc. [47], and there have been numerous studies that have examined different PHES technologies and their feasibility in electricity grid scenarios. One such study by Smallbone et al. [48] proposed a PHES method, then calculated its LCOS and compared it to other storage technologies. The concept is shown in Figure 2- 7 and explained as follows. Both a hot storage and a cold storage are utilized storing hot, high pressure (HP) gas and cold, LP gas respectively. When there is an excess of low-cost electricity in the grid, electricity is purchased to compress ambient gas in the hot piston and store it in the hot storage. Simultaneously, ambient gas is expanded in the cold piston and stored in the cold storage, recovering some mechanical power. Both TES tanks are discharged when the electricity demand and prices are high. The hot piston is used to expand the gas from the hot storage and the gas in the cold storage is compressed to ambient conditions.

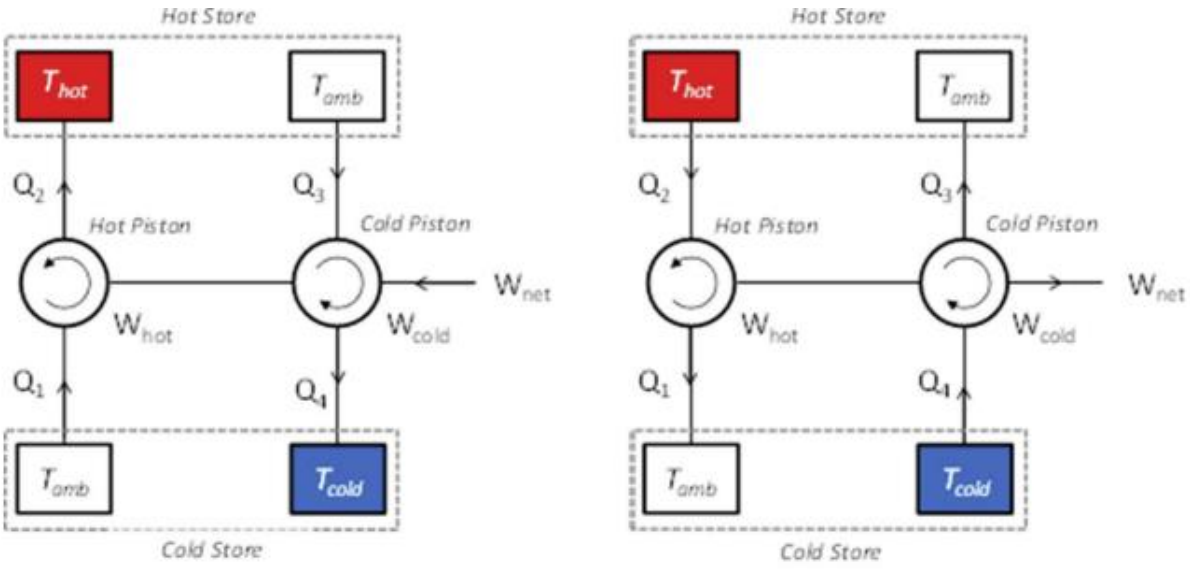

Figure 2- 7: Pumped heat thermal energy storage [48]

Smallbone et al. determined that the LCOS of PHES was in the range of $0.10/kWh to $0.17/kWh, which is lower on average than the LCOS of batteries [4]. In addition, PHES technologies have less expensive capital costs than competing storage technologies such as pumped hydro and compressed air energy storage on a power basis ($/kW). It's energy-based capital costs ($/kWh) is more expensive than pumped hydro but cheaper than compressed air energy storage.

The hot storage mediums used in the technologies previously discussed have included molten salts, steam, and gas storages. While most storages that are currently being used utilize fluid sensible heat (such as molten salts), other mediums have been discussed in previous research and include sensible, latent and chemical techniques [49]. The most promising new prospect for thermal energy storage are solid, sensible heat mediums like ceramics and concrete [49]. This is because they offer a wide operating temperature range with high densities and heat capacities. In

addition, the storage medium cost is very low. However, these storages require heat exchangers to charge and discharge which can add to the overall technology cost required for their use.

2.3.2 Cold Thermal Storage

To understand the importance of cold storage in power generation, the effect of ambient temperatures on gas power generation must first be considered. As ambient temperature changes, so does the density of the inlet air to the plant. For hot climates, the air has lower densities and therefore lower mass flowrates. The result is a decrease the power output and efficiency of the gas turbine as well as the steam turbines if the plant is a combined cycle [50]. A typical power plant suffers a 0.1% loss in thermal efficiency and a 0.5-0.9% loss in gross power output for every 1°C rise in ambient temperature [51,52].

Many strategies have been developed to cool the inlet to the plant to avoid suffering performance losses and to produce higher net power outputs then those achievable using ambient conditions. The current primary methods used include evaporative cooling, inlet fogging, mechanical refrigeration, and absorption chilling. Evaporative cooling techniques mix water with the gas turbine inlet air stream. The air is cooled via the latent heat of the water evaporating into the steam. Inlet fogging techniques use atomizing nozzles to spray very fine water droplets into the inlet stream before it enters the gas cycle. Fogging is considered a separate method to evaporative cooling because an excess moisture is achievable, and the efficiency of humidification is much higher [53]. Mechanical refrigeration primarily uses vapor compression cycle cool the intake air through heat exchange with the evaporating refrigerant. Absorption chilling techniques utilize waste heat from the power plant to power are refrigeration cycle using multiple working fluids.

Inlet chilling requires some amount of parasitic power draw from the plant. While the parasitic load is very low for evaporative cooling and inlet fogging techniques, these methods are highly dependent on the ambient conditions and have limited potential in humid regions [53]. Furthermore, humid air corresponds to lower gas power outputs than dry air when the temperature and pressure are equal [52]. Additionally, these methods use large quantities of water and can correspond to large pressure losses in the inlet stream [53]. Low parasitic power draw is also achievable through absorption chilling methods, but these techniques come with their own set of disadvantages. First, absorption technology requires more expensive, higher capacity equipment than other technologies [53]. Second, high operating and maintenance costs are required for the supply and treatment of the chemicals used in the process [53]. Third, some fluids used in absorption technology are corrosive, which leads to a reduction in technology lifetime [53].

While mechanical refrigeration technologies have comparatively high parasitic power draw, they allow for a wide range of inlet conditioning, they are not dependent on ambient conditions, they have reliable and simple designs, and they have lower equipment costs than absorption technologies [53]. In addition, it is possible to offset the parasitic power load associated with mechanical refrigeration by employing cold TES. The concept is illustrated in Figure 2- 8 and described as follows. To charge the TES, electricity is used to power drive the chiller compressor, to increase the pressure and temperature of a refrigerant. The refrigerant is then condensed at a high pressure in the cooling tower. Next, the refrigerant pressure is reduced and it is evaporated inside the TES, which consequently removes heat from the storage. To discharge the TES, the thermal storage is used to cool the inlet air the power plant.

Multiple studies have examined the impact that cold thermal storage can have on power plant operation and economics. Palestra et al. [54] determined that a significant economic benefit

is achieved when the TES is used to increase electric power production during the day when electricity prices and ambient temperatures are high, and the TES is charged at night when electricity is cheaper. Barigozzi et al. [55] developed an economics model to optimize cold storage size and evaluate the technologies' NPV in New Orleans, Pheonix, and Abu Dhubi. They found that climate conditions including temperature, pressure, and relative humidity had large impacts on plant economics. They also found that the optimal storage size was different for each climate.

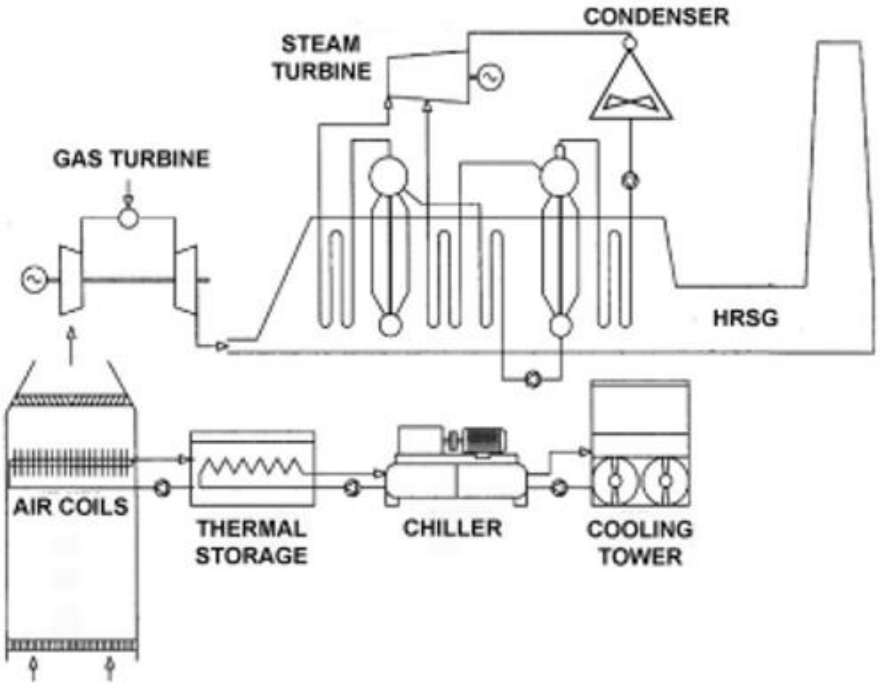

Figure 2- 8: Refrigeration cooling with cold TES [55]

Various methods exist for storing cold energy. Most technologies use water/ice as the storage medium in different mechanisms such as stratified chilled water, ice-on-tube, submerged water/glycol, ice harvesting, and ice slurries. In stratified chilled water mechanisms, multiple layers of water exist at different temperatures. The temperature zones are based on the density of water and the thermocline range is 0.3-1m. These storages are charged with water that is

approximately 4-6°C. During discharge, cold water flows from the cold side of the storage, is used to cool the inlet air, and then re-enters the hot side of the storage. Other aqueous solutions with lower freezing temperatures like brines, calcium chloride, and glycol can be used to instead of water to decrease storage temperature, but they are often corrosive and more expensive to use. Ice-on-tube configurations utilize metallic or plastic tubes surrounded by water. To charge the storage, a cold heat transfer fluid like brine flows through the inside of the tubes, and ice is formed on the outside. To discharge the storage, a warm heat transfer fluid flows through the pipes, and its heat is transferred to the melting ice. Submerged storage mediums simply have a tank of glycol, water, or other liquid with a network of pipes in them. These storages utilize a heat transfer fluid to transfer heat to/from the matter in the tank.

Other storage mediums such as phase change materials and solid ceramics/concrete have also been considered as viable options for cold storage, though they have not been included in the current technologies. Phase change materials can be categorized into organic and inorganic substances. Organic substances are carbon based and include paraffin and non-paraffin materials. They are non-corrosive with high latent heats, but they have low thermal conductivities and experience large changes in volume during phase change. Inorganic materials include salt hydrates and composites. They have a high latent heat per volume, high conductivity, and low cost, but they can be corrosive in nature which causes lower lifetimes of the storage technology. Ceramics and concrete can also be used for the cold storage medium and are an interesting prospect for future technologies because they can be cooled well below freezing temperatures, and the materials are very inexpensive [49].

2.4 Research Needs for Flexible CCS and TES

The provided literature review has outlined the current methods used to enhance the flexibility and economics of carbon capturing power plants. Post combustion carbon capture technologies have shown to be the most compatible option with current natural gas infrastructure, however only two post combustion carbon capture methods have been previously economically examined. The first method involves bypassing the carbon capture unit, which drastically increases CO_2 emissions. The second method involves the implementation of solvent storage, which increases the cost of the carbon capture unit since more solvent must be treated to regenerate the storages. Furthermore, when both bypass and solvent storage techniques are in use, the power plant must also be in use. Therefore, neither option has the capability to use very cheap electricity from excess renewable generation to offset the parasitic power penalty of the CCS unit without also operating the power plant. Other mechanisms for post combustion carbon capture flexibility that do not increase the emissions or the capacity of the CCS unit and can use very cheap electricity from the grid to offset CCS parasitic power need to be economically examined.

This literature review has also described the current applications that TES technologies have to the electricity grid. Both hot and cold storage have been shown to provide useful services to the grid, and they have both had economic success. However, the use TES as a method for flexible carbon capture has not been previously studied from an economic point of view. Therefore, mechanisms used to integrate TES with a carbon capturing power plant need to be realized and economically evaluated. This thesis addresses the research needs of existing literature because it proposes a novel electric resistance approach to heat a hot thermal storage, coupled with a previously examined vapor compression refrigeration cycle used to cool a cold thermal storage, to be used in combination with a NGCC with post combustion CCS. The proposed hot and cold

storage technologies have a minimal impact on the quantity of CO_2 emissions, require minimal capital investment, and have the ability to charge the storage using cheap grid electricity without operating the NGCC.

CHAPTER 3 Modeling Approach

This research proposes to use thermal energy storage to increase the flexibility and economics of NGCCs with CCS technology. Both hot and cold thermal storages are used in this project. The National Energy Technology Laboratory's (NETL) cases B31A (NGCC) and B31B (NGCC + CCS) power plants from the *Cost and Performance Baseline for Fossil Energy Plants* [16] were selected as the base power plants in this analysis. Concrete is used as a thermal energy storage medium. The storage initial designs are based off the BolderBlock modules pioneered by Storworks power. Future electricity market scenarios generated and published using the capacity expansion models GenX [21] and ReEDS [22] were used to evaluate the proposed technologies. This chapter first details the concept and working principles for the proposed technology. Next, an overview of the modeling process is presented. Then, each component of the modeling process is explained, including the technology, optimization, and economics models. The modeling methods for other similar technologies used for economic comparison are also explained. Finally, the methodology used to assess the effect of ambient temperature on cold storage economics is presented.

3.1 Project Concept

Where previous research has used bypass and solvent storage techniques to offset the parasitic load imposed on the power plant by the CCS technology, this project proposes hot thermal storage to recover the lost power output. In Case B31B, LP steam is extracted from the inlet to the LP steam turbine to provide 172 MW of heat for solvent regeneration in the CCS stripper. The steam extraction results in a decrease in net power output of 50 MW. By utilizing hot thermal storage to provide the steam for solvent regeneration, all the LP steam can again be expanded in the LP turbine, recovering the 50 MW power output. This research also evaluates cold storage,

which can be discharged to chill the inlet air to the plant, which results in an increase in power output and efficiency, as described in section 2.3.2 of this thesis. While the cold storage charging and discharging technique used for this research is not a novel concept, it has not yet been implemented to augment the economic potential of flexible carbon capture power plants, and concrete has not been examined extensively as a medium for cold storage.

The hot storage unit increases power plant economics by providing the base NGCC + CCS with electricity arbitrage capabilities. Since a high level of variability is expected in future price signals due to the high concentrations of renewable generators, cheap electricity can be purchased to charge the storage. Then, the storage can be discharged to generate additional electricity when the price is high. This operation concept is illustrated in Figure 3- 1 and described as follows. During long periods of intermediate level electricity prices, the base NGCC + CCS power plant operates the same as it would without any thermal storage, as shown by Figure 3- 1a. This is referred to as the "neutral mode of operation", and ambient air is used by the NGCC to create electricity, and the carbon capture unit uses power plant steam to separate CO_2 from the exhaust. Then, during periods of low electricity prices, the base power plant is shut off and cheap electricity is purchased to charge the hot storage using an electric resistance heating cycle. This is designated as the "charging mode of operation", and is as shown in Figure 3- 1b. Next, during periods of high electricity prices, the base power plant comes back online, and the hot storage provides the steam required for carbon capture. This is defined as the "discharging mode of operation", and as shown in Figure 3- 1c. It should be noted that the charging mode can occur either when the NGCC + CCS power plant is operating, or when the NGCC + CCS power plant is offline, but the discharging mode necessitates the operation of the power plant.

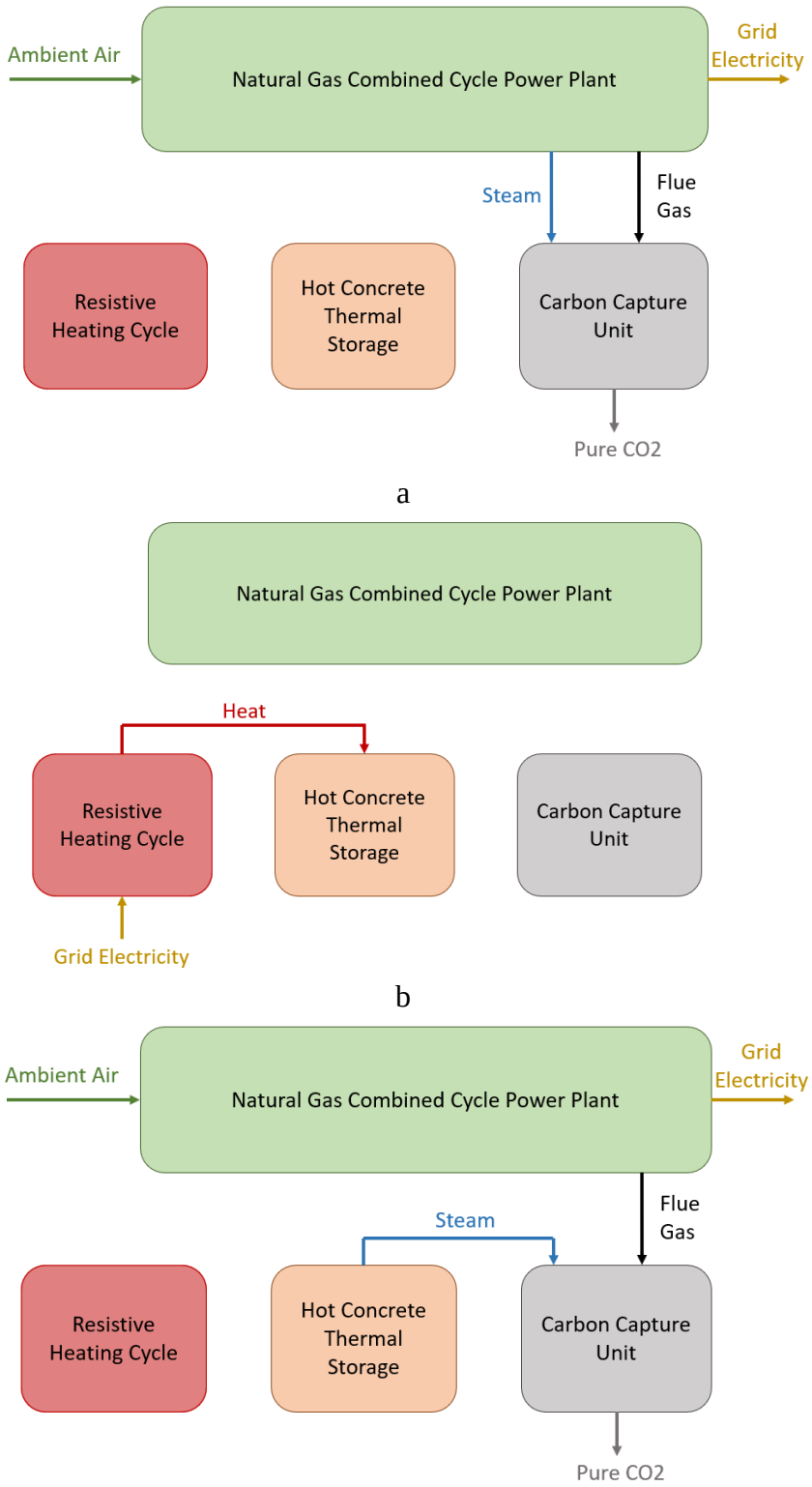

Figure 3- 1: Operation schematic of the hot storage technology for a) neutral mode, b) charging mode, and c) discharging mode

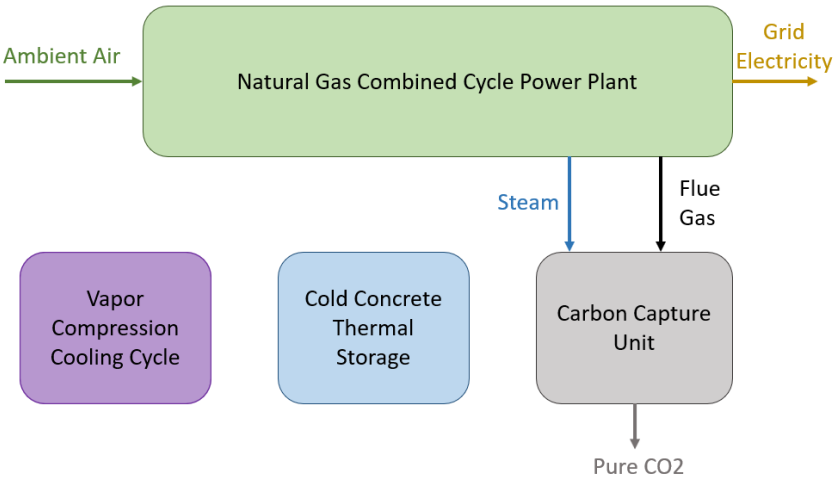
Ambient Air
Natural Gas Combined Cycle Power Plant
Grid Electricity
Steam
Flue Gas
Vapor Compression Cooling Cycle
Cold Concrete Thermal Storage
Carbon Capture Unit
Pure CO2

a

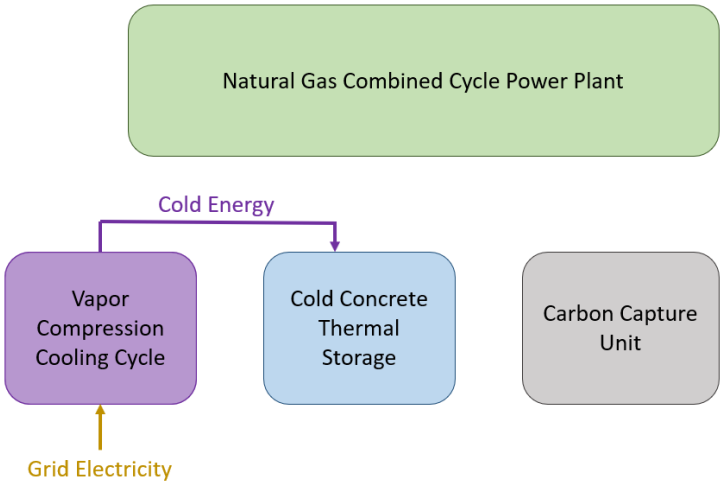
Natural Gas Combined Cycle Power Plant
Cold Energy
Vapor Compression Cooling Cycle
Cold Concrete Thermal Storage
Carbon Capture Unit
Grid Electricity

b

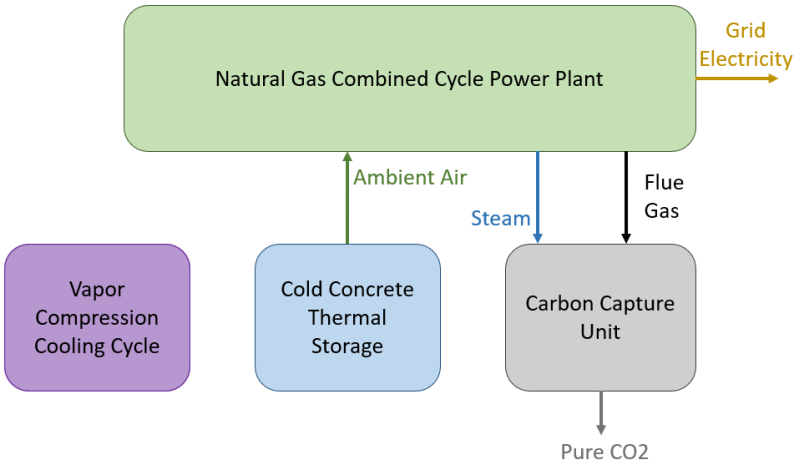
Natural Gas Combined Cycle Power Plant
Grid Electricity
Ambient Air
Steam
Flue Gas
Vapor Compression Cooling Cycle
Cold Concrete Thermal Storage
Carbon Capture Unit
Pure CO2

c

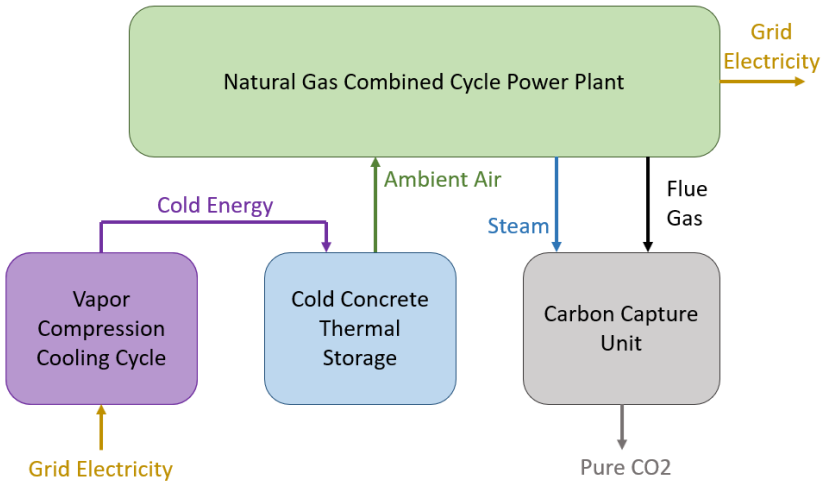

d

Figure 3- 2: Operation schematic of the cold storage technology for a) neutral mode, b) charging mode, c) discharging mode, and d) boosting mode

Like the hot storage unit, the cold storage unit provides electricity arbitrage capabilities, but it can also increase the steady state capacity of the power plant. The cold storage operation is illustrated in Figure 3- 2 and described as follows. Just like the hot storage unit, the cold storage unit can operate in neutral mode, where the power plant operates without charging or discharging thermal storage, as shown by Figure 3- 2a. Then, when the price of electricity is low, the cold TES unit can operate in the charging mode, where grid electricity can be purchased to power a mechanical vapor compression refrigeration cycle that cools the cold storage, as shown in Figure 3- 2b. When the price of electricity is very high, the cold storage can be discharged to cool the inlet air to the plant, as shown in Figure 3- 2c. The cold storage unit offers an additional capability, where it can simultaneously charge and discharge, in a process referred to as the "boosting mode of operation" as illustrated in Figure 3- 2d. This is analogous to steady state inlet chilling techniques used in previous research.

3.2 Modeling Process Overview

This research uses a combination of three models (technology, optimization, and economic) to calculate the net present value (NPV) of the proposed thermal storage technologies. Net present value (NPV) is used as the primary economic metric to describe the financial capabilities of the hot and cold storages in this analysis. NPV was chosen over LCOE because it accounts for all costs (capital and operational) associated with the proposed technology, in addition to the profits associated with actual electricity grid data. LCOE does not account for the impact of variations in electricity pricing, which is a key factor for the feasibility of the proposed technology. The inputs, outputs, and process of each model is summarized in Figure 3- 3. The technology model was constructed in engineering equation solver (EES). It applies the first and second laws of thermodynamics to each component in the base plant and the storage technologies (compressors, turbines, pumps, heat exchangers, etc.) to determine the thermodynamic states of the working fluids. The technology model also determines the mass and energy flows associated with each component, including mass flowrates, power consumption of pumps and compressors, power production of turbines, and heat transfer in the combustor, condenser, carbon capture unit, heat exchangers, and storages. The power and energy flows are used to determine key performance and cost parameters. The technology model outputs a spreadsheet which includes the net power output for each operation mode, the fuel consumption for each operation mode, the CO_2 emissions captured for each operation mode, and the configuration component costs.

The operation model was created in MATLAB. It receives the spreadsheet outputted by the technology model in addition electricity price data, natural gas data, and future CO_2 tax assumptions. The operation model decides how the plant should operate in accordance with the given electricity price profile to maximize NPV. It calculates the revenue, fuel cost, other operating

costs, and total capital cost throughout a given year, which are used to inform the economic model. The economic model is also created in MATLAB and is run by the operation model. It assumes a fixed internal rate of return and a total plant lifetime to perform a discounted cash flow analysis calculate to calculate NPV.

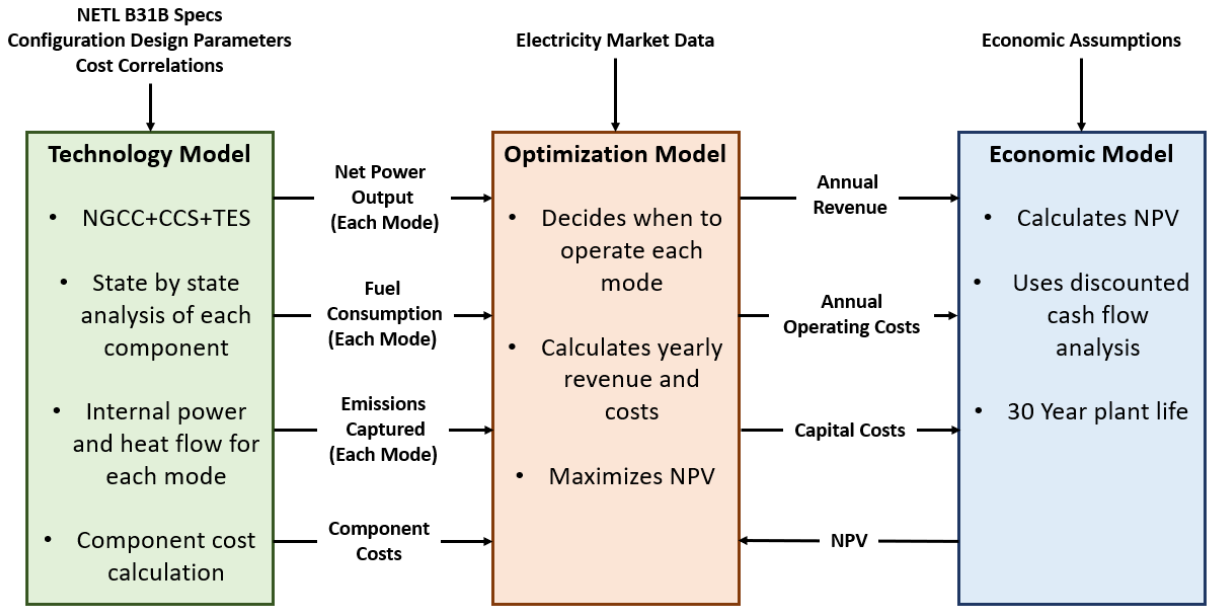

Figure 3- 3: Modeling process overview

3.3 Technology Model

The technology model is a primary focus of this thesis because the modeling details of the operation and economic models will be published in subsequent work. This section includes the base power plant (NGCC+CCS) modeling methodology, including the gas cycle, steam cycle, and carbon capture unit, as well as the thermal energy storage modeling methodology, including the resistively heated hot storage, the vapor compression cooled cold storage, the cost calculations, and the model outputs.

3.3.1 Base Plant Modeling

The technology configurations analyzed in this research use NETL case B31B NGCC+CCS power plant as a starting point. This powerplant was first replicated in EES so that the implications of each thermal storage design could be accurately understood. It should be noted that the modeling methodology of the Case B31A power plant is identical to the Case B31B power plant except it excludes the carbon capture unit. Therefore, it is sufficient to present the methodology of B31B only. Figure 3- 4 shows a process flow diagram of the base case B31B power plant as it is modeled in EES. The stars in the figure indicate the stream points that interact with the thermal energy storage components and will be discussed in sections 3.3.2 and 3.3.6. The model consists of a gas cycle, a steam cycle, and the CANSOLV carbon capture unit. The gas cycle includes the gas compressor, combustor, gas turbine, and HRSG. In this cycle, ambient air is compressed in the gas compressor, and then mixed with natural gas and ignited in the combustor. The resulting flue gas is expanded to create power in the gas turbine before its remaining heat is transferred to the water/steam in the HRSG. The gas exiting the HRSG then enters the carbon capture unit, which separates and compresses the CO2 for transport.

The steam cycle includes a condensate pump, CCS pump, multiple HRSG internal heat exchangers, HP pump, IP pump, HP turbine, IP Turbine, LP turbine, and condenser. The internal HRSG heat exchangers include the LP economizer, LP heat exchanger, IP heat exchanger, IP reheater, and HP heat exchanger. In this cycle, the water exiting the condensate pump is mixed with the water exiting the ccs pump, and the resulting stream is heated in the LP economizer. The LP economizer exit is split into 3 streams: one is boiled and superheated in the LP heat exchanger, one is pumped to a high pressure in the HP pump, and one is pumped to an intermediate pressure in the IP pump. The exit from the HP pump is boiled and superheated in the HP heat exchanger

before being expanded to create power in the HP turbine. The exhaust from the HP turbine is reheated in the IP reheater. The exit stream from the IP pump is boiled and superheated in the IP heat exchanger, mixed with the IP reheater exit stream, and expanded to create power in the IP turbine. The exhaust from the IP turbine is mixed with the LP heat exchanger exit stream and split into two streams: One of which is condensed to provide the heat for solvent regeneration in the carbon capture unit and the other is expanded in the LP turbine to create power. The LP turbine exhaust is condensed in the condenser and then pressurized in the condensate pump. The condensate exiting the carbon capture unit is pressurized in the CCS pump, mixed with the exit stream of the condensate pump, and the steam cycle is restarted.

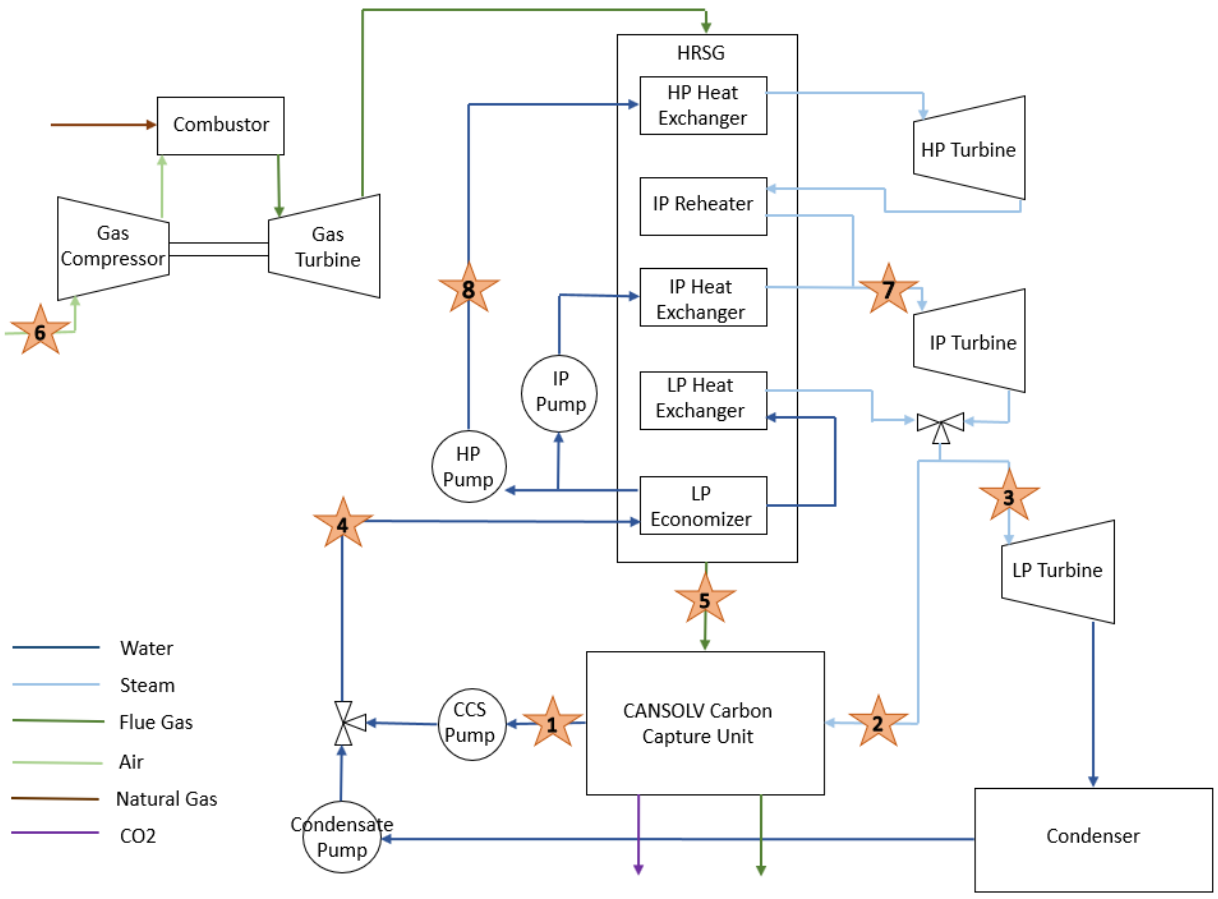

Figure 3- 4: Process flow diagram of the case B31B base plant

The internal operation of the CANSOLV carbon capture unit operation is proprietary, and therefore not reported by NETL or the current research. Instead, the capture unit is assumed to be a heat sink that requires a specific heat duty of condensing steam, delivered at a specified temperature and pressure, to enable the removal of CO2. All CCS parameters are constrained in the model to be equal to those specified by NETL throughout the entirety of the plant operation. In addition, the amount of CO2 captured is always held constant to keep the CANSOLV unit always operating at design point conditions. This means that any additional CO2 created due to thermal storage discharge is vented to the atmosphere.

Table 3- 1 lists all the assumptions used in the creation of the base plant model. Most of the assumed information was extracted from the *Cost and Performance Baseline for Fossil Energy plants* [16], and the additional assumptions can dither be found in the supplemental information for the model created for *Techno-Economic Analysis of Waste Heat Recovery Systems for Wet-Cooled Combined Cycle Power Plants* [50], or were manually selected to ensure reasonable performance of base plant components.

Table 3- 1: Base Plant Modeling Assumptions

Assumption Number	Parameter	Value	Source
1	Design Point Ambient Temperature	15.00 °C	[16]
2	Design Point Ambient Pressure	100.0 kPa	[16]
3	Volumetric Flow Rate	880.9 $m^3/_s$	[16]
4	Gas Compressor Pressure Ratio	20.00	[50]
5	Gas Compressor Isentropic Efficiency	85.00 %	[50]
6	Combustor Temperature	1371 °C	[50]
7	No Combustor Pressure Drop	NA	NA
8	Heat of Combustion	44.87 MJ/kg	[16]

Table 3- 1 Continued

9	Gas Turbine Outlet Pressure	110.0 kPa	[16]
10	Gas HRSG Outlet Pressure	100.0 kPa	[16]
11	Gas Turbine Efficiency	95.0 %	[50]
12	Design Point Low Pressure Steam Flowrate	20.04 kg/s	[16]
13	Design Point IP Steam Flowrate	19.02	[16]
14	Condensate Pump Inlet Quality	Saturated Liquid	NA
15	Condensate Pump Outlet Pressure	599.8 kPa	[16]
16	Condensate Pump Isentropic Efficiency	71.00 %	[50]
17	LP Economizer Outlet Temperature	154.8 °C	NA
18	LP Steam HRSG outlet Pressure	540.7 kPa	[16]
19	LP Steam HRSG Outlet Temperature	306.1 °C	NA
20	IP Pump Outlet Pressure	4385 kPa	[16]
21	IP Pump Isentropic Efficiency	71.00 %	[50]
22	IP Steam HRSG outlet Pressure	3509 [kPa]	[16]
23	Intermediate Steam HRSG Outlet Temperature	554.4 °C	NA
24	HP Pump Outlet Pressure	24.00	[16]
25	HP Pump Isentropic Efficiency	71.00 %	[50]
26	HP Steam HRSG outlet Pressure	16500 kPa	[16]
27	High Steam HRSG Outlet Temperature	554.4	NA
28	HP Turbine Outlet Pressure	3737 kPa	[16]
29	HP Turbine Isentropic Efficiency	85.00 %	[50]
30	IP Reheater Outlet Pressure	3509 kPa	[16]

Table 3- 1 Continued

31	IP Turbine Outlet Pressure	517.1 kPa	[16]
32	IP Turbine Isentropic Efficiency	91.00 %	[50]
33	LP Turbine Outlet Pressure	6.895 kPa	[16]
34	LP Turbine Isentropic Efficiency	93.00 %	[50]
35	Carbon Capture Stripper Heat Duty	172,000 kW	[16]
36	Carbon Capture Stripper Inlet Steam Pressure	510.2 kPa	[16]
37	Carbon Capture Stripper Outlet Steam Pressure	490.4 kPa	[16]
38	Base Plant Auxiliary Power	44.00 MW	[16]

3.3.1.1 Gas Cycle

The thermodynamic state of the inlet air to the gas compressor at the design point is defined by the assumed ambient temperature and pressure (assumptions 1 and 2 of Table 3- 1). The thermodynamic data base in EES is used to find the corresponding density, enthalpy, and entropy. The air mass flowrate is determined using equation (3.1).

$$\dot{m}_a = \rho_{a,GCI}\dot{V}_a \tag{3.1}$$

The compressor outlet pressure is determined using equation (3.2) and the compressor outlet enthalpy is determined using equation (3.3). The EES thermodynamic data base is used to find the compressor outlet temperature and entropy. Equation (3.4) is used to determine the compressor power requirement.

$$P_{a,GC,O} = Pr_{GC}P_{a,GC,O} \tag{3.2}$$

$$\eta_{GC} = \frac{h_{a,i,GC,O} - h_{a,GC,I}}{h_{a,GC,O} - h_{a,GC,I}} \tag{3.3}$$

$$\dot{W}_{GC} = \dot{m}_a (h_{a,GC,O} - h_{a,GC,I}) \tag{3.4}$$

The combustor inlet state is equal to the compressor outlet state. The combustor outlet pressure is assumed to be the same as the combustor inlet pressure (assumption 7 of Table 3- 1) and the combustor outlet temperature is defined by assumption 8 of Table 3- 1. The EES thermodynamic data base is used to determine the enthalpy and entropy at the combustor outlet. The total heat addition of the combustor is determined by equation (3.5) and the fuel mass flow rate is determined by equation (3.6). The flue gas mass flow rate is determined by equation (3.7).

$$\dot{Q}_{CMB} = \dot{m}_g (h_{g,CMB,O} - h_{a,CMB,I}) \tag{3.5}$$

$$\dot{Q}_{CMB} = HV_f \dot{m}_f \tag{3.6}$$

$$\dot{m}_g = \dot{m}_a + \dot{m}_f \tag{3.7}$$

The gas turbine inlet state is equal to the gas combustor outlet state. The gas turbine outlet pressure is defined by assumption 9 of Table 3- 1 and the gas turbine outlet enthalpy is determined by equation (3.8). The gas turbine outlet temperature and entropy are determined using the EES thermodynamic data base. The gas turbine gross power is determined by equation (3.9) and the gas turbine net power is determined by equation (3.10).

$$\eta_{GT} = \frac{h_{g,GT,I} - h_{g,GT,O}}{h_{g,GT,I} - h_{g,i,GT,O}} \tag{3.8}$$

$$\dot{W}_{GT} = \dot{m}_g (h_{g,GT,I} - h_{g,GT,O}) \tag{3.9}$$

$$\dot{W}_{net,GT} = \dot{W}_{GT} - \dot{W}_{GC} \tag{3.10}$$

The gas HRSG inlet state is equal to the gas turbine outlet state. The gas HRSG outlet pressure is defined by assumption 24 of Table 3- 1 and the gas HRSG outlet temperature was assumed initially, and then iteratively changed until proper HRSG heat transfer was achieved. The gas enthalpy and entropy were determined using the thermodynamic data base in EES. The HRSG heat transfer was determined by equation (3.11).

$$\dot{Q}_{HRSG} = \dot{m}_g(h_{g,HRSG,I} - h_{g,HRSG,O}) \tag{3.11}$$

3.3.1.2 Steam Cycle

The LP, IP, and HP water/steam flowrates were determined first in the steam cycle model. The LP and IP flowrates at design point conditions are stated in Table 3- 1 assumptions 12 and 13 respectively. The LP and IP are determined for all conditions using equations (3.12) and (3.13) respectively.

$$\dot{m}_{LP} = \dot{m}_{LP,DP}\frac{\dot{m}_g}{\dot{m}_{g,DP}} \tag{3.12}$$

$$\dot{m}_{IP} = \dot{m}_{IP,DP}\frac{\dot{m}_g}{\dot{m}_{g,DP}} \tag{3.13}$$

All enthalpy values in equations (3.14) through (3.20) are determined from the thermodynamic data base in EES, given the HRSG temperature and pressure assumptions (Table 3- 1 assumptions 18, 19, 22, 23, 26, and 27) and the pump & HRSG equations described later in this section. Additionally, the HRSG heat transfer was determined in the gas cycle analysis. Therefore, equations (3.14) through (3.20) define a closed set of 7 equations and unknowns that were solved iteratively in EES for remaining flowrates and heat transfer values.

$$\dot{m}_s = \dot{m}_{LP} + \dot{m}_{IP} + \dot{m}_{HP} \tag{3.14}$$

$$\dot{Q}_{HRSG} = \dot{Q}_{LPEC} + \dot{Q}_{LPHX} + \dot{Q}_{IPHX} + \dot{Q}_{HPHX} + \dot{Q}_{IPR} \quad (3.15)$$

$$\dot{Q}_{LPEC} = \dot{m}_s(h_{s,LPEC,O} - h_{s,LPEC,I}) \quad (3.16)$$

$$\dot{Q}_{LPHX} = \dot{m}_{LP}(h_{s,LPHX,O} - h_{s,LPHX,I}) \quad (3.17)$$

$$\dot{Q}_{IPHX} = \dot{m}_{IP}(h_{s,IPHX,O} - h_{s,IPHX,I}) \quad (3.18)$$

$$\dot{Q}_{HPHX} = \dot{m}_{HP}(h_{s,HPHX,O} - h_{s,HPHX,I}) \quad (3.19)$$

$$\dot{Q}_{IPR} = \dot{m}_{HP}(h_{s,IPR,O} - h_{s,IPR,I}) \quad (3.20)$$

The first component modeled in the steam cycle is the condensate pump. The inlet water stream was assumed to be a saturated liquid and the inlet temperature was set equal to that of the condenser outlet. The pressure, enthalpy, and entropy of the condensate pump inlet were determined using the thermodynamic database in EES. The condensate pump outlet pressure is defined in assumption 15 of Table 3- 1 and the pump efficiency is defined in assumption 16 of Table 3- 1. The condensate pump outlet enthalpy is determined from equation (3.21). The thermodynamic data base in EES is used to determine the condensate pump outlet temperature and enthalpy. The condensate pump power requirement is determined from equation (3.22).

$$\eta_{SCP} = \frac{h_{s,i,CP,O} - h_{s,CP,I}}{h_{s,CP,O} - h_{s,CP,I}} \quad (3.21)$$

$$\dot{W}_{SCP} = \dot{m}_{LPT}(h_{s,CP,O} - h_{s,CP,I}) \quad (3.22)$$

The carbon capture mixing valve mixes the stream coming from the steam condensate pump outlet and the stream from the carbon capture pump outlet. The carbon capture mixing valve outlet pressure was set equal to the inlet pressures. The carbon capture mixing valve outlet enthalpy

was determined using equation (3.23). The carbon capture mixing valve outlet temperature and entropy are determined using the thermodynamic data base in EES.

$$\dot{m}_s h_{s,CMV,O} = \dot{m}_{LPT} h_{s,CP,O} + \dot{m}_{cc} h_{s,CCP,O} \tag{3.23}$$

The LP economizer inlet state is equal to the carbon capture mixing valve outlet state. The LP economizer outlet was assumed to be a saturated liquid and the LP economizer outlet pressure is defined by Table 3- 1 assumption 17. The LP economizer outlet enthalpy and entropy are defined using the thermodynamic database in EES.

The LP heat exchanger inlet state is equal to the LP economizer outlet state. The LP heat exchanger outlet temperature and pressure are defined by Table 3- 1 assumptions 17 and 18. The LP heat exchanger outlet entropy and enthalpy are determined using the thermodynamic data base in EES.

The IP pump inlet state is equal to the LP economizer outlet state. The IP pump outlet pressure and isentropic efficiency are defined by Table 3- 1 assumptions 19 and 20 respectively. The IP pump outlet enthalpy is determined using equation (3.24) and the IP pump power is determined using equation (3.25). The IP pump outlet temperature and entropy are determined using the thermodynamic database in EES.

$$\eta_{IPP} = \frac{h_{s,i,IPP,O} - h_{s,IPP,I}}{h_{s,IPP,O} - h_{s,IPP,I}} \tag{3.24}$$

$$\dot{W}_{IPP} = \dot{m}_{IP}(h_{s,IPP,O} - h_{s,IPP,I}) \tag{3.25}$$

The IP heat exchanger inlet state is equal to the IP pump outlet state. The IP heat exchanger outlet temperature and pressure are defined by Table 3- 1 assumptions 21 and 22 respectively. The

IP heat exchanger outlet enthalpy and entropy are determined by the thermodynamic database in EES.

The HP pump inlet state is equal to the LP economizer outlet state. The HP pump outlet pressure and isentropic efficiency are defined by Table 3- 1 assumptions 23 and 24 respectively. The HP pump outlet enthalpy is determined using equation (3.26). The HP pump outlet temperature and entropy are determined using the thermodynamic database in EES. The HP pump power is determined using equation (3.27).

$$\eta_{HPP} = \frac{h_{s,i,HPP,O} - h_{s,HPP,I}}{h_{s,HPPO} - h_{s,HPPI}} \tag{3.26}$$

$$\dot{W}_{HPP} = \dot{m}_{HP}(h_{s,HPP,O} - h_{s,HPP,I}) \tag{3.27}$$

The HP heat exchanger inlet state is equal to the HP pump outlet state. The HP heat exchanger outlet temperature and pressure are defined by Table 3- 1 assumptions 25 and 26 respectively. The HP heat exchanger outlet enthalpy and entropy are determined by the thermodynamic database in EES.

The HP turbine inlet state is equal to the HP heat exchanger outlet state. The HP turbine outlet pressure and isentropic efficiency are defined in Table 3- 1 assumptions 27 and 28 respectively. The HP turbine mass flow rate is determined in equation (3.28). The HP turbine outlet enthalpy is determined using equation (3.29). The HP turbine outlet temperature and entropy are determined using the thermodynamic database in EES. The HP turbine power is determined using equation (3.30).

$$\dot{m}_{HPT} = \dot{m}_{HP} \tag{3.28}$$

$$\eta_{HPT} = \frac{h_{s,HPT,I} - h_{s,HPT,O}}{h_{s,HPT,I} - h_{s,i,HPT,O}} \tag{3.29}$$

$$\dot{W}_{HPT} = \dot{m}_{HPT}(h_{s,HPT,I} - h_{s,HPT,O}) \tag{3.30}$$

The IP reheater inlet state is equal to the HP turbine outlet state. The IP reheater outlet temperature and pressure are defined by Table 3- 1 assumptions 29 and 30 respectively. The IP reheater outlet enthalpy and entropy are determined using the thermodynamic database in EES.

The IP turbine inlet state is equal to that of the IP heat exchanger and IP reheater. The IP turbine outlet pressure and isentropic efficiency are defined in Table 3- 1 assumptions 31 and 32 respectively. The IP turbine mass flow rate is determined in equation (3.31). The IP turbine outlet enthalpy is determined using equation (3.32). The IP turbine outlet temperature and entropy are determined using the thermodynamic database in EES. The IP turbine power is determined using (3.33).

$$\dot{m}_{IPT} = \dot{m}_{HP} + \dot{m}_{IP} \tag{3.31}$$

$$\eta_{IPT} = \frac{h_{s,IPT,I} - h_{s,IPT,O}}{h_{s,IPT,I} - h_{s,i,IPT,O}} \tag{3.32}$$

$$\dot{W}_{IPT} = \dot{m}_{IPT}(h_{s,IPT,I} - h_{s,IPT,O}) \tag{3.33}$$

After the steam exits the IP turbine, it is combined with the steam exiting the LP heat exchanger. Then, some of the steam is routed to the carbon capture unit while the remaining steam enters the LP turbine. The carbon capture unit and LP turbine inlet states are therefore set equal to the state of the combined steam from the IP turbine and LP heat exchanger. The carbon capture unit outlet was assumed to be a saturated liquid at the temperature defined in Table 3- 1 assumption 34. The carbon capture unit outlet pressure, entropy, and enthalpy are determined using the

thermodynamic database in EES. The carbon capture unit heat duty is defined in Table 3- 1 assumption 33. Equation (3.34) is used to determine the mass flowrate through the carbon capture unit.

$$\dot{Q}_{CC} = \dot{m}_{CC}(h_{s,CC,O} - h_{s,CC,I}) \tag{3.34}$$

The LP turbine outlet pressure and isentropic efficiency are defined in Table 3- 1 assumptions 36 and 37 respectively. The LP turbine mass flow rate is determined in equation (3.35). The LP turbine outlet enthalpy is determined using (3.36). The LP turbine outlet temperature and entropy are determined using the thermodynamic database in EES. The LP turbine power is determined using equation (3.37).

$$\dot{m}_{LPT} = \dot{m}_{IPT} + \dot{m}_{LP} - \dot{m}_{CC} \tag{3.35}$$

$$\eta_{LPT} = \frac{h_{s,LPT,I} - h_{s,LPT,O}}{h_{s,LPT,I} - h_{s,i,LPT,O}} \tag{3.36}$$

$$\dot{W}_{LPT} = \dot{m}_{LPT}(h_{s,LPT,I} - h_{s,LPT,O}) \tag{3.37}$$

The condenser inlet state is equal to the LP turbine outlet state. The condenser outlet state is assumed to be a saturated liquid at the condenser inlet pressure. The condenser outlet temperature, enthalpy, and entropy are determined using the thermodynamic database in EES. The condenser heat duty is determined using equation (3.38).

$$\dot{Q}_{CND} = \dot{m}_{CND}(h_{s,CND,I} - h_{s,CND,O}) \tag{3.38}$$

The electrical auxiliary power requirement for the base plant is defined in Table 3- 1 assumption 38. In [16], the auxiliary power includes the pumping power, so the auxiliary power

without the pumps is determined in (3.39). The total steam power output is determined in equation (3.40) and the net power output for the base plant is determined in equation (3.41).

$$\dot{W}_{AUX} = \dot{W}_{AUX,DP} - \dot{W}_{HPP} - \dot{W}_{IPP} - \dot{W}_{CP} \tag{3.39}$$

$$\dot{W}_{ST} = \dot{W}_{HPT} + \dot{W}_{IPT} + \dot{W}_{LPT} \tag{3.40}$$

$$\dot{W}_{BP} = \dot{W}_{net,GT} + \dot{W}_{ST} - \dot{W}_{AUX} - \dot{W}_{HPP} - \dot{W}_{IPP} - \dot{W}_{CP} \tag{3.41}$$

3.3.1.3 Base Plant Technology Model Outputs

The base plant technology model outputs 9 parameters that are used in the optimization model. These parameters are listed in Table 3- 2. The power output and fuel consumption are calculated in the base plant, designated by the variables $\dot{W}_{BP}$ and $\dot{m}_f$ respectively. The capture percent, capital costs, fixed operating and maintenance (FOM) costs, and variable operating and maintenance (VOM) costs are identical to those reported by NETL and were extracted directly from [16].

Table 3- 2: Base plant technology model outputs

Parameter	Variable
Power Output (MW)	PO_{BP}
Fuel Consumption (kg/s)	FC_{BP}
Emissions Captured (%)	ECP_{BP}
NGCC Capital Cost (MM$)	CC_{NGCC}
NGCC FOM (MM$/yr)	FOM_{NGCC}
NGCC VOM (MM$/MWh)	VOM_{NGCC}
CCS Capital Cost (MM$)	CC_{CCS}
CCS FOM (MM$/yr)	FOM_{CCS}
CCS VOM (MM$/tonne)	VOM_{CCS}

3.3.2 Thermal Energy Storage Technology Modeling

Both hot and cold storage technologies are used to augment the power output of the base B31B power plant by interacting with the streams indicated with numbered stars. Section 3.3.2.1 details the modeling methodology of the hot storage while section 3.3.2.2 details the modeling methodology of the cold storage.

3.3.2.1 Hot Storage

The hot storage medium used in this research consists of modular concrete blocks with cavities for airflow, as illustrated in Figure 3- 5. The additional equipment required for the hot storage unit include a blower, a heat exchanger referred to as the hot storage steam generator (HSSG), a resistance heater, and a pump. The methods used to charge and discharge the storage unit are shown by the process flow diagrams in Figure 3- 6a and b respectively. To charge TES, air is blown through the resistance heater to increase its temperature. The hot air then passes through the cavities in the storage medium, which heats up the storage while cooling the air. The cooler air then re-enters the blower. To discharge the storage, cooler air is blown through the cavities the storage medium, which increases the air temperature while cooling off the storage. The hot air then transfers its heat to boiling steam inside the HSSG before reentering the blower. The steam generated inside the HSSG is routed to the CANSOLV CCS unit inlet of the base plant, designated by orange star 1 in Figure 3- 4 and Figure 3- 6, where it is condensed to provide the heat necessary to separate the CO2 from the flue gas. The condensate exiting the CCS unit is pumped before re-entering the HSSG. By using the hot storage to generate the steam required for CO2 removal, the base plant no longer needs to provide steam to the CCS unit. Instead, all low-pressure steam in the base plant is used for power generation.

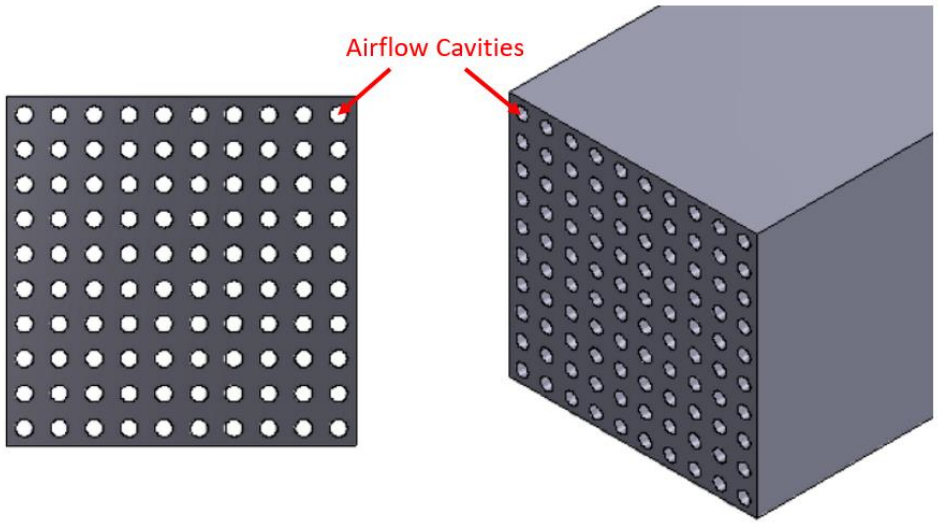

Figure 3- 5: Hot storage module concept

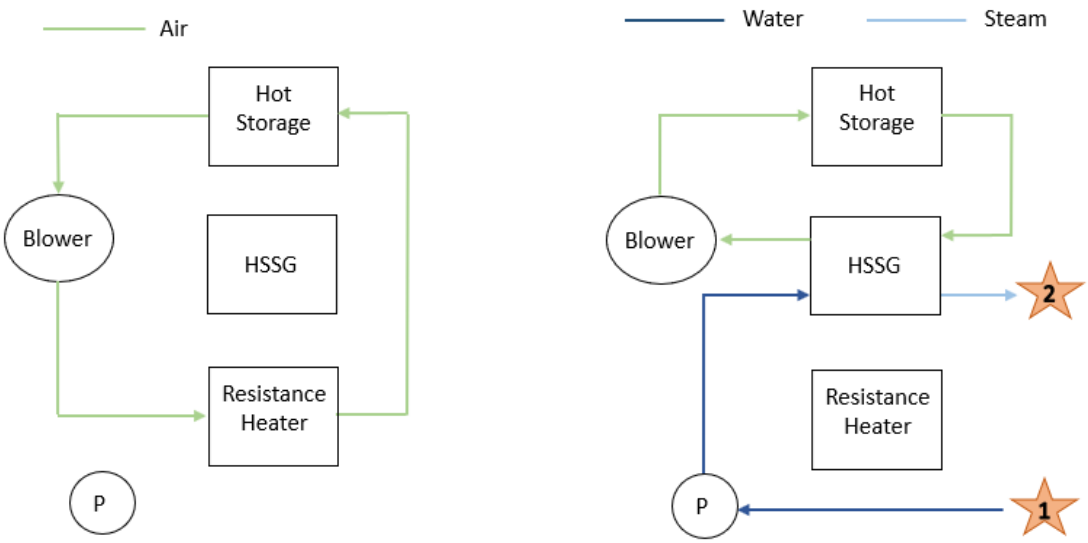

a b

Figure 3- 6: Process flow diagrams of the hot storage unit for a) charging mode and b) discharging mode

Because the hot storage medium is charged and discharged with air, no pipes are required internally to rout working fluids through the storage. Therefore, the storage medium can be composed of pure concrete. Furthermore, since the storage medium is charged via electric resistance, very high temperatures (up to 600°C) are achievable. The steam used by the carbon

capture unit condenses at only 152°C. Therefore, the concrete medium is allowed to change temperature significantly during the charge and discharge processes. Equation (3.24) shows the heat stored in the concrete (Q) as a function of the storage mass (m), the storage specific heat (cp) and the concrete temperature change during charging and discharging (ΔT).

$$Q = m * cp * \Delta T \tag{3.42}$$

Because a large temperature change is acceptable, equation (3.42) dictates that a lesser mass of concrete is required to store the desired heat. The result of having a pure concrete storage medium with a small mass per heat capacity and no internally routed pipes is a very low capital cost per amount of heat stored (6250 $/MWh$_{th}$).

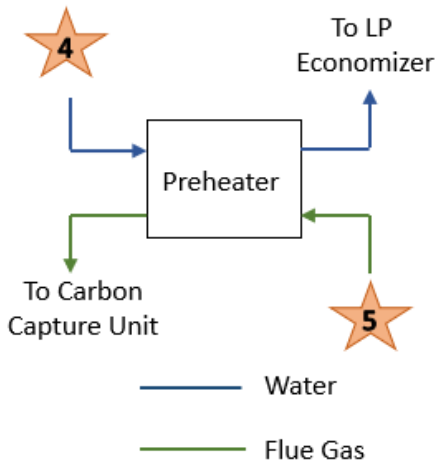

Figure 3- 7: Process flow diagram of the preheater

During the hot storage discharging operation, the condensate exiting the carbon capture unit does not mix with the condensate exiting the condenser like it does in standard base plant operation. Because the temperature of condensate exiting the carbon capture unit is much higher than the temperature exiting the condenser, a feed water preheater is required to achieve the correct temperature entering the LP economizer. A process flow diagram of the preheater is shown in

Figure 3- 7. It extracts temperature from the gas exiting the HRSG (orange star number 5 in Figure 3- 4 and Figure 3- **7**) to heat the water exiting the condenser (orange star number 4 in Figure 3- 4 and Figure 3- **7**).

The assumptions used to model the hot storage technology are listed in Table 3- 3. The methodology used to model the charging mechanism (Figure 3- 6a) is described as follows. The blower charging inlet temperature and pressure are defined by Table 3- 3 assumption 1 and 2 respectively. The blower charging inlet enthalpy and entropy are determined using the thermodynamic database in EES. The blower isentropic efficiency and charging outlet pressure are defined by Table 3- 3 assumptions 3 and 4 respectively. The blower charging outlet enthalpy is determined using equation (3.43) and the blower charging power is calculated using equation (3.44). The blower charging outlet temperature and entropy are determined using the thermodynamic database in EES.

Table 3- 3: Hot storage technology modeling assumptions

Assumption Number	Parameter	Value
1	Blower Charging Inlet Temperature	350.0 °C
2	Blower Charging Inlet Pressure	100.0 [kPa]
3	Blower Isentropic Efficiency	65.00%
4	Blower Pressure Ratio	3.000%
5	Resistance Heater Outlet Temperature	600.0 °C
7	Hot Storage Pressure Drop	1.500 %
8	Blower Discharging Inlet Temperature	180.0 °C
9	Blower Discharging Inlet Pressure	100.0 [kPa]
10	Hot Storage Discharging Outlet Temperature	436.0 °C
11	Pump Pressure Ratio	6.000%
12	Pump Isentropic Efficiency	71.00%
13	HSSG Air Side Pressure Drop	1.500%
14	HSSG Water Side Pressure Drop	3.000%
15	HSSG Outlet Quality	Saturated Vapor
16	Preheater Gas Side Pressure Drop	0.000%

$$\eta_B = \frac{h_{a,i,BC,O} - h_{a,BC,I}}{h_{a,BC,O} - h_{a,BC,I}} \tag{3.43}$$

$$\dot{W}_{BC} = \dot{m}_{a,HSC}(h_{a,BC,O} - h_{a,BC,I}) \tag{3.44}$$

The resistance heater inlet state is equal to the blower charging outlet state. The resistance heater outlet temperature and pressure are defined by Table 3- 3 assumptions 5 and 6 respectively. The resistance heater outlet enthalpy and entropy are determined using the thermodynamic data base in EES. The resistance heater heat duty is determined using equation (3.45).

$$\dot{Q}_{RH} = \dot{m}_{a,HSC}(h_{a,RH,O} - h_{a,RH,I}) \tag{3.45}$$

The hot storage charging inlet state is equal to the resistance heater outlet state. The hot storage charging outlet state is equal to the blower charging inlet state. Equation (3.46) is used to determine the hot storage charging heat duty given the hot storage discharging heat duty and equation (3.47) is used to determine the flow rate in the hot storage charging cycle.

$$\dot{Q}_{HSC} = \dot{Q}_{HSD} \tag{3.46}$$

$$\dot{Q}_{HSC} = \dot{m}_{a,HSC}(h_{a,HSC,I} - h_{a,HSC,O}) \tag{3.47}$$

The methodology used to model the hot storage discharging mechanism (Figure 3- 6b) is described as follows. The blower discharging inlet temperature and pressure are defined by Table 3- 3 assumption 8 and 4 respectively. The blower discharging inlet enthalpy and entropy are determined using the thermodynamic database in EES. The blower discharging outlet pressure is defined by assumption 9. The blower discharging outlet enthalpy is determined using equation (3.48) and the blower discharging power is calculated using equation (3.49). The blower

discharging outlet temperature and entropy are determined using the thermodynamic database in EES.

$$\eta_B = \frac{h_{a,i,BD,O} - h_{a,BD,I}}{h_{a,BD,O} - h_{a,BD,I}} \tag{3.48}$$

$$\dot{W}_{BD} = \dot{m}_{a,HSD}(h_{a,BD,O} - h_{a,BD,I}) \tag{3.49}$$

The hot storage discharging inlet state is equal to the blower discharging outlet state. The hot storage discharging temperature and pressure are defined by Table 3- 3 assumptions 10 and 7 respectively. Equation (3.50) is used to determine the hot storage discharging heat duty.

$$\dot{Q}_{HSC} = \dot{m}_{a,HSC}(h_{a,HSC,O} - h_{a,HSC,I}) \tag{3.50}$$

The HSSG air side inlet state is equal to the hot storage discharging outlet state. The HSSG air side outlet state is equal to the blower discharging inlet state. The HSSG heat duty is determined using equation (3.51) given the carbon capture heat duty, and the air flow rate for the discharging cycle is determined using equation (3.52).

$$\dot{Q}_{HSSG} = \dot{Q}_{CC} \tag{3.51}$$

$$\dot{Q}_{HSSG} = \dot{m}_{a,HSD}(h_{a,HSSG,I} - h_{a,HSSG,O}) \tag{3.52}$$

The pump inlet state is equal to the state of the condensate exiting the carbon capture unit. The pump outlet pressure and isentropic efficiency are defined by Table 3- 3 assumptions 11 and 12 respectively. The pump outlet enthalpy is determined using equation (3.53) and the pump power is calculated using equation (3.54). The pump outlet temperature and entropy are determined using the thermodynamic database in EES.

$$\eta_P = \frac{h_{s,i,P,O} - h_{s,P,I}}{h_{s,P,O} - h_{s,P,I}} \tag{3.53}$$

$$\dot{W}_P = \dot{m}_{s,HSD}(h_{s,P,O} - h_{s,P,I}) \tag{3.54}$$

The HSSG water side inlet state is equal to the pump outlet state. The HSSG outlet pressure and quality are defined by Table 3- 3 assumptions 13 and 14 respectively. The HSSG outlet temperature, enthalpy, and entropy are determined using the thermodynamic data base in EES. Equation (3.55) is used to determine the steam flowrate used in the hot storage discharge cycle.

$$\dot{Q}_{HSSG} = \dot{m}_{s,HSD}(h_{s,HSSG,I} - h_{s,HSSG,O}) \tag{3.55}$$

The methodology used to model the preheater (Figure 3- 7) is described as follows. The preheater water side inlet state is equal to the carbon capture mixing valve outlet state. The preheater water side exit state is equal to the LP economizer inlet state during neutral power plant operation. The preheater heat duty is determined by equation (3.56).

$$\dot{Q}_{PH} = \dot{m}_s(h_{s,PH,O} - h_{s,PH,I}) \tag{3.56}$$

The preheater gas side inlet state is equal to the HRSG gas outlet state. The preheater gas side outlet pressure is defined by Table 3- 3 assumption 16. The preheater gas side outlet enthalpy is determined using equation (3.57). The preheater gas side outlet temperature and entropy are determined using the thermodynamic database in EES.

$$\dot{Q}_{PH} = \dot{m}_g(h_{g,PH,I} - h_{g,PH,O}) \tag{3.57}$$

3.3.2.2 Cold Storage

The cold storage medium used in this research consists of modular concrete blocks with both air cavities and internal steel pipes, illustrated by Figure 3- 8. The additional equipment

required for the cold storage unit includes a compressor, cooling tower, and expansion valve. Figure 3- 9a and Figure 3- 9b show the mechanisms used to charge and discharge the storage unit respectively. To charge TES, ammonia is compressed and then condensed in the cooling tower. The liquid ammonia then expands through the throttling valve before it is routed through the steel pipes of the cold storage medium. While inside the storage medium, the ammonia evaporates, consequently cooling off the concrete. To discharge the cold storage unit, ambient air is pulled through the air cavities in the storage medium by suction of the gas compressor of the base plant. This cools the air down at the inlet to the NGCC and increases power production.

The cold storage unit was designed such that the ambient air is cooled from the NETL design point temperature of 15.00°C to 0.66°C (just above freezing). This was done for two reasons. First, this range of cooling results in an increase in power output within the 10% design point generator oversize specified by NETL. Second, inlet chilling can cause condensation in the inlet air. By keeping the inlet air at above freezing temperatures, ice formation (which is detrimental to gas turbine equipment) is avoided.

It should be noted that the cold storage is charged with evaporating ammonia but discharged with air. This requires the concrete module to include both pipes to rout the ammonia and cavities for the air to flow through. Additionally, the ammonia evaporates in the storage at -26°C, and the storage is used to cool air to approximately 1°C. Therefore, the allowable temperature change of the concrete during charging and discharging is much less significant than that of the hot storage. Consequently, the cold storage medium is much more expensive per heat capacity than the hot storage, with a cost of 71,560 $/MWh$_{th}$.

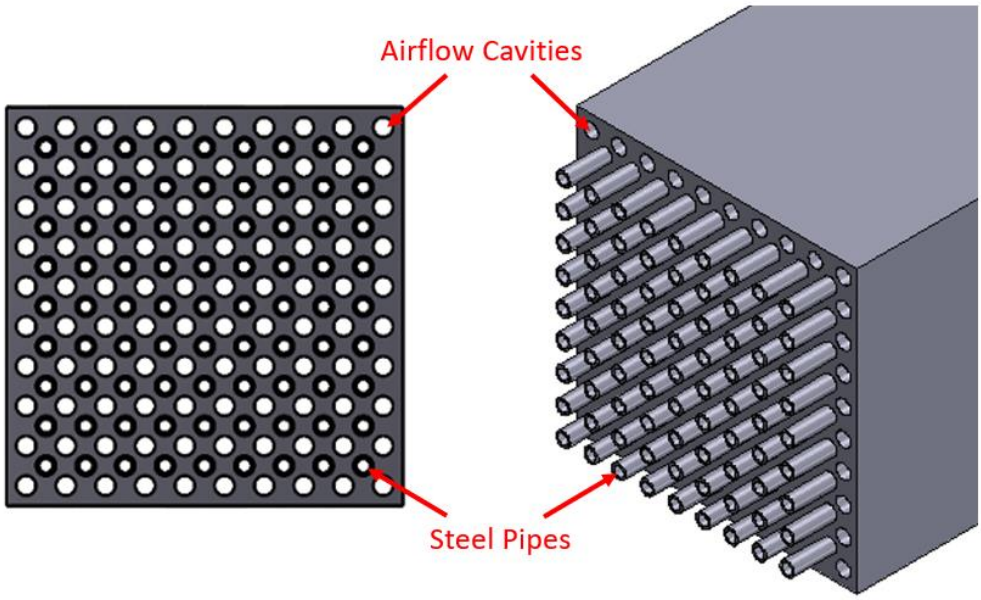

Figure 3- 8: Cold storage module concept

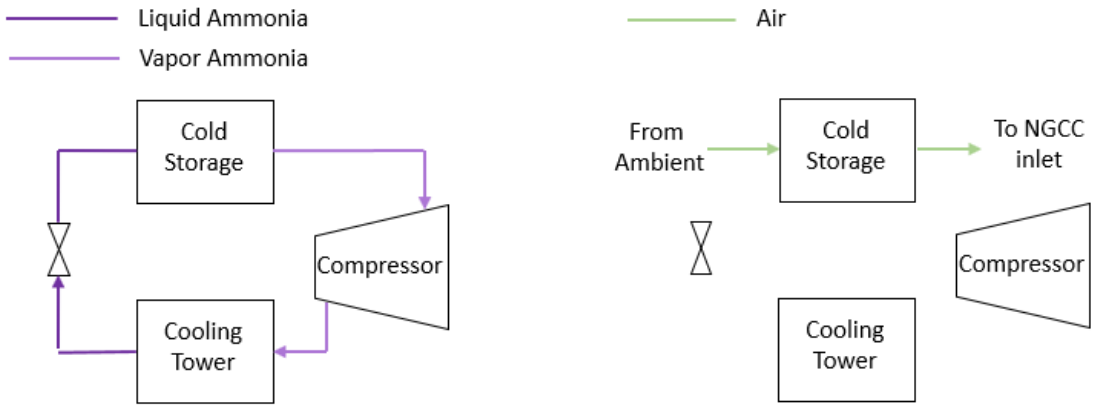

a b

Figure 3- 9: Process flow diagrams of the cold TES unit for a) charging mode and b) discharging mode

The assumptions used to model the cold storage technology are listed in Table 3- 4. The methodology used to model the charging mechanism (Figure 3- 9a) is described as follows. The refrigerant mass flowrate and compressor inlet quality are defined by Table 3- 4 assumptions 1 and 2 respectively. The compressor inlet temperature, enthalpy, and entropy are determined using

the thermodynamic database in EES. The compressor isentropic efficiency and charging outlet pressure are defined by Table 3- 4 assumptions 3 and 4 respectively. The compressor outlet enthalpy is determined using equation (3.58) and the compressor charging power is calculated using equation (3.59). The compressor outlet temperature and entropy are determined using the thermodynamic database in EES.

Table 3- 4: Cold storage modeling assumptions

Assumption Number	Parameter	Value
1	Refrigerant Flow Rate	15.00 [kg/s]
2	Compressor Inlet Quality	Saturated Vapor
3	Compressor Pressure Ratio	10.00
4	Compressor Isentropic Efficiency	85.00%
5	Condenser Pressure Drop	3.000%
6	Condenser Outlet Quality	Saturated Liquid
7	Condenser Difference in Temperature from Ambient	20.00 °C
8	Cold Storage Refrigerant Side Pressure Drop	3.000%
9	Cold Storage Air Side Pressure Drop	1.500%

$$\eta_{RC} = \frac{h_{r,i,C,O} - h_{r,C,I}}{h_{r,C,O} - h_{r,C,I}} \tag{3.58}$$

$$\dot{W}_{RC} = \dot{m}_r (h_{r,C,O} - h_{r,C,I}) \tag{3.59}$$

The cooling tower inlet state is equal to the compressor outlet state. The cooling tower outlet pressure and quality are defined by Table 3- 4 assumptions 5 and 6 respectively. The cooling tower outlet temperature, enthalpy, and entropy are determined using the thermodynamic database in EES. Equation (3.60) is used to determine the cooling tower heat duty and equation (3.61) is used to define the compressor inlet pressure via iteration of equations 56-58.

$$\dot{Q}_{CT} = \dot{m}_r (h_{r,CT,I} - h_{r,CT,O}) \tag{3.60}$$

$$T_{r,CTO} = T_{amb} + 20°C \tag{3.61}$$

The expansion valve inlet state is equal to the cooling tower outlet state. Equation (3.62) is used to determine the expansion valve outlet enthalpy. The expansion valve outlet pressure, entropy, and quality are determined using the thermodynamic database in EES.

$$T_{r,EV,O} = T_{r,EV,I} \tag{3.62}$$

The cold storage inlet state is equal to the expansion valve outlet state. The cold storage outlet state is equal to the compressor inlet state. The cold storage outlet pressure is also constrained by Table 3- 4 assumption 9. This allows the valve outlet temperature/cold storage inlet temperature to be iteratively determined. The cold storage heat transfer is determined by equation (3.63).

$$\dot{Q}_{CS} = \dot{m}_r(h_{r,CS,O} - h_{r,CS,I}) \tag{3.63}$$

The methodology used to model the cold storage discharging mechanism (Figure 3- 9b) is described as follows. The cold storage discharging inlet state is defined by the ambient conditions, presented by Table 3- 4 assumptions 1 and 2 in Table 3- 1. The cold storage outlet pressure is defined by assumption 1 of Table 3- 4. The cold storage outlet enthalpy is determined using equation (3.64). The cold storage outlet temperature and entropy are determined using the thermodynamic database in EES.

$$\dot{Q}_{CS} = \dot{m}_a(h_{a,CS,I} - h_{a,CS,O}) \tag{3.64}$$

3.3.2.3 Component Costs

The additional components required to operate both storage technologies are the hot storage, cold storage, resistance heater, HSSG, blower, pump, compressor, cooling tower, and

preheater. The cost estimations for the hot storage, cold storage, and resistance heater were determined from scaling factors provided by Storworks Power. These values are shown in Table 3- 5.

Table 3- 5: Cost scaling values provided by Storworks Power

Component	Scaling Factor
Hot Storage	1000 [$ °C / kWh]
Cold Storage	2000 [$ °C / kWh]
Resistance Heater	40.00 [$/kWh]

Equations (3.65) and (3.66) are used to determine the cost of the hot storage per hour of maximum steam discharge to the carbon capture unit. Equation 62 calculates the temperature change during charge and discharge. Equation 63 calculates the storage cost given the hot storage scaling factor.

$$\Delta T_{HS} = T_{a,HSC,I} - T_{a,HSD,O} \tag{3.65}$$

$$C_{HS} = \frac{SSF_{HS}\dot{Q}_{CS}}{\Delta T_{HS}} \tag{3.66}$$

Equations (3.67) and (3.68) are used to determine the cost of the cold storage per hour of maximum ambient air chilling capacity. Equation (3.67) calculates the temperature change during charge and discharge. Equation (3.68) calculates the storage cost given the cold storage scaling factor.

$$\Delta T_{CS} = T_{r,CSI} - T_{a,CSO} \tag{3.67}$$

$$C_{CS} = \frac{SSF_{CS}\dot{Q}_{CS}}{\Delta T_{CS}} \tag{3.68}$$

Equation (3.69) is used to determine the cost of the resistance heater given the resistance heater scaling factor.

$$C_{RH} = SSF_{RH}\dot{Q}_{RH} \tag{3.69}$$

The HSSG cost was calculated internally by Storworks Power given the heat rate and desired fluid temperatures. The blower, pump, compressor, and cooling tower were calculated using correlations reported by Couper et. al.'s *Chemical Process Equipment* [56]. Table 3- 6 contains the list of constants extracted for the cost correlations in [56].

Table 3- 6: Cost correlation constants extracted from [56]

Constant	Value
a_1	4.243
a_2	1.033
a_3	-0.0360
b_1	9.885
b_2	-1.616
b_3	0.0834
b_4	2.000

The blower cost is calculated using equations (3.70-3.73). Equation (3.70) determines the blower horsepower requirement. Equation (3.71) determines the number of drivers necessary to power the blower. Equation (3.72) determines the cost of the drivers and equation (3.73) determines the total blower cost.

$$BHP_B = 1.341\dot{W}_B \tag{3.70}$$

$$n_{BDR} = \frac{BHP_B}{700} \tag{3.71}$$

$$C_{BDR} = 2.2n_{BDR}\exp\left(a_1 + a_2\ln(700) + a_3(\ln(700))^2\right) \tag{3.72}$$

$$C_B = 7190 IF_{CPE} {BHP_B}^{0.61} + C_{BDR} \tag{3.73}$$

The compressor cost is calculated using equations (3.74) through (3.77). Equation (3.74) determines the compressor horsepower requirement. Equation (3.75) determines the number of drivers necessary to power the compressor. Equation (3.76) determines the cost of the compressor drivers and equation (3.77) determines the total compressor cost.

$$BHP_C = 1.341 \dot{W}_C \tag{3.74}$$

$$n_{CDR} = \frac{BHP_C}{700} \tag{3.75}$$

$$C_{CDR} = 2.2 n_{CDR} \exp\left(a_1 + a_2 \ln(700) + a_3 (\ln(700))^2\right) \tag{3.76}$$

$$C_C = 7190 IF_{CPE} {BHP_C}^{0.61} + IF_{CPE} C_{CDR} \tag{3.77}$$

The pump cost is calculated using equations (3.78-3.82). Equation (3.78) computes the pump volumetric flowrate. Equation (3.79) computes the pump head. Equations (3.80) and (3.81) calculate factors needed in the pump cost correlation. Equation (3.82) calculates the total pump cost.

$$\dot{V}_p = 15850 \frac{\dot{m}_{cc}}{\rho_w} \tag{3.78}$$

$$H_p = \frac{3281 P_{s,PO}}{\rho_w g} - \frac{3281 P_{s,PI}}{\rho_w g} \tag{3.79}$$

$$F_1 = 3\exp\left(8.833 - 0.9019 \ln\left(\dot{V}_p \sqrt{H_p}\right) + 0.0519 (\ln\left(\dot{V}_p \sqrt{H_p}\right))^2\right. \tag{3.80}$$

$$F_2 = \exp\left(b_1 + b_2 \ln\left(\dot{V}_p \sqrt{H_p}\right) + b_3 (\ln\left(\dot{V}_p \sqrt{H_p}\right))^2\right. \tag{3.81}$$

$$C_p = IF_{CPE} b_4 F_1 F_2 \tag{3.82}$$

Table 3- 7 lists the assumptions used for the cooling tower water usage and equations (3.83) through (3.85) are used to determine the cost of the cooling tower. Equation (3.83) is used to calculate the cooling tower water mass flowrate. Equation (3.84) is used to determine the cooling tower water volumetric flowrate. Equation (3.85) is used to determine the total cooling tower cost.

Table 3- 7: Cooling tower water assumptions

Assumption	Value
Inlet Water Temperature	15.00 °C
Outlet Water Temperature	30.00 °C

$$\dot{Q}_{CT} = \dot{m}_{CTW} cp_w (T_{w,CT,I} - T_{w,CT,O}) \tag{3.83}$$

$$\dot{V}_{CTW} = 15850 \frac{\dot{m}_{CTW}}{\rho_w} \tag{3.84}$$

$$C_{CT} = 328000 IF_{CPE} (\frac{\dot{V}_{CTW}}{100})^{0.61} \tag{3.85}$$

The preheater cost was determined by scaling the cost of the B31B base plant HRSG based on heat duty. The total cost of the HRSG was extracted from [16]. Equation (3.86) was used to determine the preheater cost.

$$C_{PH} = C_{HRSG} \frac{\dot{Q}_{PH}}{\dot{Q}_{HRSG}} \tag{3.86}$$

Estimations for total storage technology fixed and variable operating costs were provided by Storworks Power. These values are applicable to both hot and cold storage and can be viewed in Table 3- 8. It should be noted that the FOM costs are calculated based on the total storage capacity in the optimization model and the VOM costs are calculated per amount of total storage use in the optimization model.

Table 3- 8: Operating and maintenance costs

Component	Value
FOMC (per storage capacity)	1221 [$/MWh/yr]
VOMC (per total use)	1.500 [$/MWh]

3.3.2.4 Thermal Energy Storage Technology Model Outputs

Table 3- 9 presents the list of thermal energy storage parameters that are outputted by the technology model for use in the optimization model. These parameters are in reference to the base plant parameters in Table 3- 2.

Table 3- 9: Thermal energy storage technology model outputs

Parameter	Hot Storage Variable	Cold Storage Variable
Charging Power Decrease (MW)	CPD_{HST}	CPD_{CST}
Discharging Power Increase (MW)	DPI_{HST}	DPI_{CST}
Discharging Fuel Increase (kg/s)	NA	DFI_{CST}
Discharging Emissions Capture Percent Decrease (%)	NA	$DCPD_{CST}$
Storage Capital Cost (MM$/hr discharge)	SCC_{HST}	SCC_{CST}
Other Equipment Capital Cost (MM$)	ECC_{HST}	ECC_{CST}
Fixed Operating and Maintenance (MM$/yr)	$FOMC_{HST}$	$FOMC_{CST}$
VOM (MM$/MWh)	$VOMC_{HST}$	$VOMC_{CST}$

The charging power decrease is the total amount of power required to charge the storage technologies. This value is determined for the hot and cold storage technologies in equations (3.87) and (3.88) respectively.

$$CPD_{HST} = \frac{\dot{Q}_{RH}+\dot{W}_B}{1000} \tag{3.87}$$

$$CPD_{CST} = \frac{\dot{W}_c}{1000} \tag{3.88}$$

The discharging power increase is the difference in power between the discharge mode and the neutral mode for each storage technology. This value is determined for the hot and cold storage technologies in equations (3.89) and (3.90) respectively.

$$DPI_{HST} = \frac{\dot{W}_{BP,HSD} - \dot{W}_{BP,N} - \dot{W}_{B,HSD} - \dot{W}_P}{1000} \tag{3.89}$$

$$DPI_{CST} = \frac{\dot{W}_{BP,HSD} - \dot{W}_{BP,N} - \dot{W}_{B,HSD} - \dot{W}_P}{1000} \tag{3.90}$$

The discharging fuel increase is the difference in fuel consumption between the discharge mode and the neutral mode. This value is zero for the hot storage and is calculated using equation (3.91) for the cold storage.

$$DFI_{CST} = \dot{m}_{f,CSD} - \dot{m}_{f,N} \tag{3.91}$$

The discharging capture percent decrease is the difference in percent of CO_2 emissions captured between the discharging and neutral modes. This value is zero for the hot storage and is calculated using equation (3.92) for the cold storage.

$$DCPD_{CST} = ECP_{BP}\left(1 - \frac{\dot{m}_{f,N}}{\dot{m}_{f,CSD}}\right) \tag{3.93}$$

The storage capital costs used in the optimization model are the same as those calculated in section 3.3.2.3, as shown by equations (3.94) and (3.95) for the hot and cold storages respectively.

$$SCC_{HS} = C_{HS} \tag{3.94}$$

$$SCC_{CS} = C_{HS} \tag{3.95}$$

The capital costs of the additional equipment used to operate storages are determined by equations (3.96) and (3.97) for the hot and cold storage technologies respectively.

$$ECC_{HST} = C_{RH} + C_{HSSG} + C_B + C_{PH} + C_P \tag{3.96}$$

$$ECC_{CST} = C_C + C_{CT} \tag{3.97}$$

The fixed and variable operational costs of are the same for both hot and cold storages, and these values are defined in Table 3- 8.

3.4 Optimization Model

The optimization model used in this research was designed by Vercellino et. al., and detailed formulation is not included in this thesis because it can be accessed through [57]. The purpose of the optimization model is to simulate the operation of the technologies outlined in section 3.3 in accordance with predicted future electricity market scenarios in order to yield the maximum NPV. The optimization model calculates the annual plant revenue, annual fuel costs, annual emissions costs, total annual FOM costs, total annual VOM costs, and total capital cost to inform the economics model. This section is broken into three subsections; the first subsection presents the electricity market scenarios used in the research. The second subsection describes the methodology in which the optimization model chooses to operate the power plant. The third subsection details the methods used toc calculate the variables needed to inform the economics model.

3.3.1 Electricity Market Scenarios

In total, fourteen electricity market scenarios were evaluated in this study, all of which are presented in Table 3- 10, and include one year of hourly electricity prices. Four electricity market

scenarios were generated by GenX [21] and ten scenarios were generated by ReEDs [22]. The GenX profiles utilize a CO_2 tax of $60 per tonne, and they each represent a possible mix of future generators, for example high amounts of wind or solar generation [21]. The ReEDs scenarios consider existing regional electricity markets under carbon taxes of $100 per tonne and $150 per tonne [22]. Section 4.3 of this thesis discusses key characteristics of each price profile, and each market scenario is designated by the scenario name shown in Table 3- 10 throughout the results.

Table 3- 10: Electricity market scenarios summary

Scenario Name	Source	CO_2 Tax ($/tonne)	Situation/Region
G60-Base	GenX	60.00	Base Case
G60-HighWind	GenX	60.00	High Wind Generation
G60-HighSolar	GenX	60.00	High Solar Generation
G60-Winter	GenX	60.00	Winter/New York
R100-CAISO	ReEDS	100.0	California Independent System Operator
R150-CAISO	ReEDS	150.0	California Independent System Operator
R100-ERCOT	ReEDS	100.0	Electricity Reliability Council of Texas
R150-ERCOT	ReEDS	150.0	Electricity Reliability Council of Texas
R100-MISO	ReEDS	100.0	Midcontinent Independent System Operator
R150-MISO	ReEDS	150.0	Midcontinent Independent System Operator
R100-NYISO	ReEDS	100.0	New York Independent System Operator
R150-NYISO	ReEDS	150.0	New York Independent System Operator
R100-PJM	ReEDS	100.0	PJM Interconnection
R150-PJM	ReEDS	150.0	PJM Interconnection

3.3.2 Plant Operation

The plant operation concept involves choosing the optimal times to operate the base power plant while making the best use of TES units. The optimal operation of the base plant can be reduced to a very simple principle. If the available revenue during a given hour (the base plant power output multiplied by the electricity price) is greater than the electricity break-even price (the sum of the fuel, emissions, and variable operating and maintenance (O&M) costs) during that hour,

then there is a profit to be made and the optimization model will choose to operate the base plant at full load. Otherwise, the base power plant will be offline. This concept can be observed in Figure 3- 10, which illustrates the way the optimization model chooses to operate the base plant in collaboration with a) the hot storage unit and b) the cold storage unit. In both diagrams, the base plant is offline during all times where the electricity price is less than the break-even price and online when the electricity price is greater than breakeven price.

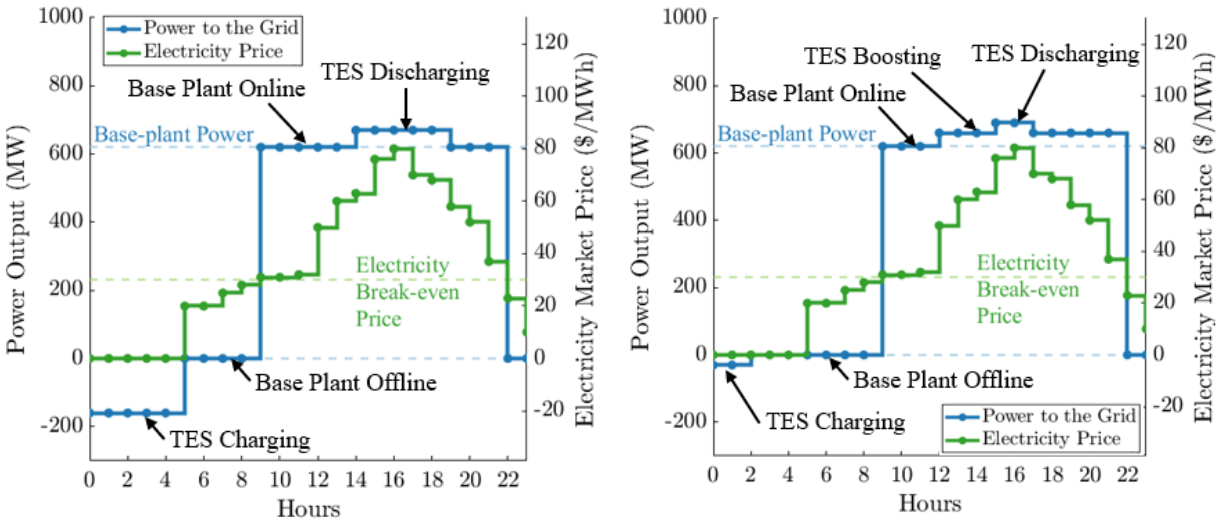

Figure 3- 10: Operation schematic of the base plant with a) the hot storage unit, and b) the cold storage unit

Both hot and cold TES units utilizes electricity price arbitrage, where the storage medium is charged during periods of the lowest electricity prices and discharged during periods of highest electricity prices, to increase the revenue of the system. This concept can also be observed in Figure 3- 10 where the optimization model chooses to charge the TES units when the electricity price is zero and discharge the TES units when the electricity prices are at a maximum. In the current research, the storage mediums charge TES at the same rate that they discharge TES. Therefore, Figure 3- 10 shows that the charging time duration is equal to the discharging time

duration for both TES units. Since the hot storage medium is less expensive per unit energy stored than the cold storage medium (described in section 3.3.2.2), long storage durations are economical. Therefore, Figure 3- 10 shows longer charging and discharging periods for the hot storage than for the cold storage.

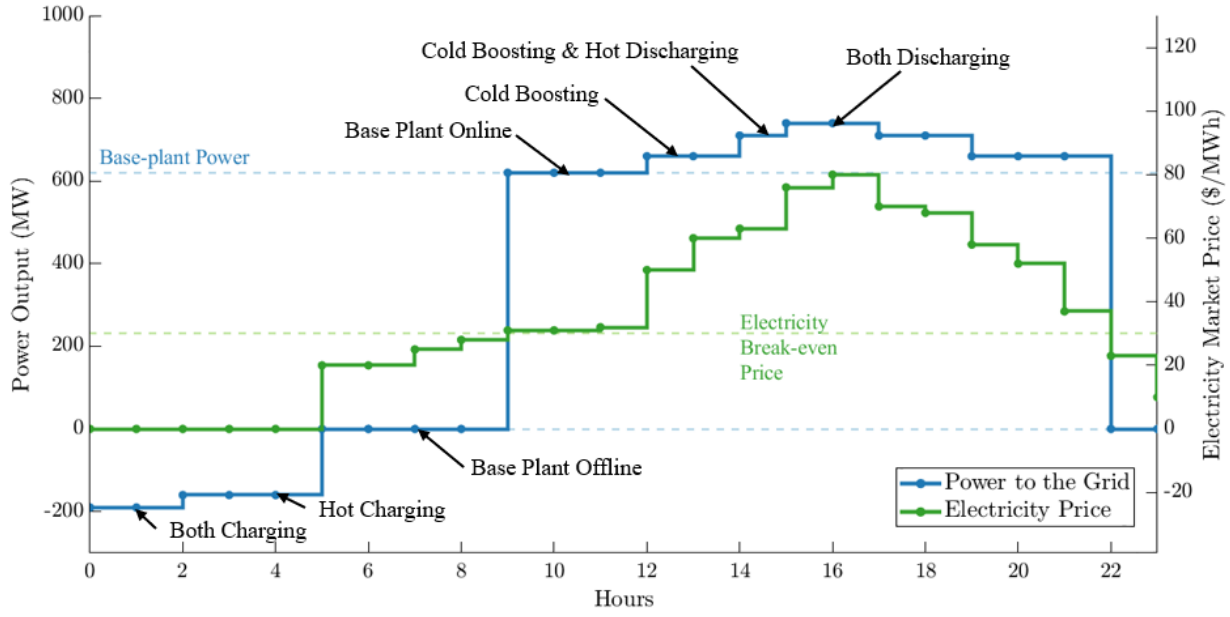

Figure 3- 11: Operation schematic of the base plant with both TES units

If the hot storage and cold storage units are operated simultaneously, the effects of each technology are combined. Figure 3- 11 shows the net power output when the hot TES unit operation shown in Figure 3- 10a is combined with the cold TES unit operation shown in Figure 3- 10b.

3.3.3 Optimization Model Simplifications

The current research utilizes the optimization model to make operational decisions for the base plant and the TES units. However, the full model also has the capability to optimize some key plant-design decisions such as the thermal capacity of the TES medium, and the energy transfer

rates to and from the TES units. Because a detailed discussion on integrated design and control optimization of this system is covered by Vercellino et al. [57], this research pre-defines both the storage duration capacities and the ratio of thermal energy charge rate to thermal energy discharge rate to simplify the analysis and to reduce computation times. The hot storage capacity is defined as 12 hours of TES discharge in this study (unless otherwise specified) because the inclusion of the hot storage unit increased the NPV of B31B in the most (12 of 14) market scenarios when 12 hours were used. However, it should be noted that different storage capacities are better suited for different market scenarios. For example, a 14-hour capacity is a more profitable option for some scenarios (see Figure 4- 5), but the NPV of B31B was only increased in 11 of 14 total scenarios when 14 hours were used. The cold storage capacity is defined as 2 hours in this study unless otherwise specified. Cold storage increases NPV in all market scenarios, so the 2-hour duration was selected because it yielded the highest average NPV. The energy transfer rates for both hot and cold TES are fixed to their nominal value so that the ratio of thermal energy charge to thermal energy discharge is set to unity. This decision was made to ensure that the exact technology introduced in section 3.3.2 was used throughout the entire analysis. Changing the ratio of thermal energy charged to thermal energy discharged alters the formulation of the outputs presented in Table 3- 9.

3.3.4 Optimization Model Economic and Performance Parameters

The parameters calculated by the optimization model that are used to inform the economics model are formulated in this section. The performance parameters include the hourly and annual power output, the hourly and annual fuel consumption, the hourly and annual CO_2 emissions, and the capacity factor. The power output, fuel consumption, and emissions at each time interval through the year are calculated using equations (3.98) through (3.100) respectively.

$$PO_j = PO_{BP,j} + DPI_{HST,j} + DPI_{CST,j} - CPD_{HST,j} - CPD_{CST,j} \quad (3.98)$$

$$FC_j = FC_{BP,j} + DFI_{CST,j} \quad (3.99)$$

$$E_j = FC_j * FTE * (1 - (ECP_{BP,j} - DCPD_{CST,j})) \quad (3.100)$$

The total annual power output, total annual fuel consumption, and total annual emissions are calculated by summing the individual values over all time intervals, as shown in equations (3.101) through (3.103) respectively.

$$TAP = \sum_{j=1}^{8760} PO_j \quad (3.101)$$

$$TAF = \sum_{j=1}^{8760} FC_j \quad (3.102)$$

$$TAE = \sum_{j=1}^{8760} E_j \quad (3.103)$$

The capacity factor is defined as the total annual power output divided by the maximum annual power output achievable by the base power plant and is calculated in equation (3.104).

$$CF = \frac{TAP}{PO_{BP} * 8760} \quad (3.104)$$

The economic parameters outputted by the optimization model include the total annual revenue, the total annual fuel costs, the total annual VOM costs, and the annual FOM costs. The total annual revenue was determined by summing the product of the power output with the corresponding electricity price over all years analyzed, as shown in equation (3.105).

$$TAR = \sum_{j=1}^{8760} PO_j * EP_j \quad (3.105)$$

The total annual fuel cost and total annual emissions cost were calculated in equations (3.106) and (3.107) respectively given the corresponding fuel and emissions prices

$$TAFC = TAF * FP \tag{3.106}$$

$$TAEC = TAE * ET \tag{3.107}$$

The total annual VOM costs were determined by summing the annual VOM costs of the NGCC, carbon capture unit, hot storage, and cold storage as shown in equation (3.108). As seen in the equation, the NGCC VOM costs scale the total annual base plant power output, the carbon capture COM costs scale the total CO_2 emissions, and the hot/cold storage VOM costs scales the total energy discharged from the storages.

$$TAVOMC = VOMC_{NGCC} * \sum_{j=0}^{8760} PO_{BP,j} + VOMC_{CC} * \sum_{j=0}^{8760} \dot{m}_{e,j} + VOMC_{HS} * PTE_{HS} * \sum_{j=0}^{8760} DPI_{HST,j} + VOMC_{CS} * PTE_{CS} * \sum_{j=0}^{8760} DPI_{CST,j} \tag{3.108}$$

The total annual FOM costs were determined by summing the annual FOM costs of the NGCC, carbon capture unit, hot storage, and cold storage as shown in equation (3.109).

$$AFOMC = FOMC_{NGCC} + FOMC_{CC} + FOMC_{HS} + FOMC_{HS} \tag{3.109}$$

The total capital costs were determined by summing the capital costs of the NGCC, carbon capture unit, hot storage technology, cold storage technology, hot storage medium, and cold storage medium, as shown in equation (3.110).

$$TCC = CC_{BP} + CC_{cc} + ECC_{HST} + ECC_{CST} + SCC_{HS} * SD_{HS} + SCC_{CS} * SD_{CS} \tag{3.110}$$

3.5 Economics Model

The optimization simulates one year of power plant operation to keep consistent with the duration of the electricity profiles used. Therefore, a discounted cash flow approach is needed to complete the 30-year NPV analysis. Table 3- 11 presents the economic assumptions used in this

approach. A 3-year build period for the technologies occurs before the start of the 30-year plant operation. 20 percent of the plant capital costs is paid in equity during the build period. A loan amount is then calculated to pay of the remaining capital throughout the lifetime of the plant. The revenue, fuel costs, emissions costs, FOM costs, and VOM costs determined in the optimization model in the first year of operation are used to determine the cash flow for the remaining years.

Table 3- 11: Economic assumptions

Item	Value	Units	Source
Loan Interest Rate	5.0	%	[58]
Loan Term	30	Years	[58]
Financed Amount	80	%	[58]
Equity Amount	20	%	[58]
Construction Interest Rate	3.5	%	[58]
Construction Period	3.0	Years	[58]
Construction Build Rate	80, 10, 10	%	[58]
MACRS Depreciation	15	Years	[58]
Tax Rate (Federal and State)	25	%	[58]
Internal Rate of Return	10	%	[58]
Natural Gas Price Increase	3.5	%/year	[59]
Electricity Price Increase	2.2	%/year	[59]

Equation (3.111) is used to determine the discount factor for each year in the analysis given the internal rate of return specified in Table 3- 11.

$$DF_k = \frac{1}{(1+IRR)^k} \tag{3.111}$$

The non-discounted revenue and fuel costs during the first year of plant operation are equal to the total annual revenue and total annual fuel costs, as shown in equations (3.112) and (3.113) respectively.

$$REV_{k=1} = TAR \tag{3.112}$$

$$FC_{k=1} = TAF \tag{3.113}$$

The non-discounted revenue and fuel costs are determined for the remaining twenty-nine years using the estimated annual increase in revenue and fuel costs specified in Table 3- 11, and are calculated in equations (3.114) and (3.115) respectively.

$$REV_k = REV_{k-1}(1 + AECI) \tag{3.114}$$

$$FC_k = FC_{k-1}(1 + AFCI) \tag{3.115}$$

The non-discounted emissions costs, FOM costs, and VOM costs are set equal to the total annual emissions cost, the annual FOM cost, and the total annual VOM cost respectively for all 30 years of operation, as shown in equations (3.116) through (3.118).

$$EC_k = TAEC \tag{3.116}$$

$$FOMC_k = AFOMC \tag{3.117}$$

$$VOMC_k = TAVOMC \tag{3.118}$$

The discounted revenue, fuel cost, emissions cost, FOM cost, and VOM cost for the entire plant life are calculated using equations (3.119) through (3.123) respectively.

$$REV_{NPV} = \sum_{k=1}^{30} REV_k * DF_k \tag{3.119}$$

$$FC_{NPV} = \sum_{k=1}^{30} FC_k * DF_k \tag{3.120}$$

$$EC_{NPV} = \sum_{k=1}^{30} EC_k * DF_k \tag{3.121}$$

$$FOMC_{NPV} = \sum_{k=1}^{30} FOMC_k * DF_k \tag{3.122}$$

$$VOMC_{NPV} = \sum_{k=1}^{30} VOMC_k * DF_k \quad (3.123)$$

The total amount paid in equity is determined using equation (3.124) and the total interest paid during the construction period is determined using equation (3.125). The total capital cost contribution to NPV is assumed to be the sum of the equity and interest paid, as shown in equation (3.126).

$$EQ_{NPV} = TCC * EF * \sum_{k=-2}^{0} CBR_k * DF_k \quad (3.124)$$

$$INT_{NPV} = TCC * LF * CIR * \sum_{k=1}^{30} CBR_k * DF_k \quad (3.125)$$

$$CAP_{NPV} = EQ_{NPV} + INT_{NPV} \quad (3.126)$$

The annual non-discounted loan payment is determined using equation (3.127). The amount of loan principle is determined using equations (3.128) and (3.129). The discounted loan amount used for the NPV calculation is determined using equation (3.130).

$$LPMT = \frac{TCC*LIR*LF}{(1-LIR)^{-30}} \quad (3.127)$$

$$LPCP_{k=1} = LPMT * 30 \quad (3.128)$$

$$LPCP_k = LPCP_{k-1} - LPMT \quad (3.129)$$

$$LPMT_{NPV} = \sum_{k=1}^{30} LPMT * DF_k \quad (3.130)$$

The taxable income is determined using the annual non-discounted revenue and costs, as shown in equation (3.131). The tax paid contributing to the NPV calculation is determined using equation (3.132).

$$TI_k = REV_k - FC_k - EC_k - VOM_k - LIR * LPCP_k - MDR_k * TCC \quad (3.131)$$

$$TAX_{NPV} = TR * \sum_{k=1}^{30} TI_k * DF_k \quad (3.132)$$

The NPV is determined by subtracting each contributing discounted cost from the discounted revenue, as shown in equation (3.133).

$$NPV = REV_{NPV} - FC_{NPV} - EC_{NPV} - FOMC_{NPV} - VOMC_{NPV} - CAP_{NPV} - LPMT_{NPV} - TAX_{NPV} \quad (3.133)$$

3.6 Other Thermal Energy Storage Technologies

The resistance heating technology proposed in this research was not the only concept considered for charging the hot storage. Other concepts that were previously evaluated include extracting IP steam from the HRSG, heat pumping the flue gas waste heat, and operating a tiered vapor compression heat pump. Process flow diagrams of these configurations are shown in Figure 3- 12a, Figure 3- 12b, and Figure 3- 12c respectively, and they are included in this thesis only as a comparison to the resistive heating configuration. The IP steam extraction configuration separates some of the steam from the IP turbine (location 7 in Figure 3- 4) to condense inside pipes running through the hot storage, consequently heating the storage. The condensate exiting the hot storage is pumped and mixed with the HP water stream entering the HRSG (location 8 in Figure 3- 4). The IP steam extraction configuration can be used in combination with the cold storage vapor compression refrigeration cycle, presented in Figure 3- 8.

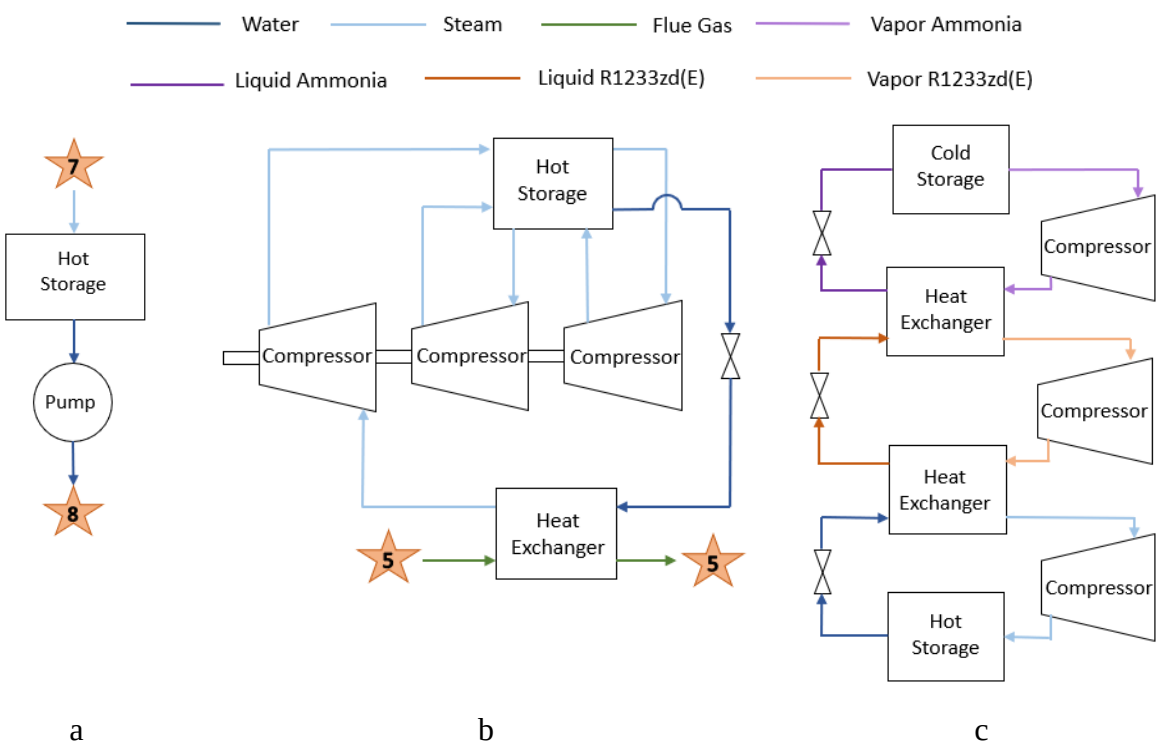

Figure 3- 12: Process flow diagrams of a) IP steam extraction b) Vapor compression heat pump using flue gas c) Tiered vapor compression heat pump

The heat pump utilizing flue gas routs the flue gas exiting the HRSG (location 5 in Figure 3- 4) through the heat exchanger before sending it to the carbon capture unit. Inside the heat exchanger, the heat from the flue gas is used to boil steam at a very low pressure. The steam exiting the HRSG is then compressed and routed through piping in the hot storage. This heats the storage while cooling the steam stream. The steam exiting the hot storage is then compressed and rerouted through the hot storage two more times. In the third pass, the steam is condensed inside the storage at a HP. The condensate exiting the hot storage is then throttled in a pressure reducing valve before re-entering the heat exchanger. The vapor compression heat pump using flue gas can also be used in combination with the cold storage vapor compression refrigeration cycle, presented in Figure 3- 8.

In the tiered vapor compression heat pump, ammonia is evaporated inside the cold storage, consequently cooling it off. The ammonia is compressed and then condensed inside the low temperature heat exchanger, transferring its heat to evaporate R1233zd(E), before being throttled and fed back into the cold storage. After evaporating, the R1233zd(E) is compressed and then condensed inside the high temperature heat exchanger, transferring heat to boil steam before being throttled for reentry to the low temperature heat exchanger. The steam is compressed and then condensed inside the hot storage, consequently heating the storage, before being rerouted to the high temperature heat exchanger. The tiered vapor compression heat pump simultaneously generates hot and cold storage.

Each component shown in Figure 3- 12 is modeled in the same way as similar components in the resistive heating and vapor compression cycles in Figure 3- 6 and Figure 3- 8. Each compressor shown in Figure 3- 12 is modeled using the same methods and assumptions as the compressor in Figure 3- 8a. Each throttling valve in Figure 3- 12 is also modeled using the same methods and assumptions as the valve in Figure 3- 8a. The heat exchangers are modeled using the same methods as the preheater in Figure 3- 6c. The pump is modeled in the same way as the pump in Figure 3- 6a. The hot and cold storages are modeled the same way in all configurations.

3.7 Ambient Temperature Considerations

Most of the research presented in this thesis has assumed that the ambient temperature remains at the design point condition of 15 °C at each time interval in order to simplify the results. However, in real climates, the power output of the base plant and the capability of the cold thermal energy storage technology changes with ambient temperature. To compare the constant ambient temperature assumptions to a more realistic temperature dependent analysis, the optimization model was made to input annual locational temperature data from the National Solar Radiation

Database [60], and the technology input parameters were adjusted for the ambient temperature at each time interval.

As discussed in section 2.3.2, the power output of the base plant increases with decreasing ambient temperature. However, the base plant turbines/generators are sized to allow a 10% increase in power production beyond the design point [16]. Without the use of thermal energy storage, the temperature dependent power output exceeds the 10% design point tolerance around freezing temperature (0°C). Therefore, the power output, fuel consumption, and carbon capture fraction are constrained for the base plant operation using equations (3.134), (3.135), and (3.136) respectively.

$$PO_{BP} \leq PO_{BP,0°C} \tag{3.134}$$

$$FC_{BP} \leq FC_{BP,0°C} \tag{3.135}$$

$$ECP_{BP} = ECP_{BP,15C} \frac{FC_{BP,15°C}}{FC_{BP}} \tag{3.136}$$

The use of the cold storage is also limited by the ambient temperature at each time interval. The inlet temperature to the gas turbine is constrained to be always above freezing temperatures when cold storage is in effect. This is necessary because inlet air is often cooled past the dew point, which causes the moisture in the air to condense. If the temperature is below freezing, sublimation can occur in the gas turbine, which is detrimental to the equipment. Although the temperature limitation (0°C) is the same for both generator sizing and sublimation reasons, the sublimation limitation imposes a more impactful constraint on the operation of the cold storage technology. The reason for this is that changes in inlet temperature due to cold storage discharge do not provide

as high of a power boost as changes in ambient temperature, because the cold storage also reduces the pressure of the inlet air while changes in ambient temperature do not.

The vapor compression cooling technology used to generate storage is sized to chill the inlet air of the power plant from 15°C to less than 1°C. Therefore, the power boost associated with cold storage discharge is limited for all temperatures less than 15°C. For temperatures less than 0°C, the cold storage is unusable. In these time intervals, the power reduction needed to charge the storage, the power increase gained from discharging the storage, the cold storage discharging fuel increase, and the decrease in the amount of CO_2 captured are all set to zero, as shown by equation (3.137).

$$IF\ (Tamb) \leq 0, \quad THEN \quad CPD_{CST} = 0,\ DPI_{CST} = 0,\ DFI_{CST} = 0,\ DCPD_{CST} = 0, \tag{3.137}$$

For temperatures between 0°C and 15°C, the cold storage is usable only at part load capacities. Operation in this temperature range is dependent on the cold limitation parameter (CLP), which is the defined as the maximum amount of cold storage discharge available for any given temperature, as shown in equation (3.138). The charging power decrease, discharging power increase, discharging fuel increase, and discharging capture percent decrease are calculated based on this parameter using equation (3.139).

$$CLP = PO_{BP,0°C} - PO_{BP,Tamb} \tag{3.138}$$

$$IF\ 0 < (Tamb) < 15°C, \quad THEN \quad CPD_{CST} = CPD_{CST,15°C}\frac{CLP}{DPI_{CST,15°C}},\ DPI_{CST} = CLP,$$

$$DFI_{CST} = CFI_{CST,15°C}\frac{CLP}{DPI_{CST,15°C}},\ DCPD_{CST} = DCPD_{CST,15°C}\frac{CLP}{DPI_{CST,15°C}} \tag{3.139}$$

For all temperatures greater than 15°C, full cold storage capabilities are available, and no limitations are placed on the characteristic parameters.

CHAPTER 4 Results and Discussion

The following sections present the results of the models created in the research and discuss the economic and performance characteristics that enable the proposed hot and cold TES configurations to be well suited for future electricity markets. Section 4.1 presents raw results from the technology model, then section 4.2 validates those results. Next, section 4.3 discusses the key characteristics of the electricity price profiles used in the research. Section 4.4 then discusses the NPV revenue and cost breakdown for a single electricity market scenario to speculate the economic effect of carbon capture and thermal storage on the base NGCC power plant. Next, section 4.5 discusses the specific roles that the hot and cold storages provide to the electricity grid and section 4.6 demonstrates the reason that electric resistance is more suited for future markets than other similar technologies. Section 4.7 summarizes the NPV results and concludes that TES helps make carbon capture more profitable. Finally, section 4.8 shows the implications of ambient temperature on TES profitability and concludes that cold storage remains beneficial in most real climates.

4.1 Technology Model Results

Table 4- 1 reports the component power production/consumption for the hot storage unit integration with the B31B base plant for each mode of operation. Positive values indicate a power is produced while negative values indicate power is consumed. All values in the neutral mode are identical to those calculated the B31B base plant components. The combustion turbine gross power output is equal to the sum of the gas compressor and gas turbine power outputs. The sum of the HP, IP, and LP turbine power outputs is equal to the gross steam turbine power output. The combustion turbine produces 70.5% of gross power while the steam turbines produce 29.5%. The operation of the pumps subtracts from the gross power output, though the pump power consumptions are small compared to the power production of the turbines. The auxiliary power

includes the CCS unit power consumption in addition to any other equipment used to enable power plant operation. The net power is the sum of all component power outputs.

Table 4- 1: Component power outputs of the base plant with the hot storage unit (MW)

Component	Neutral	Charging	Discharging
Gas Compressor	-490.08	0.00	-490.08
Gas Turbine	968.63	0.00	968.63
HP Turbine	48.74	0.00	48.74
IP Turbine	83.65	0.00	83.65
LP Turbine	67.79	0.00	116.95
HP Pump	-4.80	0.00	-4.80
IP Pump	-0.11	0.00	-0.11
Condensate Pump	-0.10	0.00	-0.18
Carbon Capture Pump	-0.03	0.00	0.00
Hot Storage Pump	0.00	0.00	0.01
Blower	0.00	-5.20	-3.93
Resistance Heater	0.00	-162.90	0.00
Auxiliary Power	-38.96	0.00	-38.96
Net Power	634.73	-168.11	679.92

The charging mode values in Table 4- 1 assume that the B31B base plant is offline, but these may be added to the neutral values if the TES unit is charged while the plant is running. The sum of the blower power and resistance heater power during the charging mode is equal to the total power reduction of the hot storage. The discharging mode values in Table 4- 1 are the same as the neutral mode values, with four exceptions. First, the discharging mode LP turbine power output is 49.16 MW higher than the neutral mode LP turbine power output since no steam extraction is required for use in the carbon capture unit during discharging mode. Second, the discharging condensate pump power is increased to accommodate a higher flowrate of condensate from the steam turbines. Third, the carbon capture pump is not operated because the hot storage

pump drives the condensate exiting the carbon capture unit instead. Fourth, the blower must be operated during discharging mode.

Table 4- 2 reports the component heat duties for the hot storage unit integration with the B31B base plant for each mode of operation. Again, the neutral values are identical to those of the B31B base plant. 1162.62 MW of heat are provided by natural gas the combustor which corresponds to a fuel flow rate of 29.51 kg/s. The HRSG heat duty is composed of the HP, IP, LP heat exchangers in addition to the IP reheater and LP economizer. Notably, the largest fraction of HRSG heat goes into boiling and superheating the HP steam because most of the feed water takes the high-pressure root through the HRSG. However, smaller fractions of the feedwater are boiled at lower pressures in the IPHX and LPHX to best use the lower grade heat at cooler locations in the HRSG. The total heat duty associated with steam condensation is the sum of the condenser and the reboiler. However, it should be noted that the steam condensation in the CCS unit occurs at a higher temperature and pressure than that of the condenser.

Table 4- 2: Component heat duties of the base plant with the hot storage unit (MW)

Component	Neutral	Charging	Discharging
Combustor	1162.62	0.00	1162.62
HPHX	363.75	0.00	363.75
IPHX	55.46	0.00	55.46
IPRH	65.39	0.00	65.39
LPHX	49.41	0.00	49.41
LPEC	49.79	0.00	49.79
HRSG	583.80	0.00	583.80
Preheater	0.00	0.00	34.13
Condenser	250.77	0.00	373.63
Hot Storage	0.00	168.10	168.10
Reboiler	172.03	0.00	172.03
Resistance Heater	0.00	162.90	0.00
HSSG	0.00	0.00	172.03

The charging column of Table 4- 2 shows that the resistance heater applies 162.90 MW of heat to the air, then the air heats the hot storage by 168.10 MW. The storage is heated by a higher duty than that of the resistance heater because the additional 5.20 MW of energy is supplied by the blower. The discharging component heat duties are identical to the neutral component heat duties with the addition of the preheater, hot storage, and HSSG. The preheater supplies 34.13 MW to the feedwater inlet to the HRSG to account for the difference in energy between the condenser outlet state and the CCS unit outlet state of the neutral mode (as discussed in section 2.3.2.1). The hot storage heats the air by 168.10 MW during discharge, then the air imparts 172.03 MW to the boiling steam in the HSSG. Again, the difference in duty of 3.93 MW is accounted for by the blower power during discharge.

Table 4- 3 reports the component power outputs of the base plant with the cold storage unit during each mode of operation. The neutral values are the same as those reported for the hot storage in Table 4- 1. The VC compressor consumes 6.21 MW to operate the cold storage unit during the charging mode and is the only component that consumes or produces power during charging. Unlike the hot storage unit, the cold storage unit alters most of the power outputs of the neutral mode during discharge. The magnitude of the gas compressor is decreased even though the mass flow rate is increased, because the air inlet pressure is decreased due to cold storage pressure drop, while the inlet temperature is decreased due to the cooling effect, and the pressure ratio is held constant. The gas turbine power output is increased because both the air and fuel flowrates have been increased. It should be noted that the fuel to air ratio is increased during discharge to ensure that the combustor temperature does not change. This means that while the temperature of the air entering the gas compressor during discharging is lower than the temperature during charging, the temperature of the air entering the gas turbine during discharging remains unchanged. The

magnitude of all steam turbines and pumps has also increased during discharge because of the increased feed water flowrates. The auxiliary power is unchanged primarily because almost all of the auxiliary power requirement is associated with the carbon capture unit, which is operated at design conditions for the entire time that the NGCC is online. The only power difference between the boosting mode and the discharging mode is that the compressor is operated during boosting, which subtracts from net power output.

Table 4- 3: Component power outputs of the base plant with the cold storage unit (MW)

Component	Neutral	Charging	Discharging	Boosting
Gas Compressor	-490.08	0.00	-483.30	-483.30
Gas Turbine	968.63	0.00	1001.49	1001.49
HP Turbine	48.74	0.00	50.95	50.95
IP Turbine	83.65	0.00	87.36	87.36
LP Turbine	67.79	0.00	72.88	72.88
HP Pump	-4.80	0.00	-5.02	-5.02
IP Pump	-0.11	0.00	-0.11	-0.11
Condensate Pump	-0.10	0.00	-0.19	-0.19
Carbon Capture Pump	-0.03	0.00	-0.03	-0.03
VC Compressor	0.00	-6.21	0.00	-6.21
Auxiliary Power	-38.96	0.00	-38.96	-38.96
Net Power	634.73	-6.21	681.13	674.94

Table 4- 4 reports the heat duties of the base plant with the cold storage components during each mode of operation. The neutral heat duties shown in Table 4- 4 are the same as those shown in Table 4- 2. The ammonia extracts 15.93 MW from the cold storage, then rejects 22.14 MW of heat to ambient in the cooling tower during charging mode. It should be noted that the cold storage heat duty is an order of magnitude less than the hot storage heat duty. This is why the selection of the low-cost resistive heating technology was needed the hot storage, where the higher cost vapor compression equipment is acceptable for the cold storage. The difference between these heat amounts is accounted for by the VC compressor. The discharging mode of the cold storage

increases all neutral mode heat duties except for the CCS reboiler. The combustor heat duty increases by 7.35% (corresponding to an increase in fuel consumption of 1.9 kg/s) while the remaining heat duties increase by around 4% depending on the component. The combustor heat duty increases by a higher percentage than the other component heat duties because the air enters the combustor at a cooler temperature during discharging than during neutral mode, but it is heated to the same combustor exit temperature. The other heat duties are only increased because of the increased in flue gas and steam flowrates. The reboiler duty remains unchanged between neutral and discharging modes because the carbon capture unit remains operated at design point conditions during discharge. The boosting mode heat duties are the same as the discharging mode heat duties with the addition of the cooling tower due to simultaneous cold storage charge and discharge.

Table 4- 4: Component heat duties of the power plant with the cold storage unit

Component	Neutral	Charging	Discharging	Boosting
Combustor	1162.62	0.00	1248.09	1248.09
HPHX	363.75	0.00	380.21	380.21
IPHX	55.46	0.00	57.55	57.55
IPRH	65.39	0.00	68.35	68.35
LPHX	49.41	0.00	51.27	51.27
LPEC	49.79	0.00	51.95	51.95
HRSG	583.80	0.00	609.33	609.33
Preheater	0.00	0.00	0.00	0.00
Condenser	250.77	0.00	261.73	261.73
Reboiler	172.03	0.00	172.03	172.03
Cold Storage	0.00	15.93	15.93	15.93
Cooling Tower	0.00	22.14	0.00	22.14

Table 4- 5 presents all cost parameters determined in the technology model. The cost of the base plants and CCS unit were extracted directly from NETL Case B31B. The differential generator cost accounts for the increase in capacity of the LP turbine, resulting from hot storage discharge. The preheater cost accounts for the increase in HRSG inlet temperature between neutral

and discharging modes. The hot storage equipment costs include the differential generator, preheater, hot storage, hot storage pump, blower, resistance heater, and HSSG. The total hot storage equipment cost is 38.33 MM$. The cold storage equipment costs include the cold storage, compressor, and cooling tower. The total cold storage equipment cost is 4.62 MM$. Notably, the sum of the hot and cold storage costs are only 3.4% of the total base plant and CCS costs. These costs were kept to a minimum to enable economic success.

Table 4- 5: Technology model cost parameters

Component	Cost
Base Plant	537.72
CCS Unit	743.60
Differential Generator	10.20
Preheater	4.46
Hot Storage	12.59
Cold Storage	2.28
Hot Storage Pump	0.01
Blower	2.05
Resistance Heater	6.52
HSSG	2.50
Compressor	1.30
Cooling Tower	1.04
Total	1325.26

4.2 Technology Model Validation

The primary validation method used in this research is to demonstrate that the base plant and TES unit models are consistent with the first and second laws of thermodynamics. This is accomplished by presenting detailed process flow diagrams with all thermodynamic state points labeled in addition to the power and heat flows of all power plant and TES unit components included in the diagrams. Appendix A.1 consists of the supplemental information for the B31A and B31B base power plants where Figure A- 1 shows the B31A process flow diagram, Table A-

1 reports B31A component power, Table A- 2 reports B31A component heat duty, Figure A- 2 shows the B31B process flow diagram, Table A- 3 reports B31B component power, and Table A- 4 reports B31B component heat duty. Appendix A.2 consists of the supplemental information for the Hot Storage Unit where Figure A- 3 shows the charging process flow diagram, Figure A- 4 shows the discharging process flow diagram, Table A- 5 reports the component power, and Table A- 6 reports the component heat duty. Appendix A.3 consists of the supplemental information for the Cold Storage Unit where Figure A- 5 shows the charging process flow diagram, Figure A- 6 shows the discharging process flow diagram, Figure A- 7 shows the boosting process flow diagram, Table A- 7 reports the component power, and Table A- 8 reports the component heat duty. Appendix A.4 consists of the supplemental information for the simultaneous operation of the storage units where Figure A- 8 shows the combined charging process flow diagram, Figure A- 9 shows the combined discharging process flow diagram, Table A- 9 reports the combined power output, and Table A- 10 reports the combined heat duty.

Table 4- 6: Comparison between reported and calculated base plant parameters

Component	Reported B31A (MW)	Calculated B31A (MW)	Reported B31B (MW)	Calculated B31B (MW)
Combustion Turbine Net	477.00	478.56	477.00	478.56
HP Turbine	55.48	48.79	55.53	48.74
IP Turbine	86.63	83.71	86.51	83.65
LP Turbine	120.89	117.05	70.96	67.79
Feed Water Pumps	4.83	4.94	4.83	4.80
Condensate Pumps	0.15	0.18	0.17	0.13
Combustor (HHV)	1355.00	1355.00	1355.00	1355.00
HRSG	636.90	618.39	603.90	583.80
Condenser	390.60	373.90	219.70	250.80
Net Power Output	727.00	714.10	646.00	634.70

It should be noted that the B31A and B31B base plant models formulated in this research are simplified versions of those reported by NETL. They were simplified for ease of use and

integration with the thermal energy storage units. To validate the accuracy of the models, the primary power outputs and heat rates are compared to those reported by NETL in Table 4- 6. It should be noted that all calculated values in Table 4- 6 are close to the corresponding reported value. The largest difference in values occurs between the steam turbine power outputs and the HRSG heat transfer, but this only results in a calculated net power outputs 1.7-1.8% lower than reported net power outputs.

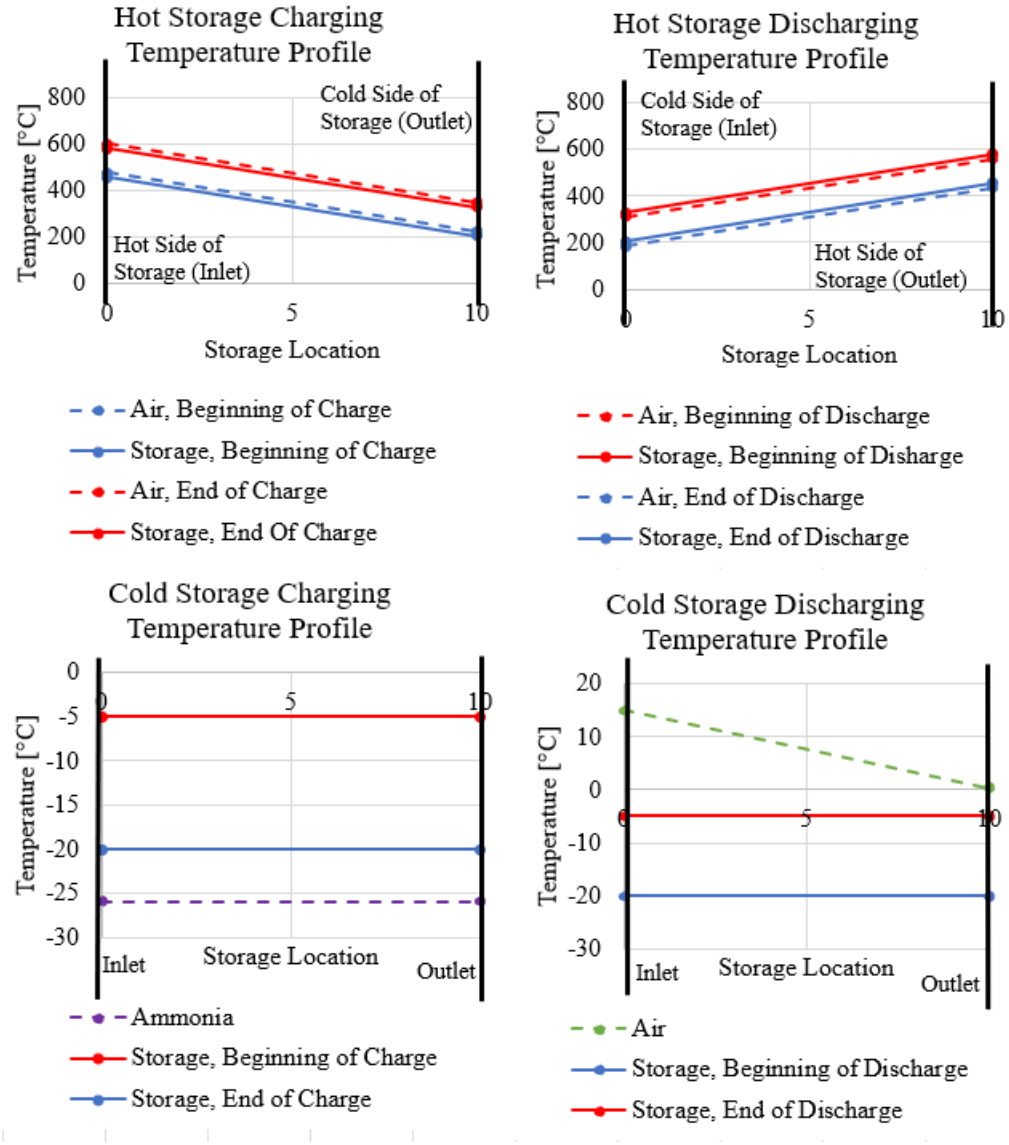

Figure 4- 1: Charging and discharging temperature profiles of the hot and cold storages

In the current study, the charging and discharging modes of the storage units are modeled as steady state processes. However, the storage mediums change temperature throughout charging and discharging. This temperature change has been accounted for in the modeling approach by considering only the limiting scenarios for heat transfer. This means that charging has been modeled at the very end of the charge periods when the hot storage medium has already been heated to its maximum temperature and the cold storage medium has already been cooled to its minimum temperature. Similarly, discharging is modeled at the very end of the discharge periods when the hot storage medium is at its minimum temperature and the cold storage medium is at its maximum temperature. This modeling approach allows for the appropriate temperature fluctuation of the storages, as is illustrated by Figure 4- 1a and b for the hot storage and cold storage respectively.

4.3 Electricity Market Scenarios

The economic feasibility of the proposed technology is extremely dependent on the electricity market scenarios used in the research. Since the proposed technologies use electricity arbitrage to increase their revenue, a high amount of variability in electricity price signal is crucial to economic success. The market scenarios introduced in Table 3- 10 include the hourly electricity market prices needed to enable the operation of the lowest cost mix of generators under a variety of expected future technologies and policies. Figure 4- 2 and Figure 4- 3 show the concentration of electricity prices in each price range with a $10 per MWh granularity for the GenX and ReEDS market scenarios respectively.

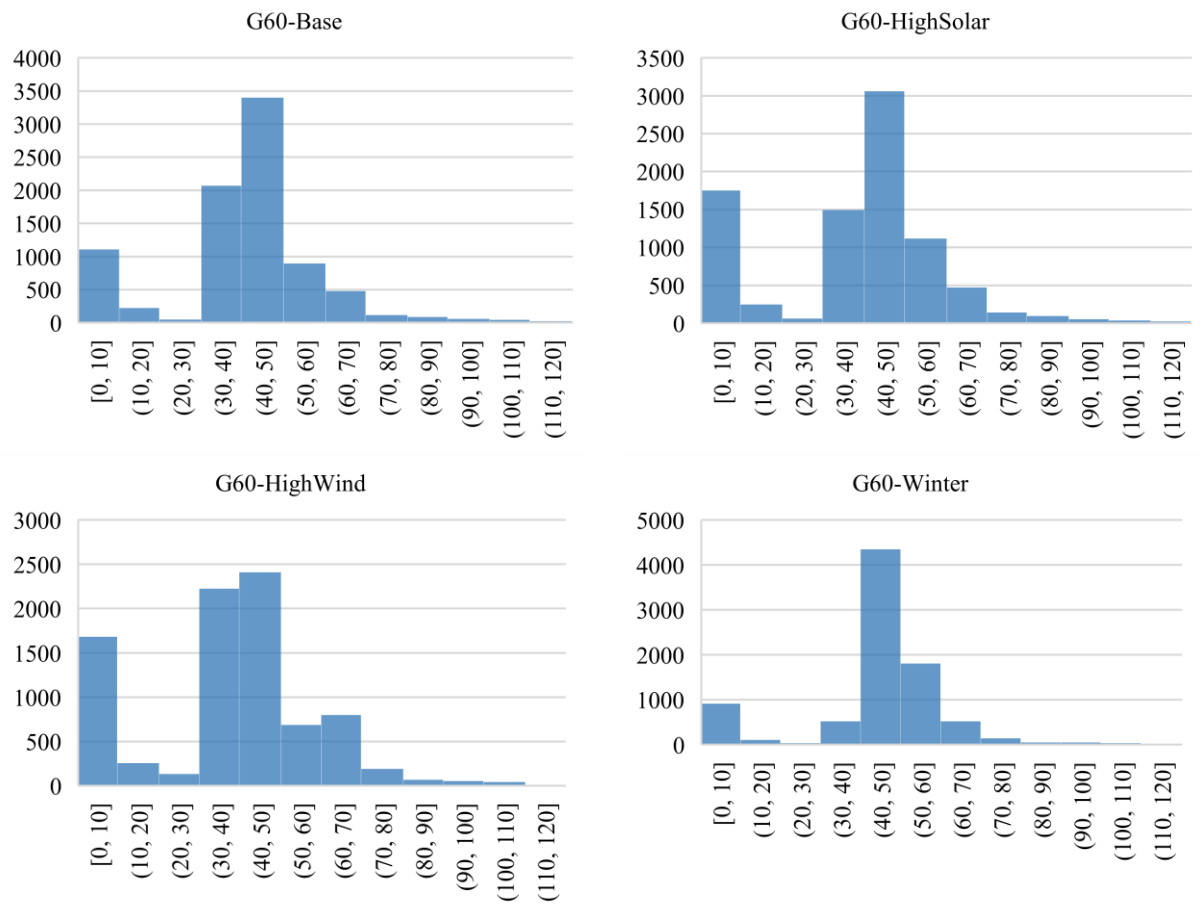

Figure 4- 2: Electricity price concentration for the GenX market scenarios

The four GenX profiles in Figure 4- 2 all show a high frequency of mid-range prices ($40-50 per MWh) across all scenarios. This is the range of prices that causes the difference between the revenue and the operation costs of the primary load following generators (such as natural gas power plants) to be high enough to motivate the operation of those technologies. These market scenarios also have a high frequency of very low prices ($0-10 per MWh), especially for the scenarios with high renewable generation. There are two reasons for this. First, the renewable generators have minimal operating costs, so very low prices are sufficient to justify power production. Second, during periods of high renewable resource availability, there is an access of electricity available, which causes the electricity price to be zero. It should also be noted from Figure 4- 2 that there is a very low frequency of prices between $10 and $30 per MWh. This is

because this range is too low to motivate the non-renewable resource power plants and higher than the prices required to motivate wind and solar operation.

The price concentrations of the 10 electricity profiles generated by ReEDS are shown in Figure 4- 3. ReEDS evaluated the electricity markets based on carbon taxes of $100 per tonne and $150 per tonne where GenX evaluated carbon taxes at $60 per tonne. This difference in CO_2 taxes has some interesting implications on the nature of the price profiles. First, the concentration of prices in the $0-10 per MWh range is higher for higher CO_2 taxes. This concentration was 10-20% for the $60 per tonne GenX prices, but is 31-55% and 36-67% for the $100 per tonne and $150 per tonne ReEDS prices respectively. The increase is explicable because higher CO_2 taxes motivate higher deployment of carbon free renewable energy, which results in a higher frequency of time periods that have an excess of grid electricity. Second, higher CO_2 taxes require higher prices to motivate the load following technologies. For the $60 per tonne GenX profiles, there was a high frequency of prices in the $40-50 per ton range. For the ReEDS $100 per tonne and $150 per tonne scenarios, a significant fraction of the prices are in the $60-100 per MWh and $90-150 per MWh ranges respectively. There are two explanations for the shift in electricity price. The first is that the operating costs of the fossil fuel load following technologies increases with CO_2 tax. Therefore, plant operation requires higher electricity prices to be profitable. The second reason is that the increased concentration of near zero prices decreases the capacity factor of the load following generators. Higher electricity prices are required to economically justify building new technologies that operate infrequently.

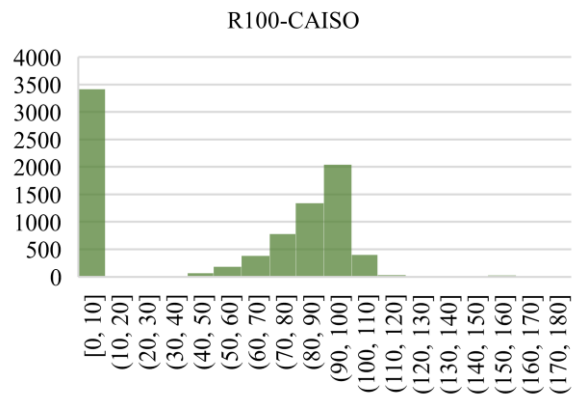
R100-CAISO
4000
3500
3000
2500
2000
1500
1000
500
0
[0, 10]
(10, 20]
(20, 30]
(30, 40]
(40, 50]
(50, 60]
(60, 70]
(70, 80]
(80, 90]
(90, 100]
(100, 110]
(110, 120]
(120, 130]
(130, 140]
(140, 150]
(150, 160]
(160, 170]
(170, 180]

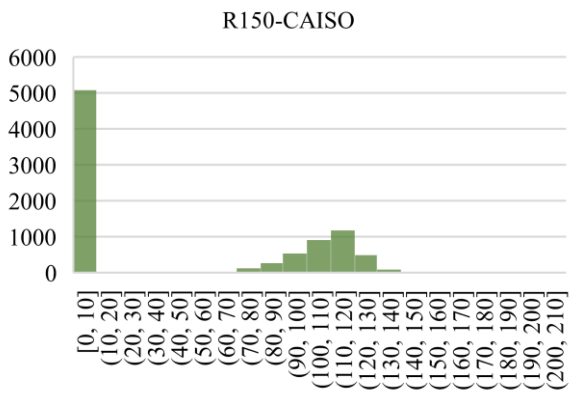
R150-CAISO
6000
5000
4000
3000
2000
1000
0
[0, 10]
(10, 20]
(20, 30]
(30, 40]
(40, 50]
(50, 60]
(60, 70]
(70, 80]
(80, 90]
(90, 100]
(100, 110]
(110, 120]
(120, 130]
(130, 140]
(140, 150]
(150, 160]
(160, 170]
(170, 180]
(180, 190]
(190, 200]
(200, 210]

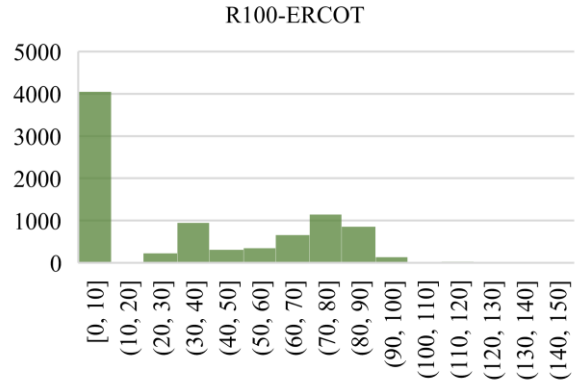
R100-ERCOT
5000
4000
3000
2000
1000
0
[0, 10]
(10, 20]
(20, 30]
(30, 40]
(40, 50]
(50, 60]
(60, 70]
(70, 80]
(80, 90]
(90, 100]
(100, 110]
(110, 120]
(120, 130]
(130, 140]
(140, 150]

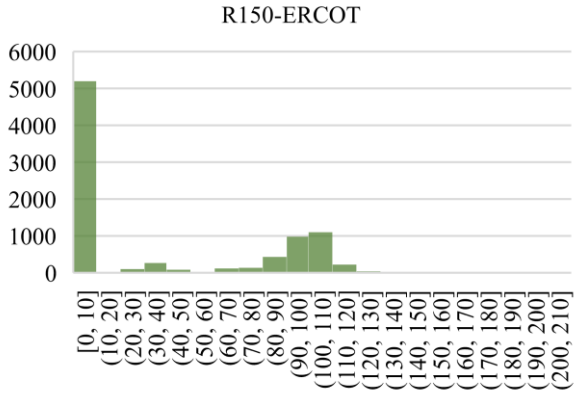
R150-ERCOT
6000
5000
4000
3000
2000
1000
0
[0, 10]
(10, 20]
(20, 30]
(30, 40]
(40, 50]
(50, 60]
(60, 70]
(70, 80]
(80, 90]
(90, 100]
(100, 110]
(110, 120]
(120, 130]
(130, 140]
(140, 150]
(150, 160]
(160, 170]
(170, 180]
(180, 190]
(190, 200]
(200, 210]

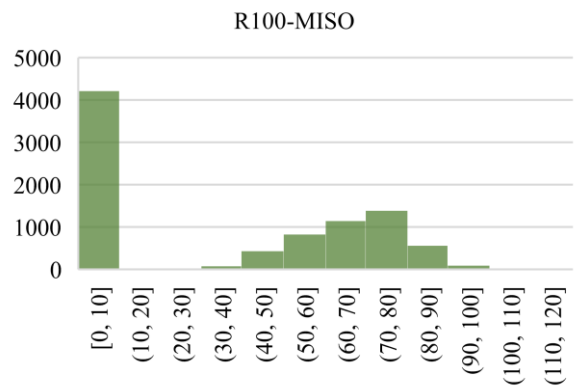
R100-MISO
5000
4000
3000
2000
1000
0
[0, 10]
(10, 20]
(20, 30]
(30, 40]
(40, 50]
(50, 60]
(60, 70]
(70, 80]
(80, 90]
(90, 100]
(100, 110]
(110, 120]

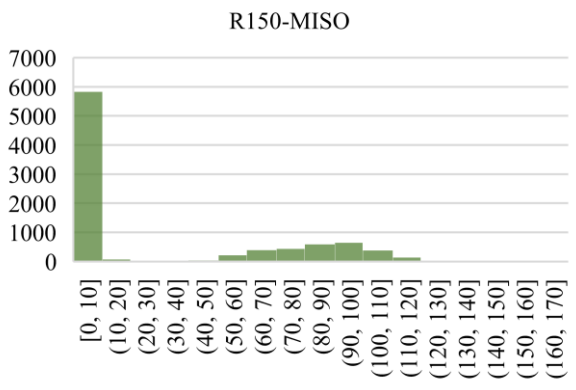
R150-MISO
7000
6000
5000
4000
3000
2000
1000
0
[0, 10]
(10, 20]
(20, 30]
(30, 40]
(40, 50]
(50, 60]
(60, 70]
(70, 80]
(80, 90]
(90, 100]
(100, 110]
(110, 120]
(120, 130]
(130, 140]
(140, 150]
(150, 160]
(160, 170]

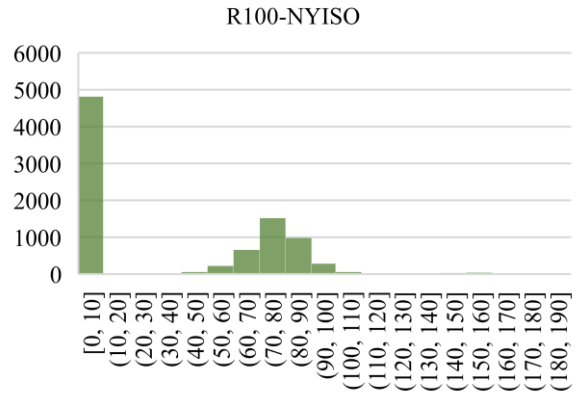
R100-NYISO
6000
5000
4000
3000
2000
1000
0
[0, 10]
(10, 20]
(20, 30]
(30, 40]
(40, 50]
(50, 60]
(60, 70]
(70, 80]
(80, 90]
(90, 100]
(100, 110]
(110, 120]
(120, 130]
(130, 140]
(140, 150]
(150, 160]
(160, 170]
(170, 180]
(180, 190]

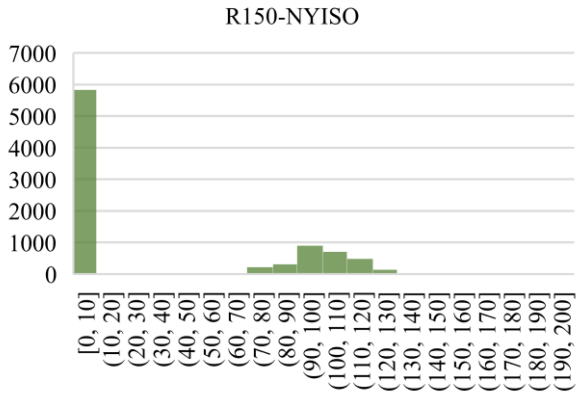
R150-NYISO
7000
6000
5000
4000
3000
2000
1000
0
[0, 10]
(10, 20]
(20, 30]
(30, 40]
(40, 50]
(50, 60]
(60, 70]
(70, 80]
(80, 90]
(90, 100]
(100, 110]
(110, 120]
(120, 130]
(130, 140]
(140, 150]
(150, 160]
(160, 170]
(170, 180]
(180, 190]
(190, 200]

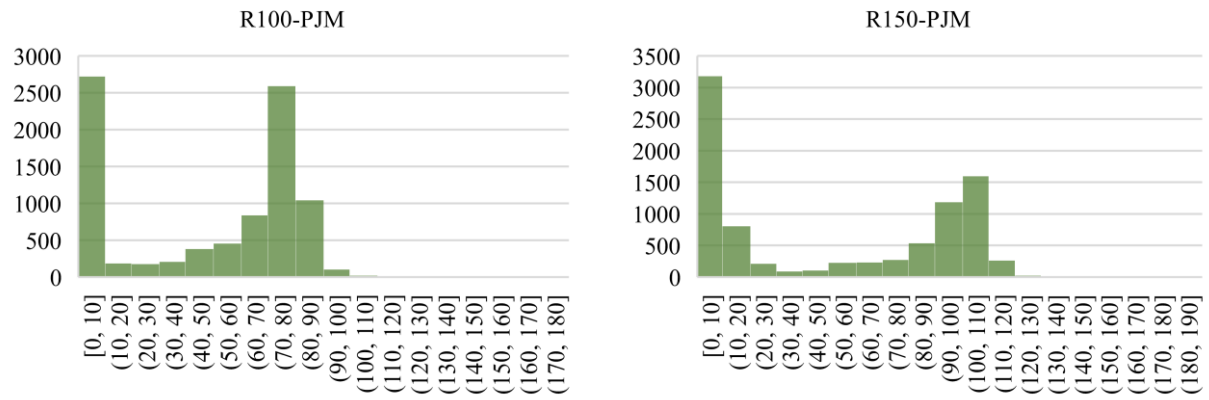

Figure 4- 3: Electricity price concentration for the ReEDS market scenarios

4.4 NPV Revenue/Cost Makeup

Figure 4- 4 shows the revenue (electricity sales) vs plant costs that contribute to the NPV of each analyzed power plant configuration for the R150-CAISO market scenario. R150-CAISO was selected for this discussion for two reasons. First, the impact of TES on the NPV of the B31B base plant in the R150-CAISO scenario is representative of the impact of TES in most of the other scenarios. Second, R150-CAISO yields an NPV of B31B that is higher than the NPV of B31A, which indicates that carbon capture is financially feasible. While this is not the case for every scenario analyzed in research, it is important to show results for a scenario in which carbon capture is likely to be implemented. The revenue vs cost breakdowns for all other scenarios are included in Appendix A.3.

In Figure 4- 4, the NPV of each configuration (each power plant type on the horizontal axis) is equal to the difference between the electricity sales and the sum of the costs. By comparing the cost/revenue breakdown of B31A to B31B, the impact of carbon capture on plant economics can be extracted. It can be seen in Figure 4- 4 that the electricity sales from B31A are $320 million higher than those of B31B while the fuel costs are $20 million lower. This is the result of the

efficiency and maximum power penalty imposed by the CCS unit. Furthermore, B31B has much higher capital, loan, tax, FOM, and VOM costs due to the additional technology required for carbon capture. On the other hand, the 150 $/tonne carbon tax imposes a staggeringly high emissions cost on B31A that is $1230 million higher than that of B31B. This has outweighed the effect of the decreased electricity sales and increased equipment costs. The result is the NPV of B31B is $60 million higher than that of B31A for the R150-CAISO scenario.

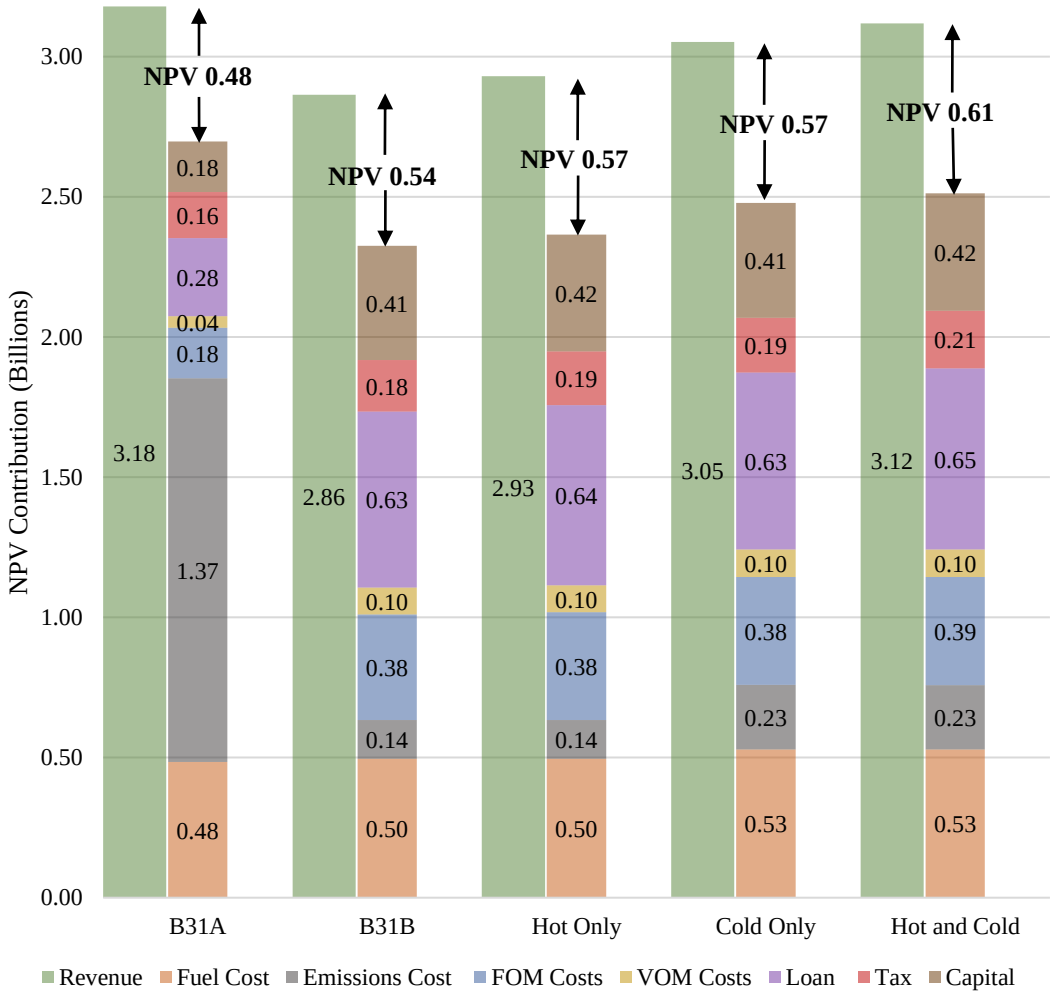

Figure 4- 4: Electricity sales and component cost makeup of the net present value calculation for the R150-CAISO electricity market scenario

The comparison between B31A and B31B also provides important insight to the nature of the R150-CASIO market scenario. The similar fuel costs in Figure 4- 4 between B31A and B31B are indicative of similar capacity factors. For this scenario, the capacity factor of B31A is 41% and the capacity factor of B31B is 42%. The closeness of the capacity factors is counter intuitive because the inclusion of the emissions tax necessitates a higher electricity price to for B31A to come online. B31A requires the electricity price to be at least $74 per MWh to come online while B31B only needs an electricity price of $27 per MWh to come online. For an even spread of electricity prices, this difference would indicate a significantly lower capacity factor for B31A than for B31B. However, as shown in Figure 4- 3 and described in section 4.3, the spread of electricity prices in R150-CAISO is not even, and the prices jump from lower than $27 per MWh to higher than $74 per MWh with a low frequency (87 of 8760 hours) of prices in between.

The impact of the individual hot and cold TES units on plant economics can also be extracted from Figure 4- 4 by comparing the hot only and cold only cost/revenue breakdowns to that of the B31B base plant. For the hot only configuration, the operation of the base power plant is identical to B31B. Since the hot storage technology does not require an increase in fuel consumption to discharge, its fuel and emissions costs are also the same as the corresponding B31B values. The inclusion of the hot storage technology does add modest additional capital, FOM, and VOM expenses, but these expenses are less than the increase in revenue due to the electricity arbitrage capabilities of the technology. Also, Figure 4- 4 reveals the advantages that the resistively heated TES method has over other previously examined flexible CCS methods such as bypass and solvent storage. Bypass methods turn off the capture unit to increase power output. While this increases plant revenue, it also increases emissions cost by a factor of 10 when the capture unit is bypassed. Figure 4- 4 suggests that this would be very detrimental to NPV. This conclusion is

supported by Oates et al. [30], who determined that bypass was not a viable option under emissions policies significant enough to economically motivate carbon capture. Previously examined solvent storage methods require either a higher capacity carbon capture solvent regenerator (which significantly increases capital and loan costs) [30,32], or a decrease in annual power production (which decreases revenue) if the CCS unit is to be operated at full capacity [30]. Therefore, Oates et al. concluded that solvent storage is not a viable option either in electricity market scenarios that motivate carbon capture. On the other hand, Figure 4- 4 shows that the resistively heated TES only adds minimal increases to the capital and loan costs, while retaining the increase in revenue.

The performance of the cold only configuration is different than the performance of the hot only configuration because fuel consumption is increased, and CO2 capture percent is decreased during thermal storage discharge and boosting operations. However, it should be noted that the amount of CO2 emitted only increases by a factor of 1.7 when cold storage is in use comparted to an increase by a factor of 10 associated with bypassing the CCS unit. Still, it can be observed in Figure 4- 4 that the fuel and emissions costs for the cold only configuration are higher than the fuel and emissions costs of the B31B and hot only configurations. The cold TES unit requires less addition capital, FOM, and VOM costs than the hot TES unit, since the cold storage thermal capacity is less than that of the hot storage (as described in section 4.1). In the end, the increase in revenue due to the arbitrage and boosting capabilities of the cold storage configuration outweighs the increase in costs, so the NPV of the cold only configuration is higher than the NPV of the B31B base plant. It should be noted that the market scenarios used in this research are better suited for the use of cold storage and inlet chilling than those that currently exists. The reason for this is inlet chilling is only useful when the power plant is operated at full capacity, but most existing NGCC power plants are used to follow load when they are at partial capacity [45]. However, Figure 4- 3

suggests that many the electricity price scenarios evaluated in this study have a more binary approach where the price is often either very low or very high. Therefore, the most profitable way to operate the power plant is to run at full capacity with inlet chilling whenever the price is very high. Additionally, the binary nature of the prices can have a higher potential for cold storage arbitrage than current pricing structures because storage can be generated at cheaper prices.

4.5 Roles of the Hot and Cold Storage Technologies

Both hot and cold storage technologies can take advantage of electricity arbitrage and their operation is motivated by the same electricity price profile. However, there is a clear difference in their optimal uses. Figure 4- 5 shows the NPV difference from the B31B base plant for a range of storage capacities for a) the hot storage technology and b) the cold storage technology. Included in each box and whisker plot are all the electricity market scenarios outlined in Table 3- 10. It can be seen from the figure that longer storage capacities (10+ hours) are clearly better than shorter storage capacities for the hot storage technology while cold storage capacity does not have a clear impact on NPV. These results suggest that the hot storage is best used for long periods of charge and discharge to mirror longer periods of high and low renewable resource availability while the cold storage is primarily used to increase the capacity of the plant and for short duration arbitrage to account for spikes in electricity prices.

The difference in optimal uses can be explained by a couple key differences in the technology. First, the hot storage is cheaper than the cold storage per energy stored, as described in section 2.3.2.2. Second, the hot and cold storage technologies have very different electrical charge to discharge efficiencies. The hot storage unit requires roughly four times as much electricity to charge TES than the energy produced by discharging TES while the cold storage unit produces nearly nine times more electricity during discharge than it requires to charge (albeit the

fuel consumption and emissions are increased during cold TES discharge). Because most of the power increase due to cold storage discharge can be accomplished by the boosting mode, Figure 4- 5b shows that increases in NPV are achievable without any cold storage capacity. In addition, increases in revenue due to increased cold storage capacity are largely balanced by the increased cost of the storage medium. Still, the average NPV increase occurs when a 2-hour capacity is utilized, so cold storage arbitrage still has a positive economic impact.

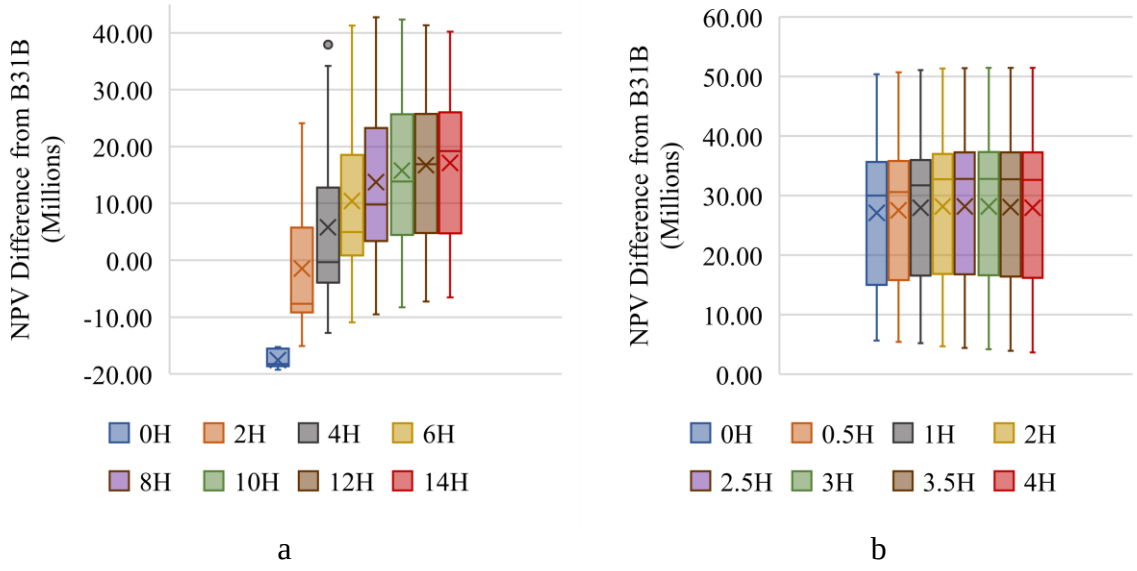

Figure 4- 5: NPV difference from case B31B over a range of storage durations for a) the hot storage only configuration and b) the cold storage only configuration

The different roles of the hot and cold storage technologies are also reflected by the capacity factors of the configurations. Figure 4- 6 shows the capacity factor of each configuration where all market scenarios are included in each box and whiskers plot. The average capacity factors across all electricity market scenarios of the B31B configuration, hot storage configuration, and cold storage configuration are 57%, 55%, and 60% respectively. The inclusion of the hot storage decreases capacity factor because it requires significantly more electricity to charge than

it provides during discharge. This means that the revenue boost comes only from its low-cost electricity arbitrage capabilities. The inclusion of the cold storage configuration increases the B31B capacity factor because it can discharge much more electricity than it requires to charge at the expense of increased fuel consumption. When both hot and cold storage technologies are deployed, the capacity factor is 57%, which implies that the effect that each technology has on capacity factor is balanced out. It should be noted that the capacity factors are calculated using net power output to the grid. For most of the time that the hot storage is being charged, the power plant is not running, so the net power output is negative and the capacity factor is reduced. In other words, the calculated capacity factors are not reflective of the amount that the technologies are being used, instead lower capacity factors indicate use of technologies that require more electricity to charge than produced during discharge while higher capacity factors indicate more electricity is produced during discharge than required to charge. It should also be noted that TES use has no effect on the operation of the base plant, so differences in the capacity factor are only dependent on the nature of the storage technologies.

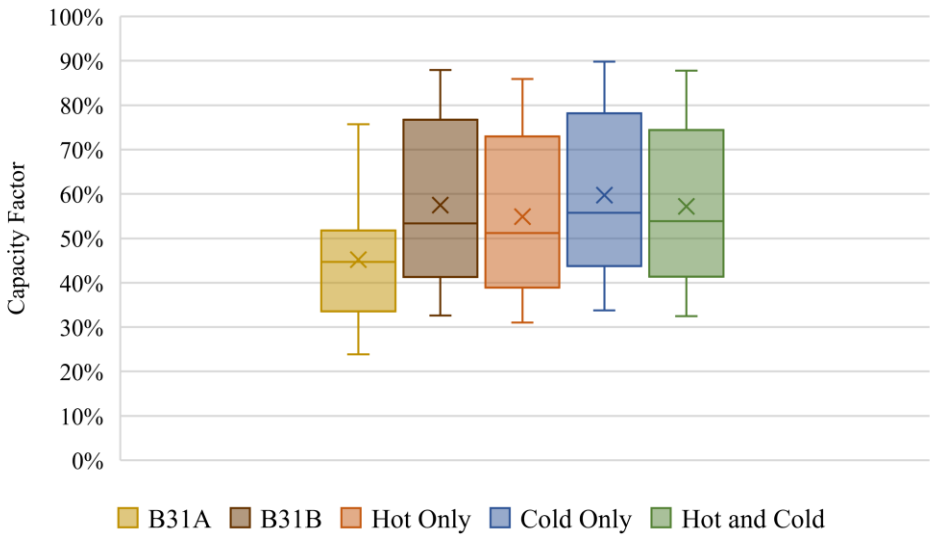

Figure 4- 6: Capacity factors of the base plants and TES units

4.6 Novelty of Resistive Heating

It is well known that resistive heating technologies are much less efficient than other forms of creating heat. In this context, it would be more efficient to use either a vapor compression heat pump to generate heat for the hot storage or to simply extract and store existing heat from the power plant (via steam or flue gas removal from the HRSG). Such techniques have also been considered in this thesis, and as introduced in section 3.6, include the IP steam extraction, the vapor compression heat pump using flue gas, and the tiered vapor compression heat pump configurations. These configurations were analyzed under the same electricity market scenarios as the resistive heating configuration. Figure 4- 7 compares the NPV difference from B31B of these technologies to those of the resistive heating configuration where all market scenarios are included in each box and whiskers plot.

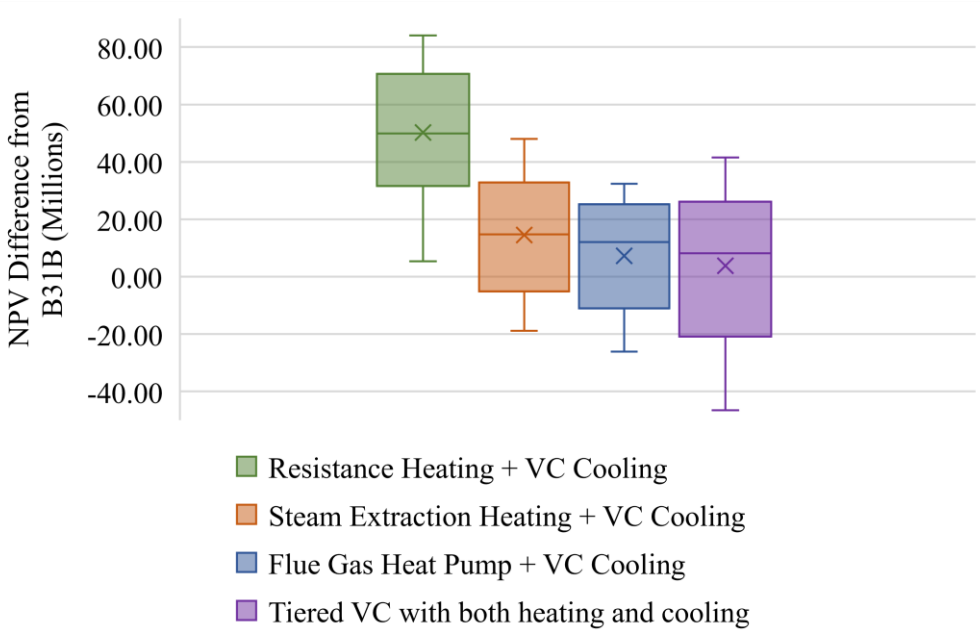

Figure 4- 7: Economic comparison of the resistive heating technology to previously examined concepts

The resistance heating with VC cooling technology yielded a higher NPV for every market scenario by a large margin. The total average NPVs of the steam extraction flue gas heat pump, and tiered VC technologies were 16.90%, 20.34%, and 22.00% lower than the current resistively heated configuration. The steam extraction and flue gas heat pump technologies performed worse than the resistive heating technology primarily because the power plant must be operating to charge the storages. This is a highly detrimental characteristic because 54.82% of the electricity price points analyzed are not high enough to motivate the operation of the base plant. Therefore, charging these thermal storage mediums requires that either the power plant operate at times when the sum of the operating expenses is higher than the revenue from electricity sales, or the power plant suffers a decrease in output due to thermal storage charge during times when its desirable to sell as much electricity as possible. Furthermore, charging the storage while running the plant does not enable the technology to remove grid congestion from high levels of renewable energy output. The tiered vapor compression configuration does enable the thermal storage to charge independently of plant operation, however the high costs of the large heat pump technology outweigh the benefit of having a higher efficiency than resistive heating.

The results also indicate that poor efficiency of the resistive heating does not have much of an impact on plant economics because hot storage charging periods happen at times of extremely low prices. Table 4- 7 shows the equivalent electrical power required for thermal storage charging and discharging, the average price in which the operation model chooses to operate each mode, and the electricity cost or sales during one hour of operation at that price level. It can be seen from the table that, as mentioned in section 4.5, it takes roughly four times as much electricity to charge the storage than to discharge it. This is indicative of the poor efficiency of resistive heating. However, the average electricity selling price is roughly sixty-three times higher than the price at

which electricity is purchased to charge the storage. The result is that the technology generates seventeen times more revenue from discharging the storage than it costs to charge the storage. In other words, the electricity purchased to charge the storage is very nearly free, so it is not important to achieve high efficiencies because the economic penalty associated with high charging power is very low.

Table 4- 7: Storage charging and discharging equivalent power output, average electricity price, and average electricity costs/sales

	Storage Equivalent Power (MW)	Average Electricity Price ($/MWh)	Average Electricity Cost/Sales ($/hr)
Charging	168.10	1.50	252.15
Discharging	45.19	93.86	4241.53

4.7 NPV Comparison

Figure 4- 8 presents the difference in NPV from the B31B base plant for the hot only configuration, cold only configuration, and hot & cold combination configuration for each market scenario considered. The hot only configuration yields higher NPVs than B31B in 12 of 14 analyzed scenarios, while the cold only configuration yield higher NPVs for all 14 grid scenarios. A combination of both thermal storage technologies is largely the most profitable option as it yields the highest NPV in all but one scenario. These results indicate that it is financially feasible to incorporate both hot and cold technologies into carbon capturing power plants.

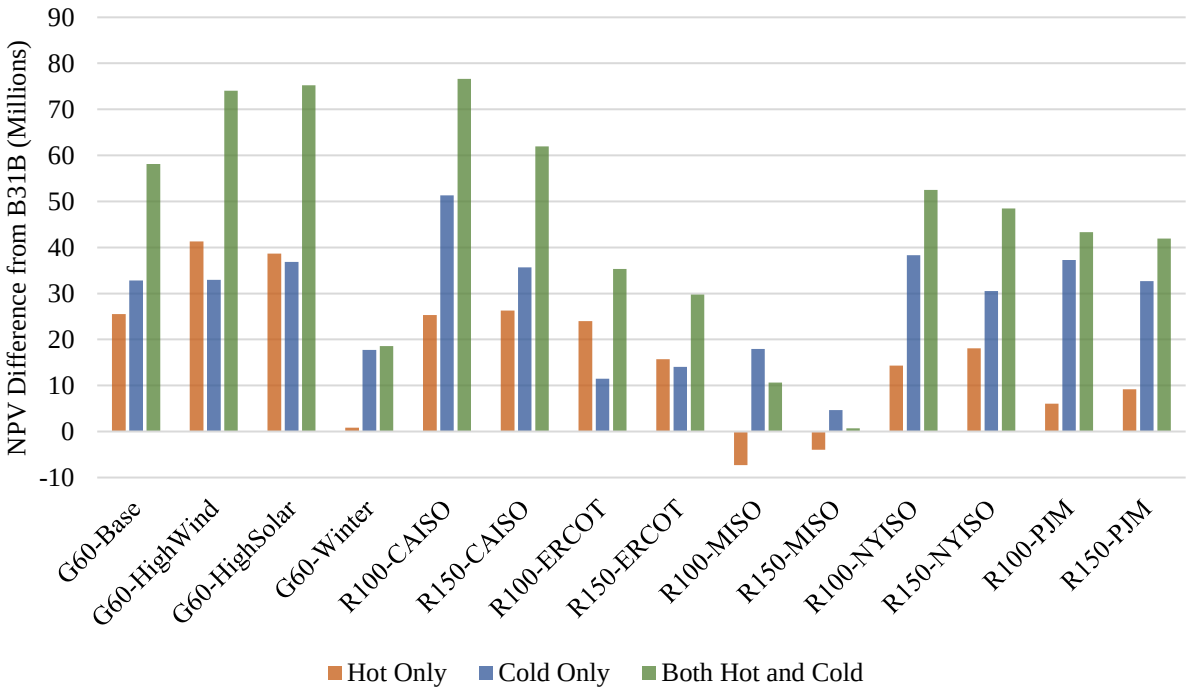

Figure 4- 8: NPV difference from B31B for the hot only, cold only, and combined configurations for all market scenarios

It should be noted that while a combination of hot and cold TES is an economical option for the B31B power plant in all market scenarios examined, carbon capture itself is not economically justified in every scenario. In this study, we define a market scenario to be sufficient to economically motivate carbon capture if the NPV of a given carbon capturing power plant is greater than the NPV of B31A. Table 4- 8 shows the NPV of B31A, B31B, and B31B plus both hot and cold TES units for each market scenario. There are only three market scenarios in which the B31B configuration yields a higher NPV than the B31A configuration: R150-CAISO, R100-PJM, and R150-PJM. B31A is a more profitable option than B31B in the remaining eleven market scenarios because its capital costs and loan payments are less than half of the B31B costs (see Figure A- 10 for cost breakdowns of each scenario) while its fuel efficiency is higher than that of B31B because there is no parasitic power draw from the CCS unit. In these scenarios, the B31A

emissions costs are not a significant enough penalty to overcome the effect of having a lower cost and higher efficiency than B31B. If TES is not used, either more severe emissions policies, or a lower cost/higher efficiency CCS unit is required to motivate carbon capture in these eleven scenarios. However, Table 4- 8 shows there are two scenarios (R100-CAISO and R150-ERCOT) where the NPV of the configuration utilizing both hot and cold TES units is greater than the NPV of B31A, even though the NPV of B31B is less than that of B31A. Therefore, while there are only three market scenarios that motivate carbon capture without TES, there are five market scenarios that motivate carbon capture when TES is utilized. This result suggests that TES can help make carbon capture more feasible.

Table 4- 8 also provides an important comparison between the economics of a power plant with and without carbon capture over a variety of carbon taxes. The table shows that market scenarios with low ($60 per tonne) carbon taxes yield positive NPVs for B31A, but negative NPVs B31B. However, in market scenarios where the NPV of B31A is negative, the NPV of B31B is also negative. Moreover, market scenarios with higher carbon taxes ($100 or $150 per tonne) that yield positive NPVs for B31A, also yield positive NPVs for B31B. These observations support the notion that higher carbon taxes are better suited for carbon capturing power plants, but they also suggest that utilizing a more cost-effective carbon capture technology could have a significant impact on the feasibility of CCS. A potential area for future research is to combine the economically advantageous TES technologies presented in this study with a lower cost/higher efficiency CCS technology suite such as the one offered by ION Clean Energy, which could potentially increase the concentration of captured CO2 to greater than 90%, while reducing the capital costs by up to 38% and the O&M costs by up to 28% [61].

The total CO_2 emissions for B31A, B31B, and B31B with the hot and cold TES units for each market scenario are also shown in Table 4- 8. B31B operation avoids 87% of the total B31A emissions on average. This number is less than the capture rate of 90% because the capacity factors of B31B are typically higher than those of B31A (see Figure 4- 6). The B31B with TES operation avoids 82% of total B31A emissions on average. B31B emits more CO2 when TES is utilized due to increased fuel consumption and emissions during cold storage discharge & boosting modes, but still avoids most emissions

Table 4- 8: NPV and CO_2 emissions for B31A, B31B, and B31B with both TES units

	NPV (Millions)			**CO_2 Emissions (Thousand Tonnes per Year)**		
	B31A	**B31B**	**B31B+TES**	**B31A**	**B31B**	**B31B+TES**
G60-Base	200	-67	-9	1181	203	239
G60-HighWind	224	-80	-6	1188	184	221
G60-HighSolar	235	-90	-14	995	184	224
G60-Winter	104	-109	-90	1816	211	258
R100-CAISO	749	710	787	1420	246	245
R150-CAISO	487	539	601	983	101	168
R100-ERCOT	-47	-262	-226	808	125	174
R150-ERCOT	72	48	78	797	94	142
R100-MISO	125	45	55	1083	124	188
R150-MISO	-147	-213	-212	573	78	108
R100-NYISO	409	242	295	1063	108	183
R150-NYISO	303	232	280	785	80	133
R100-PJM	498	555	599	1401	161	256
R150-PJM	450	700	733	1083	130	202

4.8 Ambient Temperature Considerations

The purpose of the cold storage is to reduce the temperature of the inlet air to the gas turbine. Notably, colder ambient temperatures yield higher power outputs than warm ones regardless of whether inlet chilling is in effect. While the rest of the results generated in this thesis assumed a constant temperature for simplicity, the ability to account for variations in

ambient temperature was also included in the models to validate that cold storage provides a benefit in real climates. Figure 4- 9 provides box and whiskers plots of the NPV of the B31B base plant in all market scenarios, utilizing temperature data from different geographical regions throughout 2019 from [60]. As expected, the NPV is larger for colder climates than for warmer ones. Salt Lake City, Fargo, and Syracuse all have colder climates and yield higher NPVs than Dallas, Sacramento, Pheonix, and San Diego, which all have warmer climates. The constant temperature analysis used in this research yields NPVs that are lower than those calculated for colder climates but higher than those calculated for the warmer climates.

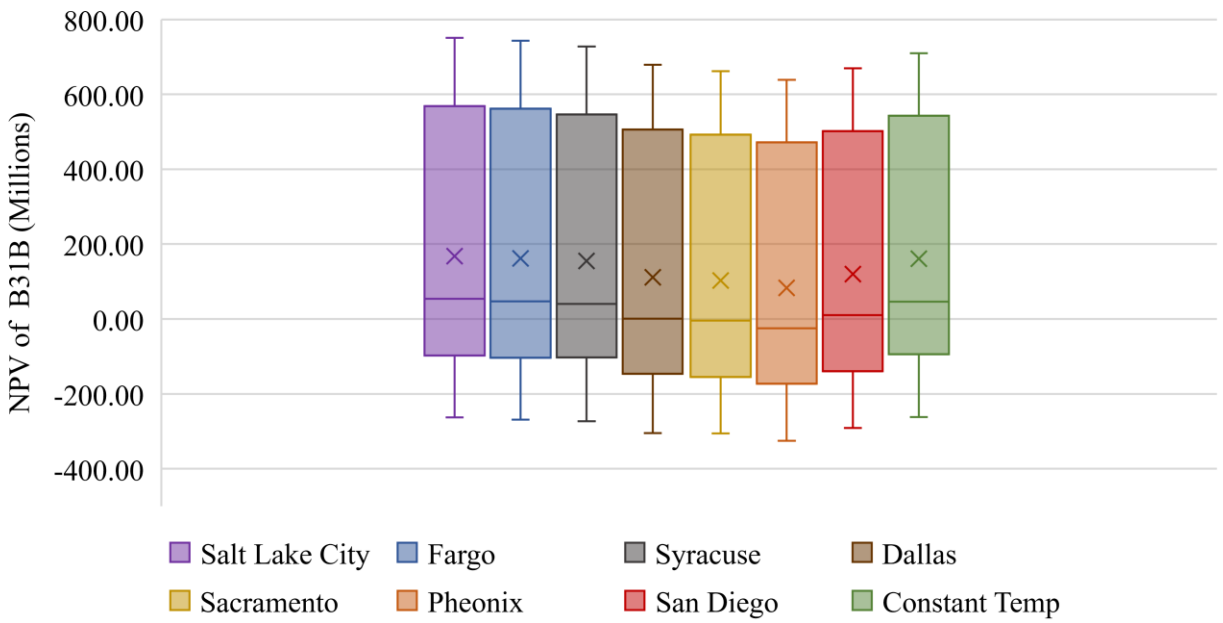

Figure 4- 9: NPV of B31B when operated in different locations

Current uses of cold storage have predominantly been demonstrated in the summer months during warm temperatures. There are two prominent reasons why cold storage is not as useful for colder ambient conditions. The first reason is the gas and steam generators have a designated capacity that cannot be exceeded, which limits the amount of useful cooling potential. The second

reason is that cooling below the dewpoint can cause icing in the gas turbine which is extremely detrimental to the equipment. In the current research, both concerns were addressed, as formulated in section 3.7. Figure 4- 10 shows the NPV difference of the base plant with only the cold storage technology from B31B over the same climates considered in Figure 4- 9. Again, all market scenarios are included in each box and whiskers plot. It can be seen from the figure that the benefit of cold storage is very dependent on the climate in which its deployed. The constant temperature case yields the highest NPV difference because full cold storage capability is always available while the base plant always operates at the design point. When real ambient temperature profiles are accounted for, cold storage provides larger benefits as the frequency of warmer temperatures increases. Regardless, Figure 4- 10 shows that cold storage still provides economic benefit in all locations, for most electricity market scenarios.

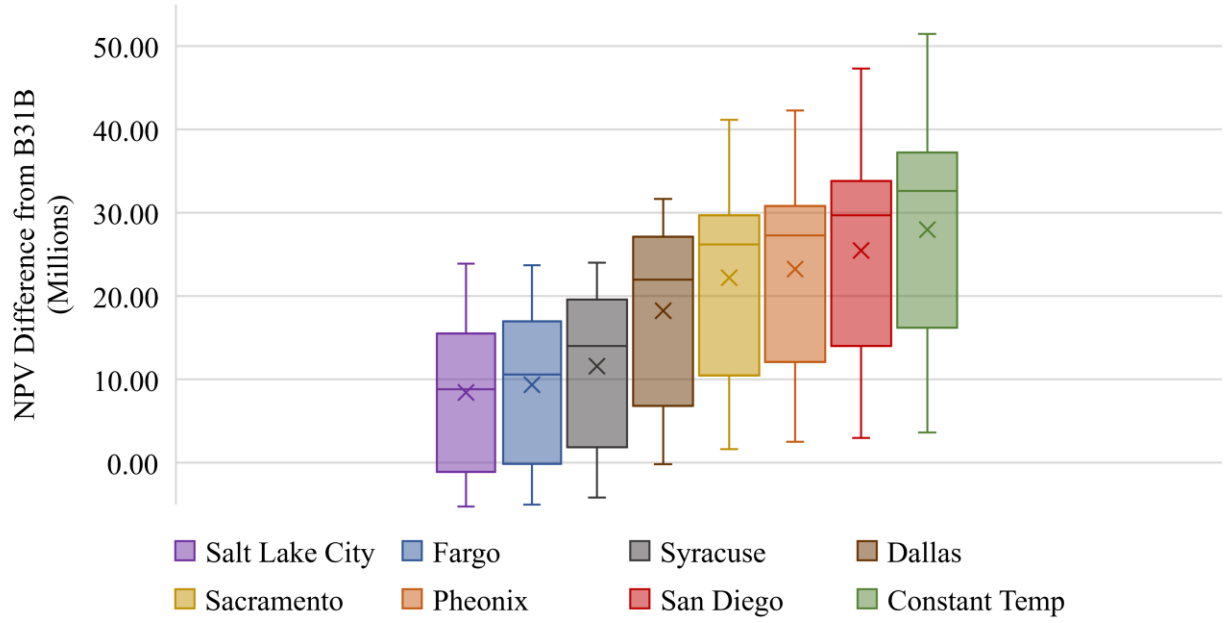

Figure 4- 10: NPV difference from B31B of the cold storage technology in different locations

CHAPTER 5 Conclusions

The present work has proposed resistively heated hot TES and vapor compression cooled cold TES to increase the flexibility and profitability of an NGCC power plant with CCS. Previous literature has explored using techniques such capture unit bypass, solvent storage, hydrogen storage, and oxygen storage to increase flexibility of carbon capturing power plants. All previous techniques showed the possibility to boost variable operating capabilities and plant revenue, however bypass and solvent storage were shown not to be profitable under market scenarios that financially motivate carbon capture while hydrogen and oxygen storage are not compatible with state-of-the-art fossil fuel power plants. Previous literature has also investigated the utilization of hot and cold TES in the context of power generation where the hot storage decouples electricity production with fuel or electricity consumption and the cold storage is used to chill the inlet air to gas plants. However, previous literature has not made the interconnection between TES and flexible CCS. This thesis has detailed a novel concept for using resistively heated hot TES to regain the parasitic power penalty imposed by the carbon capture technology, combined with previously investigated mechanical refrigeration cold storage techniques to chill the inlet to the power plant.

Thermodynamic models were created in EES for the base NGCC with CCS power plant, the resistively heated hot TES technology, and the vapor compression cooled cold TES technology. These models output key performance and cost parameters such as net power output, fuel consumption, emissions captured, capital costs, and operational costs. These parameters were then used to simulate the operation of the power plant and storage technologies at each hour for a year given an electricity price profile, fuel price, and carbon tax using a previously created optimization model. The electricity market data used in the research was provided by the capacity expansion models GenX and ReEDs. The optimization model outputs the annual revenue, fuel cost, emissions

cost, FOM cost, VOM cost, and total capital cost. These revenue and costs were then used in a discounted cash flow calculation to determine the NPV of the power plant with and without TES over a 30-year period.

The results have shown that the increase in revenue due to storage arbitrage capabilities outweighs the costs of the storage components, indicating that both hot and cold TES are a profitable option for the NETL B31B power plant. It was determined that the hot storage was best used for periods of long duration arbitrage, while the cold storage was best used to boost the steady state capacity of the power plant and to offer bursts of short duration arbitrage. The poor efficiency of the resistive heating technology used in this study was determined to have little impact on plant economics because charging periods happen at times of near zero electricity prices. Hot TES increased the NPV of B31B in 12 of 14 market scenarios and cold TES increased the NPV of B31B in 14 of 14 market scenarios. A combination of hot and cold TES was shown to have the largest economic impact overall. Furthermore, the inclusion of TES increases the number of scenarios in which carbon capture is more economically feasible than no carbon capture from 3 of 14 scenarios to 5 of 14 scenarios, which suggests that TES can help the deployment of carbon capture technologies. Additionally, results have also suggested that a reduction in CCS technology costs could have a significant impact on the feasibility of carbon capture when combined with the TES technologies presented in this study. Finally, while ambient temperature does have an impact on the usefulness of cold storage, it was shown to be largely profitable in a variety of real climates.

5.1 Recommendations for future work

Although this research has provided valuable insight into the potential value of hot and cold TES to natural gas power plants with carbon capture, there is a degree of uncertainty in the results and a few limitations that should be addressed in future work. Furthermore, this research

has provided insight for possible investigations beyond the scope of the current study. Listed below are the specific sources of error, limitations, and an additional insight for future work.

Sources of error:

- The cost assumptions used in this analysis are approximations based on previously published data, equipment type cost correlations, and from similar equipment. To improve the cost prediction accuracy, future work should leverage the expertise of engineering procurement and construction firms.
- Because the hot TES, cold TES, and CCS technologies are still in various stages of development, it is unclear how well these systems can respond to changes in the electricity grid. Therefore, there is uncertainty regarding the start-up time, shut down time, and ramp rates of the integrated NGCC + CCS + TES system. Future work should build and test and integrated pilot plant to better understand the dynamic operation of the system. Building and testing a pilot plant will also increase the readiness level of these technologies for integration with the electricity market.
- This research assumes that the power plant operational decisions are based purely on the electricity market prices, which eliminates the motivation for part load operation. However, in real grids, there is a demand for electricity that needs to be satisfied by the generation resources, so the power plant will often need to be operated at part load to not exceed the electricity demand. Future research should account for electricity demand profiles in addition to pricing structures.
- This research also neglects the interaction of the proposed technologies with other generation resources. This is significant because the price of electricity is dependent on the mix of generators used. Introducing a new generator into the mix changes the design

conditions, which intern alters the operation of the generator technologies and electricity prices. Future research should consider a grid-wide mix of generation resources to more accurately gauge operation characteristics and future pricing structures.

Limitations:

- Concrete was the only TES medium evaluated in this research for both the hot and cold TES units. Future work should consider other mediums for hot storage such as molten salts, sands, high temperature ceramics, etc., to verify that concrete is best used for flexible carbon capture. Similarly, other mediums for cold storage should be considered including water/glycol mixtures and ice.
- Carbon taxes are the only carbon capture incentive considered in this thesis. Future work should also consider other incentives such as tax credits and/or the existence of maximum allowable CO_2 emissions, which are also likely to play a role in future electricity markets.
- This research only considers the CANSOLV carbon capture technology presented by NETL in 2018. However, the results have demonstrated that the feasibility of the proposed system could be largely impacted by the performance of the carbon capture technology. More modern suites of carbon capture designs promise higher CO_2 capture rates and lower costs. Future work should consider using lower cost, higher performance carbon capture solutions.
- Only new build scenarios for NGCC power plants were considered in this research, which provides an accurate comparison between power plants with and without carbon capture over the same duration life cycle. However, carbon capture technologies are more likely to be added to existing power plants than to be deployed with new power plants. Future work should consider retrofitting existing NGCCs with CCS and TES technologies. This will

require assuming a shorter lifetime of the base NGCC power plant and considering costs of retrofit in addition to the costs of the CCS and TES equipment.

Insight for future work:

- This research has determined that resistive heating is a valuable solution to future electricity grids because it is low cost while the poor efficiency has little impact on profitability. However, this research only considered resistive heating for carbon capture applications. Additionally, most existing TES technologies currently used for stand-alone electricity storage are pumped heat systems. Future work should examine resistive heating technologies for stand-alone electricity storage systems as a solution in future electricity markets.

CHAPTER 6 References

[1] H. Shaftel, S. Callery, R. Jackson, D. Bailey, and S. Callery, “Global Climate Change,” *NASA*, Mar. 23, 2022. https://climate.nasa.gov/evidence/ (accessed Apr. 10, 2022).

[2] Intergovernmental Pannel on Climate Change (IPCC), “Summary for policy makers. In: Global warming of 1.5°C. An IPCC special report on the impacts of global warming of 1.5°C above pre-industrial levels and related global greenhouse gas emission pathways, in the context of strngthening the global response to the threat of climate change, sustainable development and efforts to eradicate poverty,” 2018.

[3] A. M. Abdilahi, M. W. Mustafa, S. Y. Abujarad, and M. Mustapha, “Harnessing flexibility potential of flexible carbon capture power plants for future low carbon power systems: Review,” *Renewable and Sustainable Energy Reviews*, vol. 81. Elsevier Ltd, pp. 3101–3110, Jan. 01, 2018. doi: 10.1016/j.rser.2017.08.085.

[4] LAZARD, “Levelized cost of energy, levelized cost of storage, and levelized cost of hydrogen,” Oct. 28, 2021. https://www.lazard.com/perspective/levelized-cost-of-energy-levelized-cost-of-storage-and-levelized-cost-of-hydrogen/ (accessed Apr. 10, 2022).

[5] U.S. Energy Information Administration, “Solar power will account for nearly half of new U.S. electric generating capacity in 2022,” Jan. 10, 2022. https://www.eia.gov/todayinenergy/detail.php?id=50818 (accessed Apr. 10, 2022).

[6] P. Lund, “Large-scale urban renewable electricity schemes - Integration and interfacing aspects,” in *Energy Conversion and Management*, Nov. 2012, vol. 63, pp. 162–172. doi: 10.1016/j.enconman.2012.01.037.

[7] T. Horiba, “Lithium-Ion Battery Systems,” *Proceedings of the IEEE*, vol. 102, no. 6, pp. 939–950, Jun. 2014, doi: 10.1109/JPROC.2014.2319832.

[8] B. R. Chalamala, T. Soundappan, G. R. Fisher, M. R. Anstey, V. v Viswanathan, and M. L. Perry, “Redox Flow Batteries: An Engineering Perspective,” *Proceedings of the IEEE*, vol. 102, no. 6, pp. 976–999, Jun. 2014, doi: 10.1109/JPROC.2014.2320317.

[9] U.S. Energy Information Administration (EIA), “Electricity generation, capacity, and sales in the United States,” Mar. 18, 2021. https://www.eia.gov/energyexplained/electricity/electricity-in-the-us-generation-capacity-and-sales.php (accessed Apr. 10, 2022).

[10] U.S. Energy Information Administration (EIA), “Coal will account for 85% of U.S. electric generating capacity retirements in 2022 - Today in Energy - U.S. Energy Information Administration (EIA),” Jan. 11, 2022. https://www.eia.gov/todayinenergy/detail.php?id=50838 (accessed Apr. 10, 2022).

[11] A. S. Brouwer, M. van den Broek, A. Seebregts, and A. Faaij, “Operational flexibility and economics of power plants in future low-carbon power systems,” *Applied Energy*, vol. 156, pp. 107–128, Oct. 2015, doi: 10.1016/j.apenergy.2015.06.065.

[12] R. Domenichini, L. Mancuso, N. Ferrari, and J. Davison, “Operating flexibility of power plants with carbon capture and storage (CCS),” in *Energy Procedia*, 2013, vol. 37, pp. 2727–2737. doi: 10.1016/j.egypro.2013.06.157.

[13] N. Ceccarelli *et al.*, “Flexibility of low-CO2 gas power plants: Integration of the CO2 capture unit with CCGT operation,” in *Energy Procedia*, 2014, vol. 63, pp. 1703–1726. doi: 10.1016/j.egypro.2014.11.179.

[14] P. D. Lund, J. Lindgren, J. Mikkola, and J. Salpakari, “Review of energy system flexibility measures to enable high levels of variable renewable electricity,” *Renewable and Sustainable Energy Reviews*, vol. 45, pp. 785–807, 2015, doi: 10.1016/j.rser.2015.01.057.

[15] H. Mikulčić *et al.*, “Flexible Carbon Capture and Utilization technologies in future energy systems and the utilization pathways of captured CO2,” *Renewable and Sustainable Energy Reviews*, vol. 114, Oct. 2019, doi: 10.1016/j.rser.2019.109338.

[16] National Energy Technology Laboratory (NETL), “Cost and Performance Baseline for Fossil Energy Plants1: Bituminous Coal and Natural Gas to Electricity,” Sep. 2019.

[17] Congressional Research Service, “The Tax Credit for Carbon Sequestration (Section 45Q),” Jun. 08, 2021. https://sgp.fas.org/crs/misc/IF11455.pdf (accessed Apr. 10, 2022).

[18] Office of Administrative Law, “Unofficial Electronic Version of the Low Carbon Fuel Standard,” Jul. 01, 2020. https://ww2.arb.ca.gov/sites/default/files/2020-07/2020_lcfs_fro_oal-approved_unofficial_06302020.pdf (accessed Apr. 10, 2022).

[19] The Regional Greenhouse Gas Initiative, “Elements of RGGI,” Mar. 15, 2021. https://www.rggi.org/program-overview-and-design/elements (accessed Apr. 10, 2022).

[20] United States Department of State, “Long Term Strategy of the United States: Pathways to Net-Zero Greenhouse Gas Emissions by 2050,” Washington DC, Nov. 2021.

[21] J. D. Jenkins, S. Chakrabarti, F. Cheng, and N. Patankar, “Summary Report of the GenX and PowerGenome runs for generating Price Series (for ARPA-E Fleccs Project),” Oct. 13, 2021. https://zenodo.org/record/5765798#.YggaBN_MJD8 (accessed Apr. 10, 2022).

[22] The National Renewable Energy Laboratory, “NREL Price Series Developed for the ARPA-E FLECCS Program,” Dec. 23, 2021. https://data.nrel.gov/submissions/181 (accessed Apr. 10, 2022).

[23] New York Independent System Operator, “Energy Market and Operational Data,” 2019. https://www.nyiso.com/energy-market-operational-data (accessed Apr. 10, 2022).

[24] The Electricity Reliability Council of Texas, “Hourly Load Data Archives,” 2019. https://www.ercot.com/gridinfo/load/load_hist (accessed Apr. 10, 2022).

[25] E. Kyritsis, J. Andersson, and A. Serletis, “Electricity prices, large-scale renewable integration, and policy implications,” *Energy Policy*, vol. 101, pp. 550–560, 2016, doi: 10.1016/j.enpol.2016.11.014.

[26] Intergovernmental Panel on Climate Change (IPCC), *Carbon Dioxide Capture and Storage*. New York: Cambridge, 2005.

[27] Global CCS Institute, “New wave of CCS activity: Ten large-scale projects announced,” Oct. 29, 2019. https://www.globalccsinstitute.com/news-media (accessed Apr. 10, 2022).

[28] P. Tait, B. Buschle, I. Ausner, P. Valluri, M. Wehrli, and M. Lucquiaud, “A pilot-scale study of dynamic response scenarios for the flexible operation of post-combustion CO2 capture,” *International Journal of Greenhouse Gas Control*, vol. 48, pp. 216–233, May 2016, doi: 10.1016/j.ijggc.2015.12.009.

[29] Q. Chen, C. Kang, Q. Xia, and D. S. Kirschen, “Optimal flexible operation of a CO 2 capture power plant in a combined energy and carbon emission market,” *IEEE Transactions on Power Systems*, vol. 27, no. 3, pp. 1602–1609, 2012, doi: 10.1109/TPWRS.2012.2185856.

[30] D. L. Oates, P. Versteeg, E. Hittinger, and P. Jaramillo, “Profitability of CCS with flue gas bypass and solvent storage,” *International Journal of Greenhouse Gas Control*, vol. 27, pp. 279–288, 2014, doi: 10.1016/j.ijggc.2014.06.003.

[31] S. M. Cohen, G. T. Rochelle, and M. E. Webber, “Optimal operation of flexible post-combustion CO2 capture in response to volatile electricity prices,” in *Energy Procedia*, 2011, vol. 4, pp. 2604–2611. doi: 10.1016/j.egypro.2011.02.159.

[32] S. M. Cohen, G. T. Rochelle, and M. E. Webber, “Optimizing post-combustion CO2 capture in response to volatile electricity prices,” *International Journal of Greenhouse Gase Control*, vol. 8, pp. 180–195, 2012.

[33] S. M. Cohen, G. T. Rochelle, and M. E. Webber, “Optimal CO2 capture operation in an advanced electric grid,” *Energy Procedia*, vol. 37, pp. 2585–2594, 2013, doi: 10.1016/J.EGYPRO.2013.06.142.

[34] S. Szima, A. M. Cormos, and C. C. Cormos, “Flexible Hydrogen and Power Co - generation based on Dry Methane Reforming with Carbon Capture,” in *Computer Aided Chemical Engineering*, vol. 43, Elsevier B.V., 2018, pp. 1281–1286. doi: 10.1016/B978-0-444-64235-6.50225-4.

[35] M. W. Ajiwibowo, A. Darmawan, and M. Aziz, “A conceptual chemical looping combustion power system design in a power-to-gas energy storage scenario,” *International Journal of Hydrogen Energy*, vol. 44, no. 19, pp. 9636–9642, Apr. 2019, doi: 10.1016/j.ijhydene.2018.11.177.

[36] J. Davison, S. Arienti, P. Cotone, and L. Mancuso, “Co-production of hydrogen and electricity with CO2 capture,” *International Journal of Greenhouse Gas Control*, vol. 4, no. 2, pp. 125–130, 2010, doi: 10.1016/j.ijggc.2009.10.007.

[37] The Integrated Environmental Control Model Team, “IECM Technical Documentation: Integrated Gasification Combined Cycle Power Plants Integrated Gasification Combined Cycle Power Plants,” Pittsburg, PA, 2019. Accessed: Apr. 10, 2022. [Online]. Available: www.iecm-online.com

[38] C. Mitchell, V. Avagyan, H. Chalmers, and M. Lucquiaud, “An initial assessment of the value of Allam Cycle power plants with liquid oxygen storage in future GB electricity system,” *International Journal of Greenhouse Gas Control*, vol. 87, pp. 1–18, Aug. 2019, doi: 10.1016/j.ijggc.2019.04.020.

[39] Y. Hu, X. Li, H. Li, and J. Yan, “Peak and off-peak operations of the air separation unit in oxy-coal combustion power generation systems,” *Applied Energy*, vol. 112, pp. 747–754, 2013, doi: 10.1016/j.apenergy.2012.12.001.

[40] Toshiba, “Toshiba Ships Turbine for World’s First Direct-Fired Supercritical Oxy-Combustion CO2 Power Cycle Demonstration Plant to U.S. | Toshiba,” Nov. 01, 2016. https://news.toshiba.com/press-releases/press-release-details/2016/Toshiba-Ships-Turbine-

for-Worlds-First-Direct-Fired-Supercritical-Oxy-Combustion-CO2-Power-Cycle-Demonstration-Plant-to-US/default.aspx (accessed Apr. 10, 2022).

[41] P. Higginbotham, V. White, K. Fogash, and G. Guvelioglu, "Oxygen supply for oxyfuel CO2 capture," *International Journal of Greenhouse Gas Control*, vol. 5, no. SUPPL. 1, 2011, doi: 10.1016/j.ijggc.2011.03.007.

[42] C. Spero, T. Yamada, P. Nelson, T. Morrison, and C. Bourhy-Weber, "Callide Oxyfuel Project: Combustion and Environmental Performance," Sep. 10, 2013.

[43] NetPower, "Making Clean Energy Cheaper," 2022. https://netpower.com/ (accessed Apr. 10, 2022).

[44] M. Medrano, A. Gil, I. Martorell, X. Potau, and L. F. Cabeza, "State of the art on high-temperature thermal energy storage for power generation. Part 2-Case studies," *Renewable and Sustainable Energy Reviews*, vol. 14, no. 1. pp. 56–72, Jan. 2010. doi: 10.1016/j.rser.2009.07.036.

[45] D. Li, Y. Hu, W. He, and J. Wang, "Dynamic Modelling and Simulation of a Combined-Cycle Power Plant Integration with Thermal Energy Storage," Sep. 2017.

[46] J. H. Chang, G. H. Lee, D. Adams, H. W. Ahn, J. C. Lee, and M. Oh, "Multiscale modeling and integration of a combined cycle power plant and a two-tank thermal energy storage system with gPROMS and SimCentral," *Korean Journal of Chemical Engineering*, vol. 38, no. 7, pp. 1333–1347, Jul. 2021, doi: 10.1007/s11814-021-0789-1.

[47] MALTA, “Malta’s electro-thermal energy storage system: A better way to enable cleaner reliable electricity on the grid,” 2021. https://www.maltainc.com/our-solution (accessed Apr. 10, 2022).

[48] A. Smallbone, V. Jülch, R. Wardle, and A. P. Roskilly, “Levelised Cost of Storage for Pumped Heat Energy Storage in comparison with other energy storage technologies,” *Energy Conversion and Management*, vol. 152, pp. 221–228, Nov. 2017, doi: 10.1016/j.enconman.2017.09.047.

[49] A. Gil *et al.*, “State of the art on high temperature thermal energy storage for power generation. Part 1-Concepts, materials and modellization,” *Renewable and Sustainable Energy Reviews*, vol. 14, no. 1. pp. 31–55, Jan. 2010. doi: 10.1016/j.rser.2009.07.035.

[50] A. Paudel and T. Bandhauer, “Techno-economic analysis of waste heat recovery systems for wet-cooled combined cycle power plants,” *Applied Thermal Engineering*, vol. 143, pp. 746–758, Oct. 2018, doi: 10.1016/j.applthermaleng.2018.07.138.

[51] V. Eveloy and P. Rodgers, “Power generation and cooling capacity enhancement of natural gas processing facilities in harsh environmental conditions through waste heat utilization,” *International Journal of Energy Research*, vol. 38, no. 15, pp. 1921–1936, Apr. 2014.

[52] A. K. Mohapatra and Sanjay, “Thermodynamic assessment of impact of inlet air cooling techniques on gas turbine and combined cycle performance,” *Energy*, vol. 68, pp. 191–203, Apr. 2014, doi: 10.1016/j.energy.2014.02.066.

[53] V. Gkoutzamanis, A. Chatziangelidou, T. Efstathiadis, A. Kalfas, A. Traverso, and J. Chiu, “Thermal Energy Storage For Gas Turbine Power Augmentation,” *Journal of the Global Power and Propulsion Society*, vol. 3, pp. 592–608, Jul. 2019, doi: 10.33737/jgpps/110254.

[54] N. Palestra, G. Barigozzi, and A. Perdichizzi, “Inlet air cooling applied to combined cycle power plants: Influence of site climate and thermal storage systems,” *Journal of Engineering for Gas Turbines and Power*, vol. 130, no. 2, Feb. 2008.

[55] G. Barigozzi, A. Perdichizzi, C. Gritti, and I. Guaiatelli, “Techno-economic analysis of gas turbine inlet air cooling for combined cycle power plant for different climatic conditions,” *Applied Thermal Engineering*, vol. 82, pp. 57–67, May 2015, doi: 10.1016/j.applthermaleng.2015.02.049.

[56] Couper James R, Penny W R, J. R. Fair, and S. M. Walas, *Chemical Process Equipment Selection and Design*. Butterworth-Heinemann, 2012.

[57] R. Vercellino *et al.*, “Control co-design optimization of natural gas power plants with carbon capture and thermal storage,” *Proceedings of the ASME,* 2022.

[58] The National Renewable Energy Laboratory (NREL), “2020 Electricity Annual Technology Baseline n.d.,” 2020. https://atb-archive.nrel.gov/electricity/2020/data.php (accessed Apr. 10, 2022).

[59] U.S. Energy Information Administration (EIA), “Annual Energy Outlook 2022,” Mar. 03, 2022. https://www.eia.gov/outlooks/aeo/ (accessed Apr. 11, 2022).

[60] National Renewable Energy Laboratory (NREL), “National Solar Radiation Database,” 2019. https://nsrdb.nrel.gov/ (accessed May 11, 2022).

[61] ION Clean Energy, “Our Technology,” 2022. https://ioncleanenergy.com/our-technology/ (accessed May 30, 2022).

Appendix

A.1 B31A and B31B Base Plant Technical Information

The main text has considered the Case B31A and Case B31B natural gas power plants specified by the National Energy Technology Laboratories' *Cost and Performance Baseline for Fossil Energy Plants* [16] as reference power plants for the proposed hot and cold thermal energy storage technologies. Therefore, both B31A and B31B were modeled in Engineering Equation Solver to accurately represent the integration with the corresponding thermal energy storage technologies. This section includes process flow diagrams of the constructed B31A and B31B models in addition to the power and heat duty of each component shown in the diagrams.

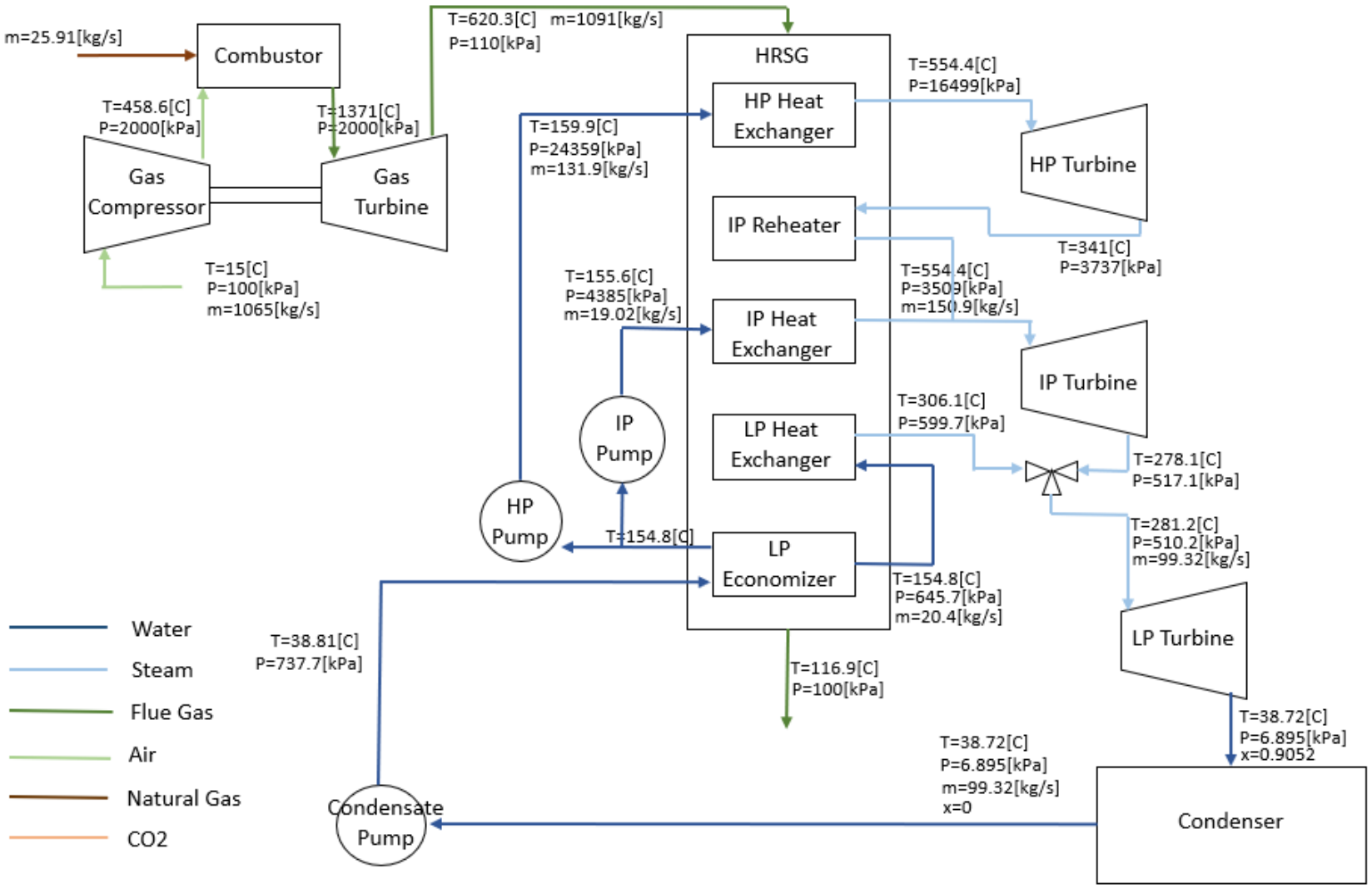

Figure A- 1: Process flow diagram of the B31A base plant

Table A- 1: B31A component power

Component	Discharging Power [MW]
Gas Compressor	-490.08
Gas Turbine	968.63
HP Turbine	48.74
IP Turbine	83.65
LP Turbine	116.95
HP Pump	-4.80
IP Pump	-0.11
Condensate Pump	-0.18
Carbon Capture Pump	0.00
Hot Storage Pump	0.00
Blower	0.00
RH Electricity Consumption	0.00
Configuration Compressor	0.00
Auxiliary Power	-8.91
Net Power	713.89

Table A- 2: B31A component heat duty

Component	Charging Heat Duty [MW]
Combustor	1162.62
HPHX	363.75
IPHX	55.46
IPRH	65.39
LPHX	49.41
LPEC	49.79
HRSG	583.80
Preheater	34.13
Condenser	373.63
Hot Storage	0.00
Reboiler	172.03
Cold Storage	0.00
Resistance Heater	0.00
Configuration HRSG	0.00
Cooling Tower	0.00

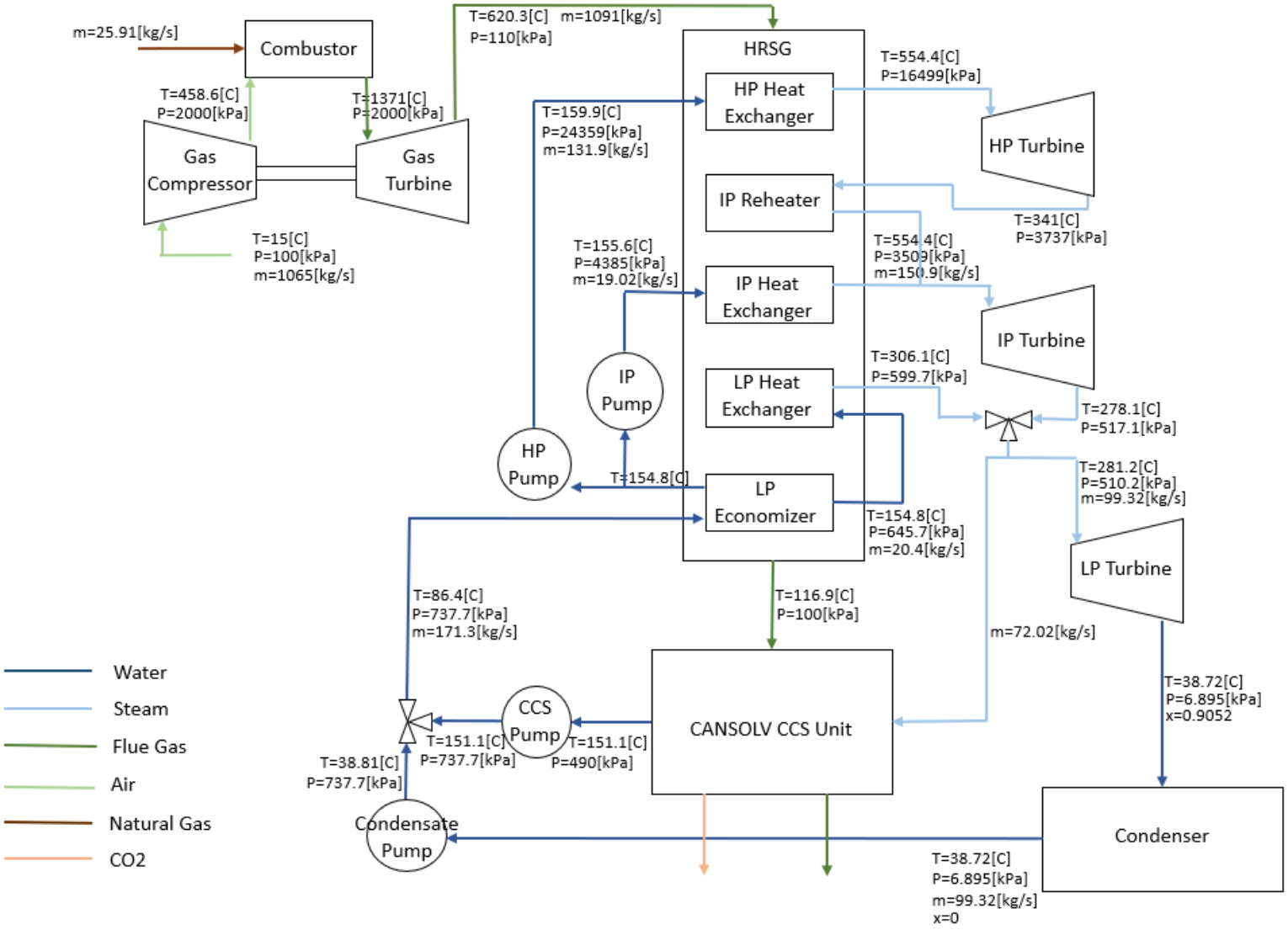

Figure A- 2: Process flow diagram of the B31B base plant

Table A- 3: B31B component power

Component	Charging Power [MW]
Gas Compressor	-490.08
Gas Turbine	968.63
HP Turbine	48.74
IP Turbine	83.65
LP Turbine	67.79
HP Pump	-4.80
IP Pump	-0.11
Condensate Pump	-0.10
Carbon Capture Pump	-0.03
Hot Storage Pump	0.00
Blower	0.00
RH Electricity Consumption	0.00
Configuration Compressor	0.00
Auxiliary Power	-38.96
Net Power	634.73

Table A- 4: B31B component heat duty

Component	Charging Heat Duty [MW]
Combustor	1162.62
HPHX	363.75
IPHX	55.46
IPRH	65.39
LPHX	49.41
LPEC	49.79
HRSG	583.80
Preheater	0.00
Condenser	250.77
Hot Storage	0.00
Reboiler	172.03
Cold Storage	0.00
Resistance Heater	0.00
Configuration HRSG	0.00
Cooling Tower	0.00

A.2 Hot Storage Unit Technical Information

The main text has considered a resistively heated hot storage unit to offset the steam requirement of the B31B carbon capture unit. This section provides charging mode and discharging mode process flow diagrams of the hot storage unit interaction with the B31B base plant and reports the power output and heat duties of the components shown in the diagrams to demonstrate the model compliance with thermodynamic laws.

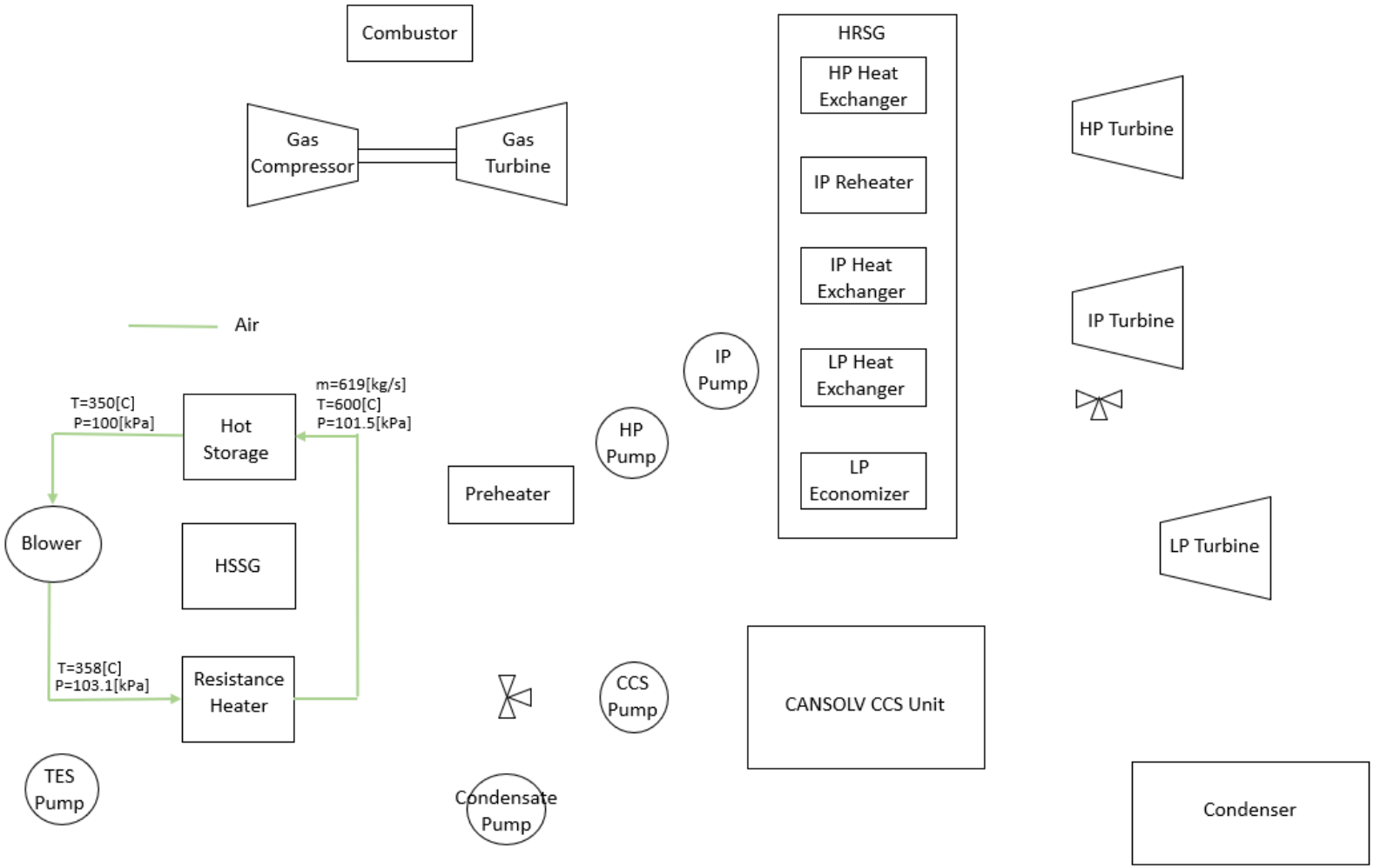

Figure A- 3: Process flow diagram of the hot storage unit charging mode

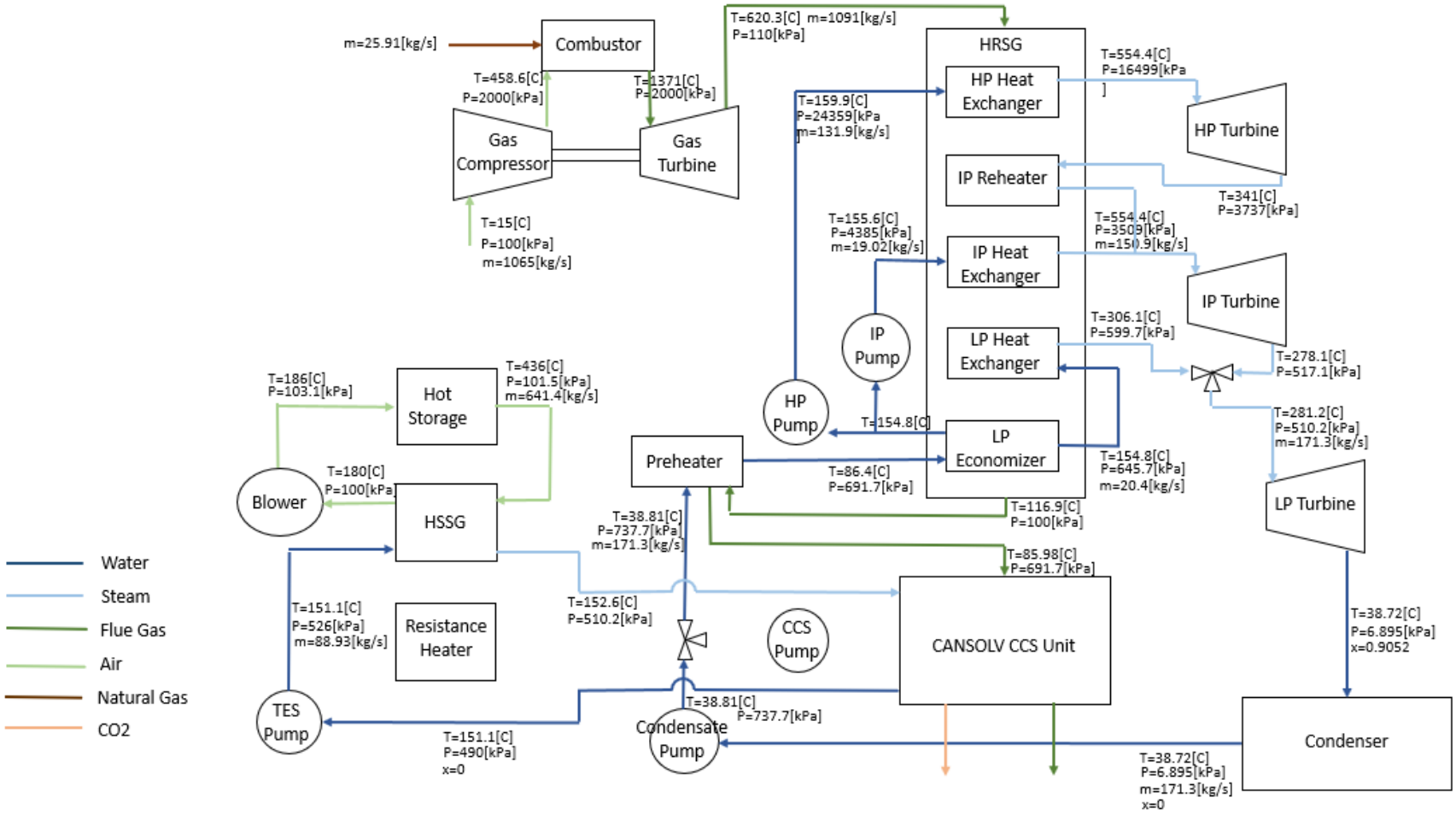

Figure A- 4: Process flow diagram of the hot storage unit discharging mode

Table A- 5: Hot storage unit component power

Component	Charging Power [MW]	Discharging Power [MW]
Gas Compressor	0.00	-490.08
Gas Turbine	0.00	968.63
HP Turbine	0.00	48.74
IP Turbine	0.00	83.65
LP Turbine	0.00	116.95
HP Pump	0.00	-4.80
IP Pump	0.00	-0.11
Condensate Pump	0.00	-0.18
Carbon Capture Pump	0.00	0.00
Hot Storage Pump	0.00	0.00
Blower	-5.21	-3.92
RH Electricity Consumption	-162.90	0.00
Configuration Compressor	0.00	0.00
Auxiliary Power	0.00	-38.96
Net Power	-168.11	679.92

Table A- 6: Hot storage unit component heat duty

Component	Charging Heat Duty [MW]	Discharging Heat Duty [MW]
Combustor	0.00	1162.62
HPHX	0.00	363.75
IPHX	0.00	55.46
IPRH	0.00	65.39
LPHX	0.00	49.41
LPEC	0.00	49.79
HRSG	0.00	583.80
Preheater	0.00	34.13
Condenser	0.00	373.63
Hot Storage	168.10	168.10
Reboiler	172.03	172.03
Cold Storage	0.00	0.00
Resistance Heater	0.00	0.00
Configuration HRSG	0.00	172.03
Cooling Tower	22.14	0.00

A.3 Cold Storage Unit Technical Information

The main text has considered a vapor compression cooled cold storage unit to chill the inlet air to the B31B power plant. This section provides charging mode, discharging mode, and boosting mode process flow diagrams of the cold storage unit interaction with the B31B base plant and reports the power output and heat duties of the components shown in the diagrams to demonstrate the model compliance with thermodynamic laws.

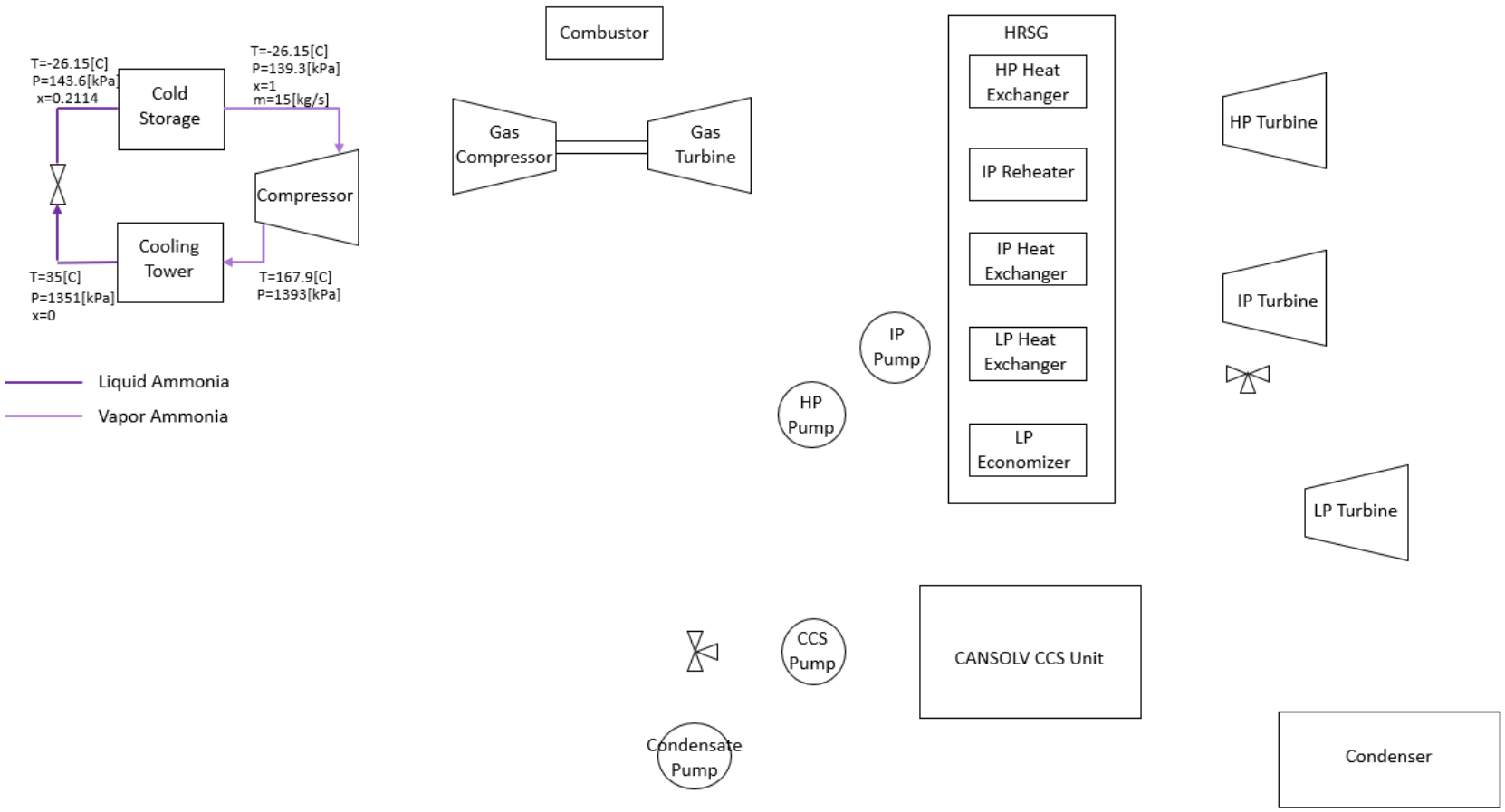

Figure A- 5: Process flow diagram of the cold storage unit charging mode

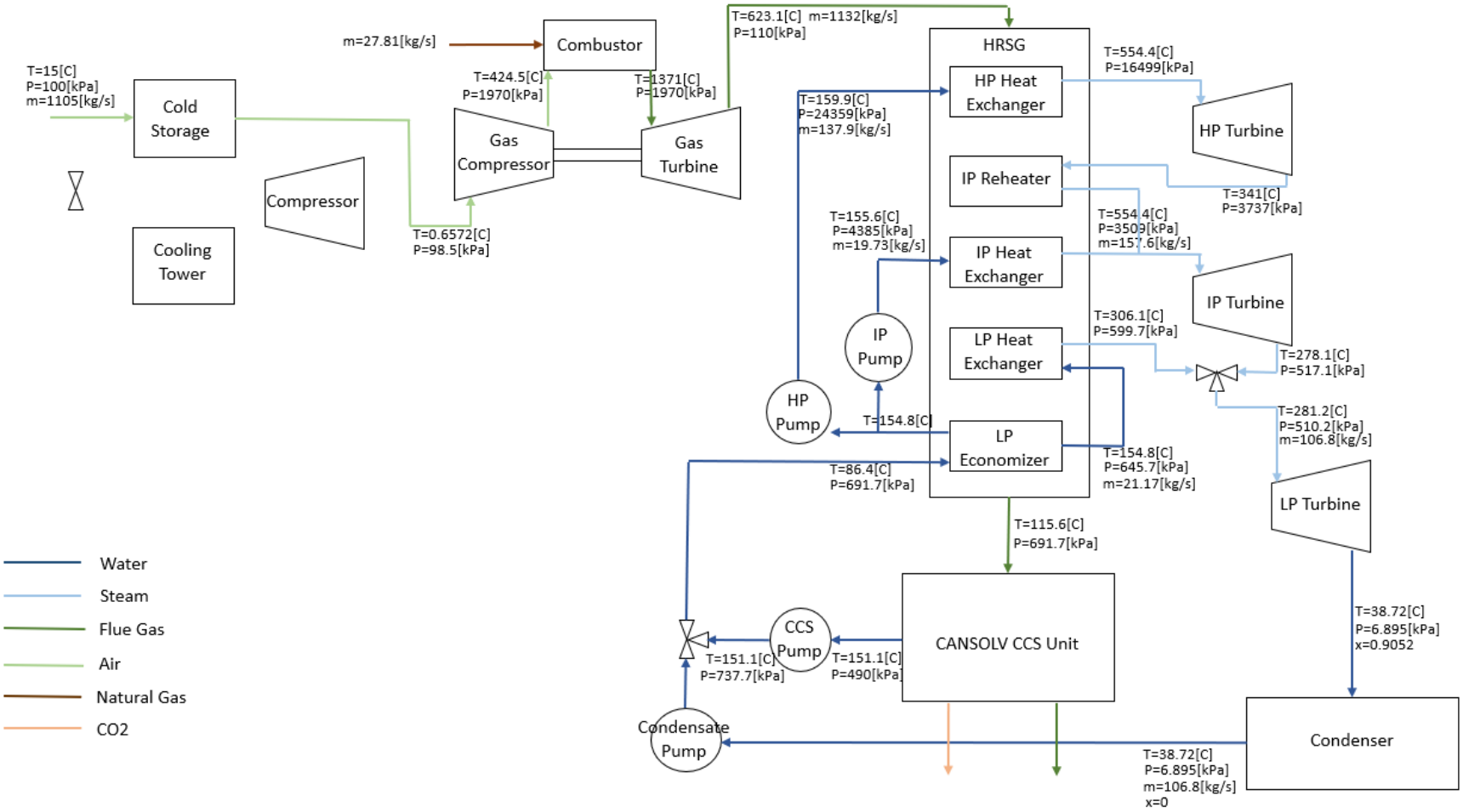

Figure A- 6: Process flow diagram of the cold storage unit discharging mode

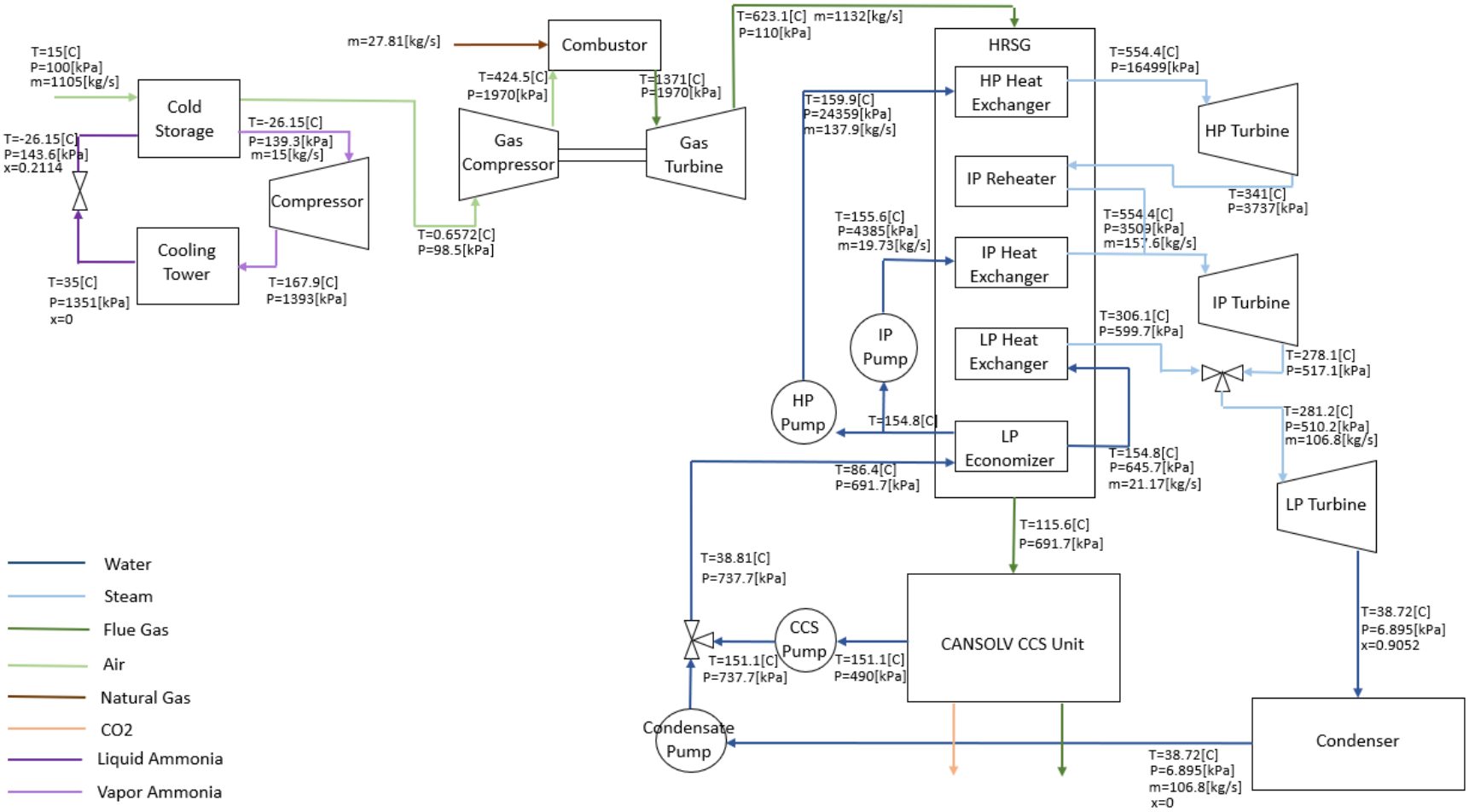

Figure A- 7: Process flow diagram of the cold storage unit boosting mode

Table A- 7: Cold storage unit component power

Component	Charging Power [MW]	Discharging Power [MW]	Boosting Power [MW]
Gas Compressor	0.00	-483.30	-483.30
Gas Turbine	0.00	1001.49	1001.49
HP Turbine	0.00	50.95	50.95
IP Turbine	0.00	87.36	87.36
LP Turbine	0.00	72.88	72.88
HP Pump	0.00	-5.02	-5.02
IP Pump	0.00	-0.11	-0.11
Condensate Pump	0.00	-0.19	-0.19
Carbon Capture Pump	0.00	-0.03	-0.03
Hot Storage Pump	0.00	0.00	0.00
Blower	0.00	-3.92	-3.92
RH Electricity Consumption	0.00	0.00	0.00
Configuration Compressor	-6.21	0.00	-6.21
Auxiliary Power	0.00	-38.96	-38.96
Net Power	-6.21	681.13	674.94

Table A- 8: Cold storage unit component heat duty

Component	Charging Heat Duty [MW]	Discharging Heat Duty [MW]	Boosting Heat Duty [MW]
Combustor	0.00	1248.09	1248.09
HPHX	0.00	380.21	380.21
IPHX	0.00	57.55	57.55
IPRH	0.00	68.35	68.35
LPHX	0.00	51.27	51.27
LPEC	0.00	51.95	51.95
HRSG	0.00	609.33	609.33
Preheater	0.00	0.00	0.00
Condenser	0.00	389.88	389.88
Hot Storage	0.00	0.00	0.00
Reboiler	0.00	172.03	172.03
Cold Storage	15.93	15.93	15.93
Resistance Heater	0.00	0.00	0.00
HSSG	0.00	0.00	0.00
Cooling Tower	22.14	0.00	22.14

A.4 Combined Hot and Cold Storage Unit Technical Information

The hot and cold storage units may be operated simultaneously. This section shows the process flow diagrams that correspond to the simultaneous charging mode and discharging mode of both hot and cold storage units and reports the power and heat duty of the components shown in the diagrams.

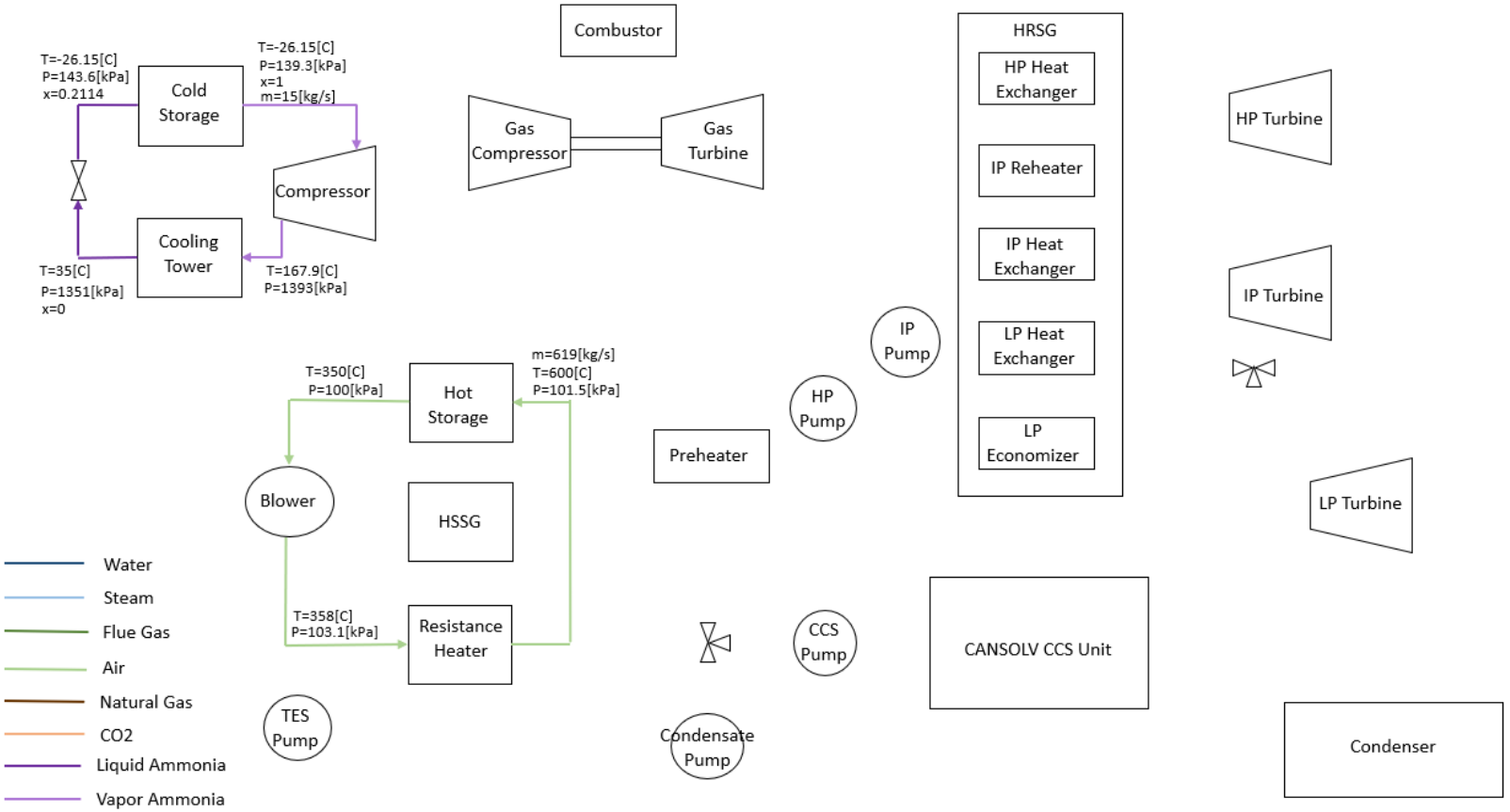

Figure A- 8: Process flow diagram of the combined hot and cold storage unit charging mode

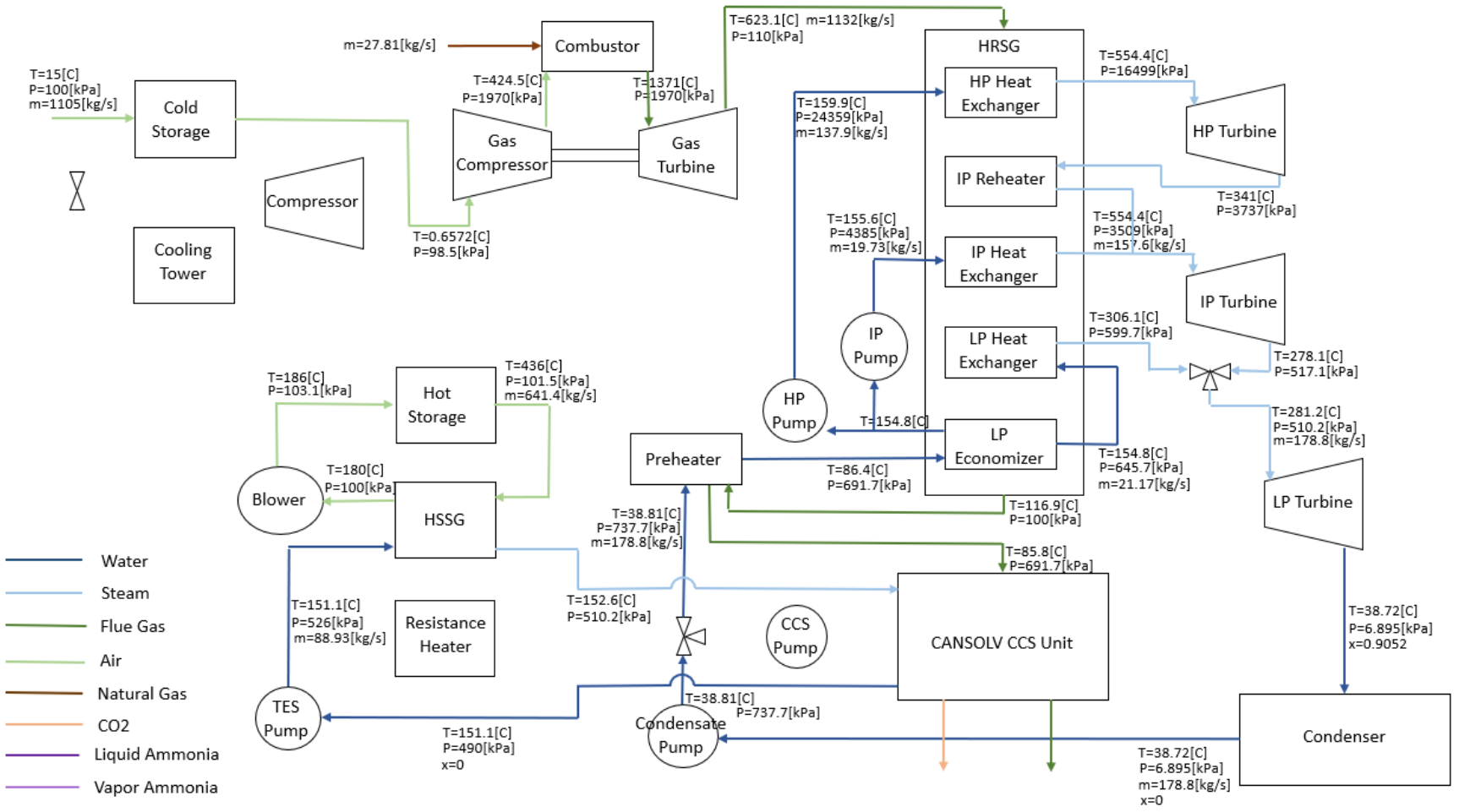

Figure A- 9: Process flow diagram of the combined hot and cold storage unit discharging mode

Table A- 9: Combined hot and cold storage unit component power

Component	Charging Power [MW]	Discharging Power [MW]
Gas Compressor	-490.08	-483.30
Gas Turbine	968.63	1001.49
HP Turbine	48.74	50.95
IP Turbine	83.65	87.36
LP Turbine	67.79	122.04
HP Pump	-4.80	-5.02
IP Pump	-0.11	-0.11
Condensate Pump	-0.10	-0.19
Carbon Capture Pump	-0.03	0.00
Hot Storage Pump	0.00	0.00
Blower	-5.21	-3.92
RH Electricity Consumption	-162.90	0.00
Configuration Compressor	-6.21	0.00
Auxiliary Power	-38.96	-38.96
Net Power	460.42	730.32

Table A- 10: Combined hot and cold storage unit component heat duty

Component	Charging Heat Duty [MW]	Discharging Heat Duty [MW]
Combustor	1162.62	1248.09
HPHX	363.75	380.21
IPHX	55.46	57.55
IPRH	65.39	68.35
LPHX	49.41	51.27
LPEC	49.79	51.95
HRSG	583.80	609.33
Preheater	0.00	35.61
Condensor	250.77	389.88
Hot Storage	168.10	168.10
Reboiler	172.03	172.03
Cold Storage	15.93	15.93
Resistance Heater	162.90	0.00
Configuration HRSG	0.00	172.03
Cooling Tower	22.14	0.00

A.3 Revenue & Cost breakdowns for all Electricity Market Scenarios

The main text presented the revenue and cost breakdown for the R150-CAISO market scenario as a representative case. This section provides the same revenue and cost breakdown for all 14 market scenarios considered in this study.

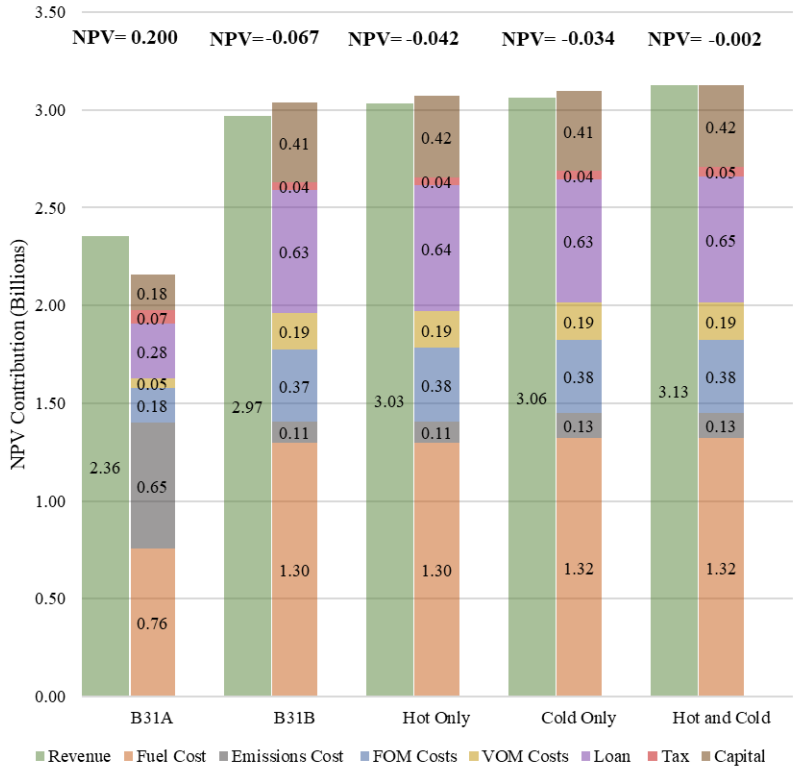

a) G60-Base

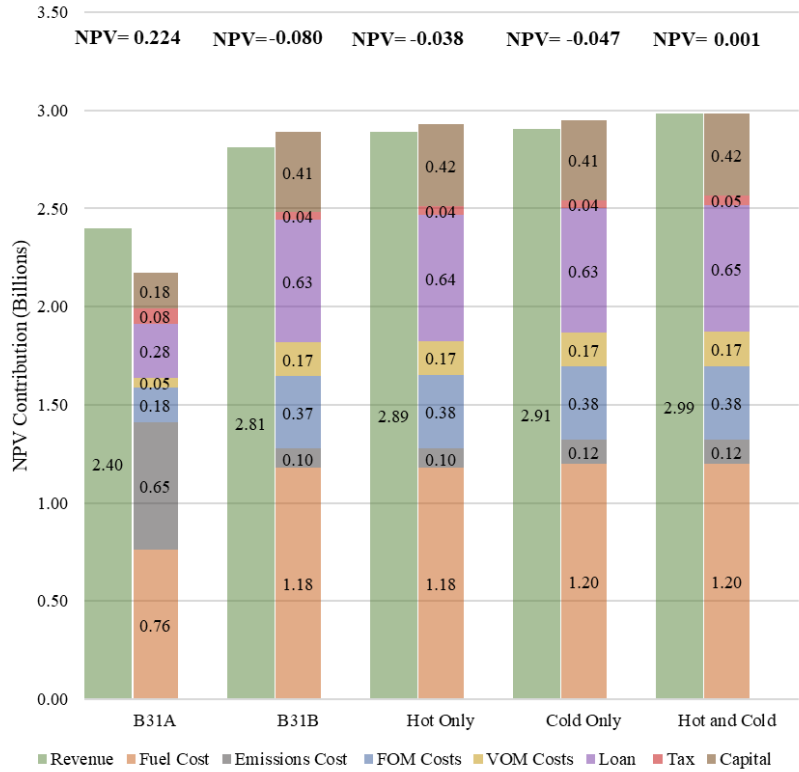

b) G60-HighWind

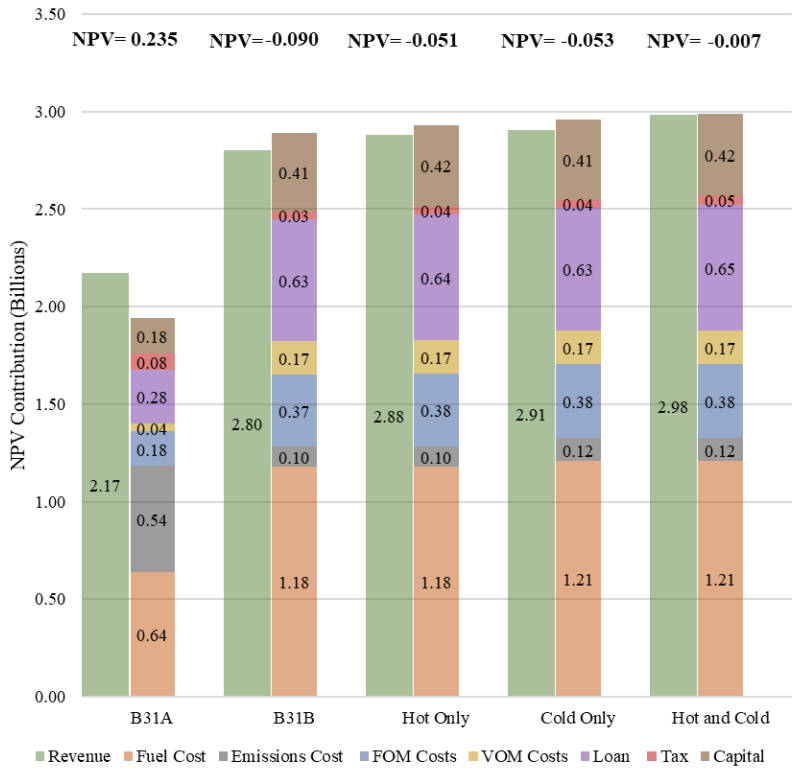

c) G60-HighSolar

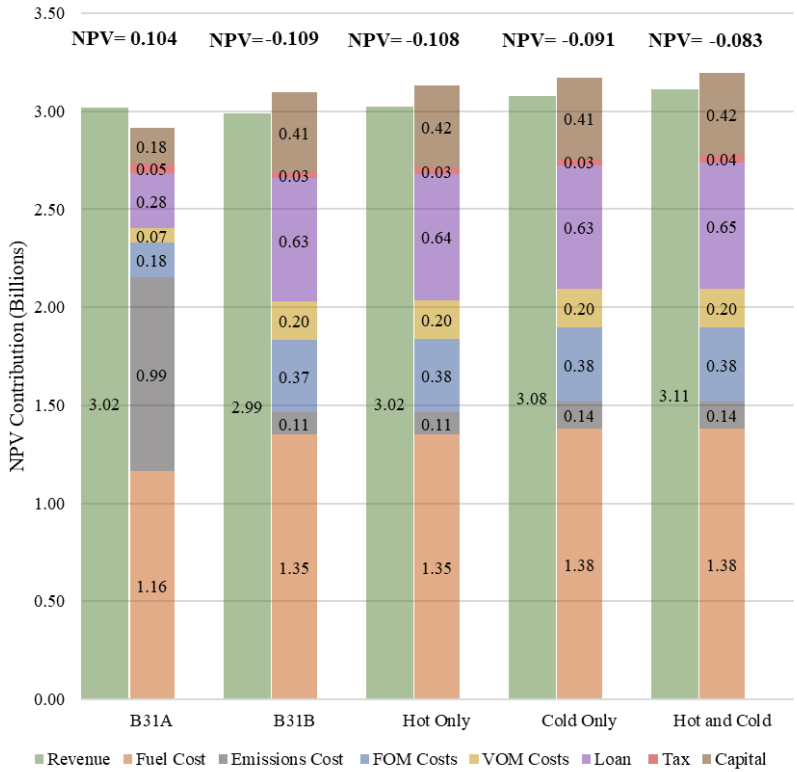

d) G60-Winter

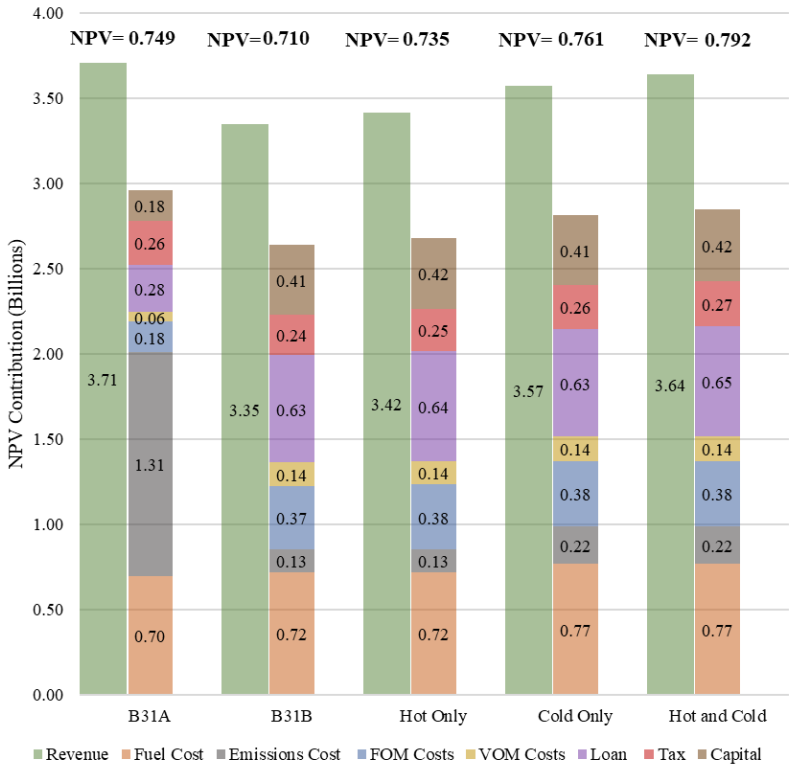

e) R100-CAISO

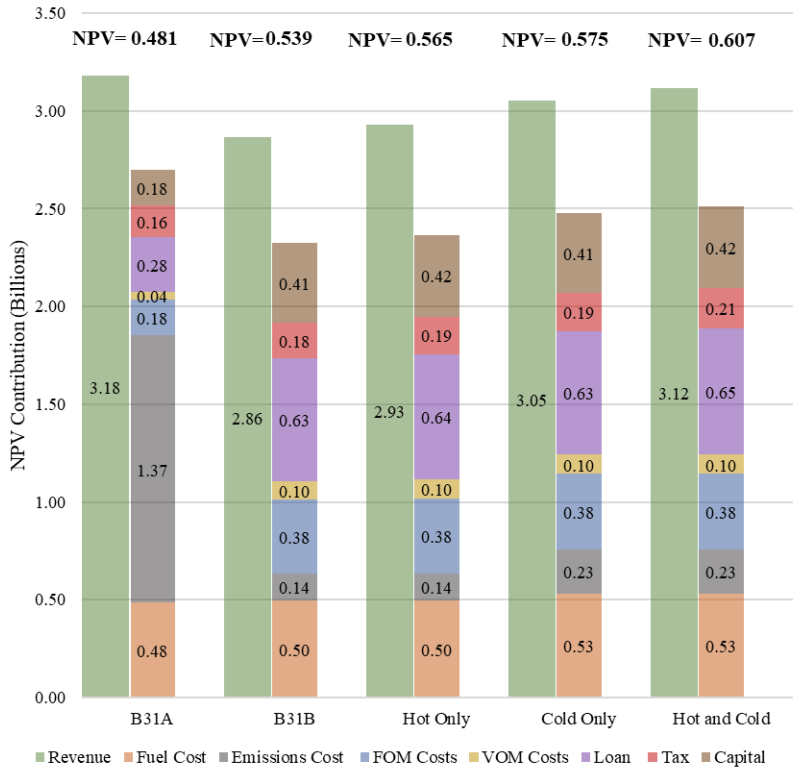

f) R150-CAISO

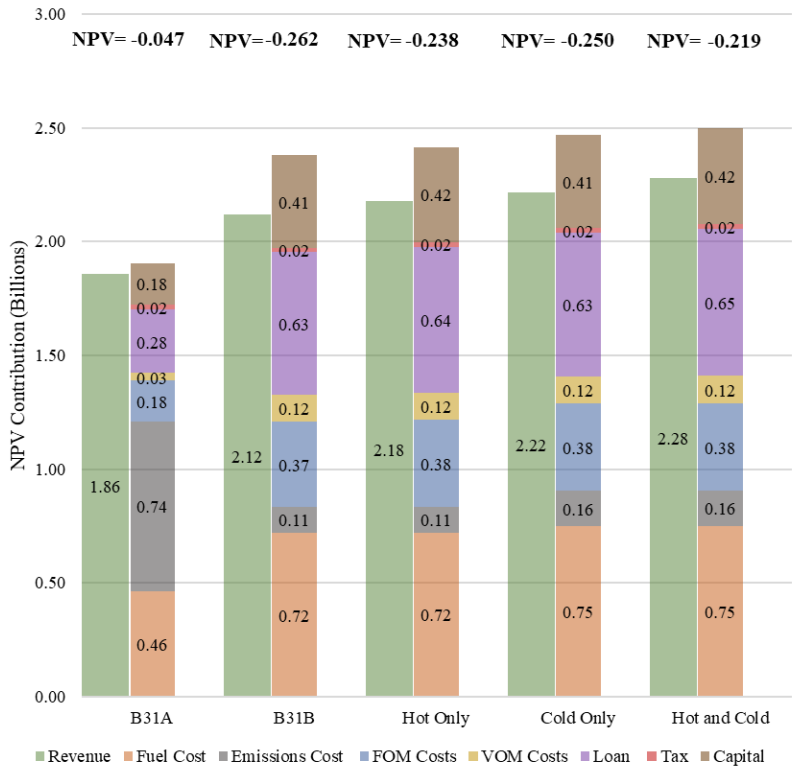

g) R100-ERCOT

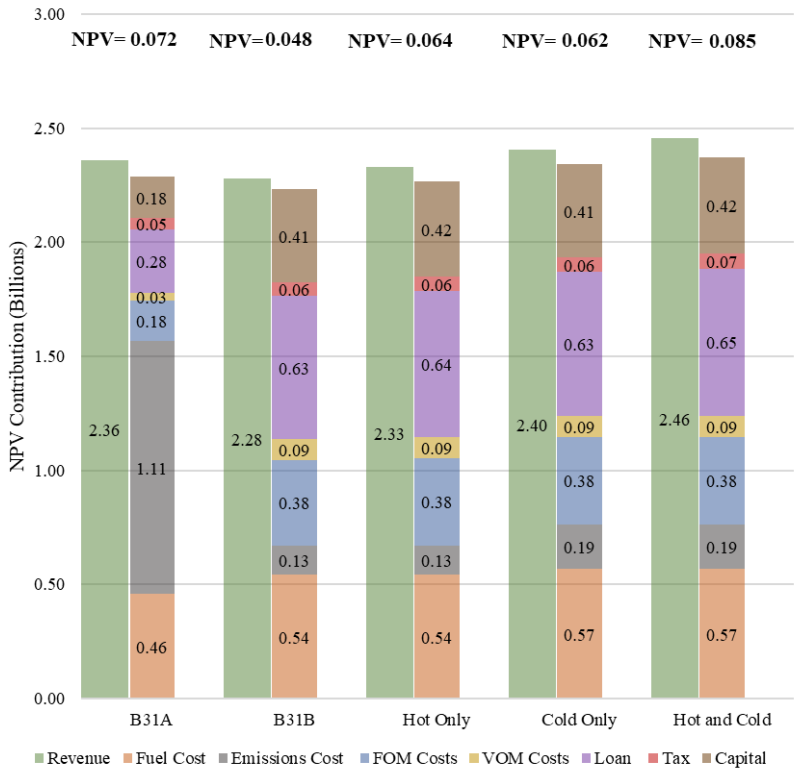

h) R150-ERCOT

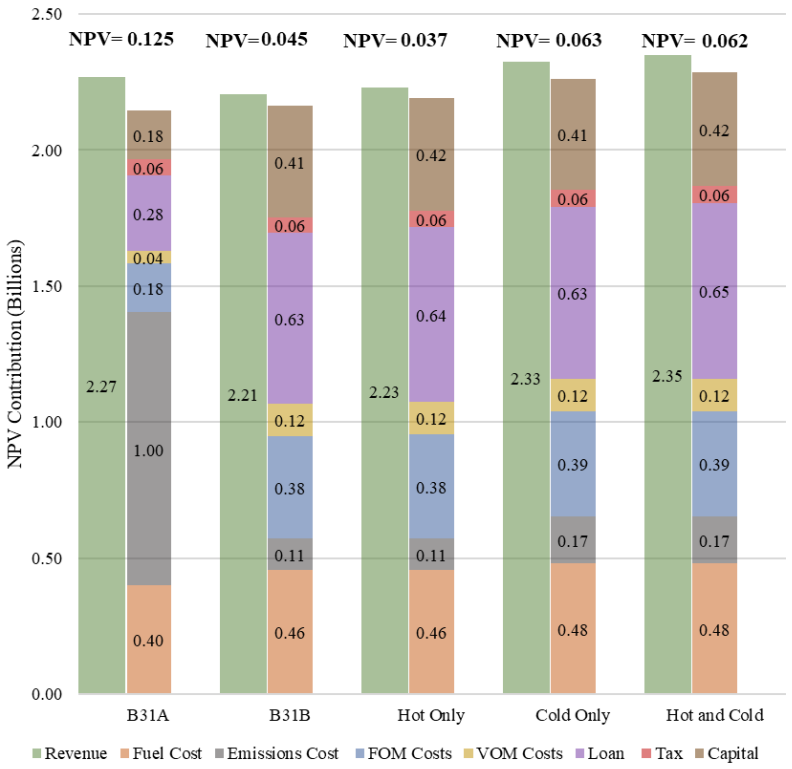

i) R100-MISO

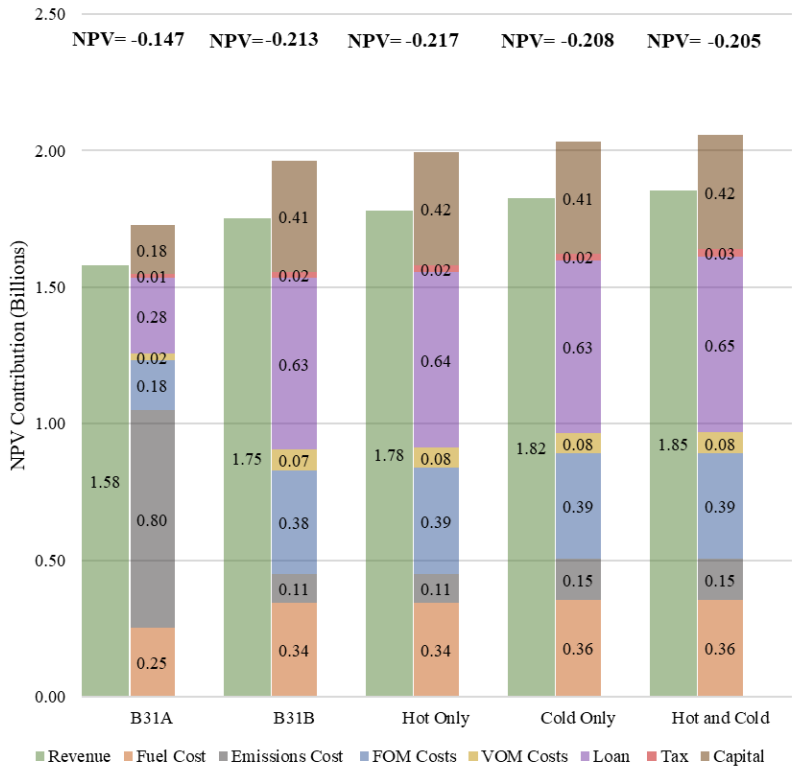

j) R150-MISO

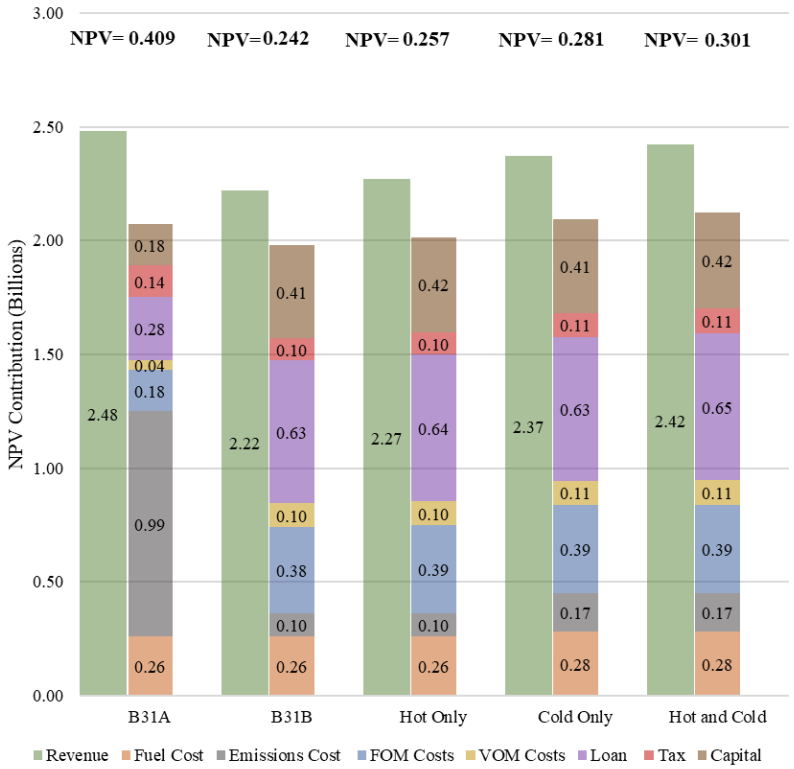

k) R100-NYISO

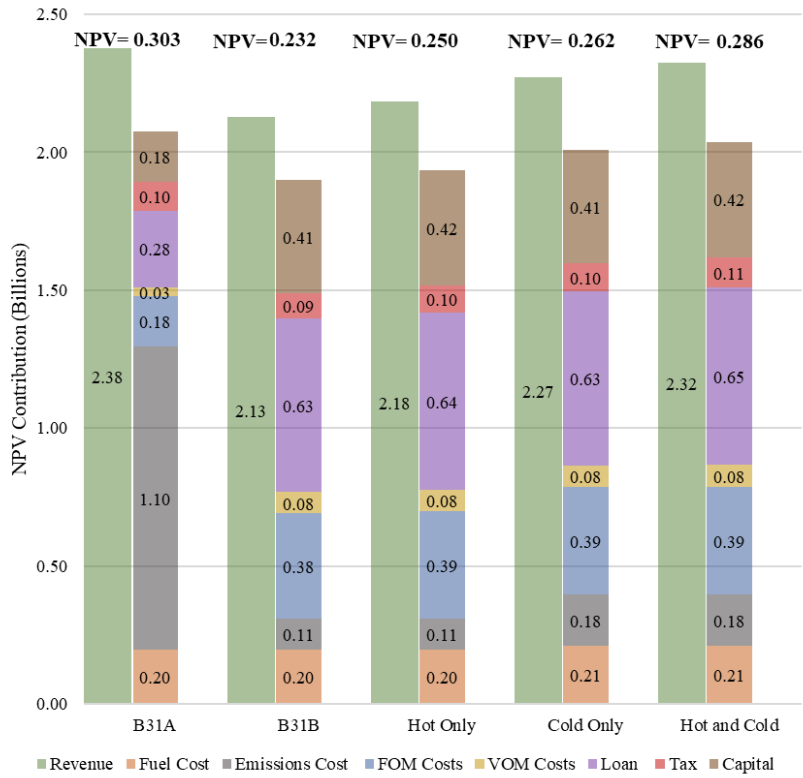

l) R150-NYISO

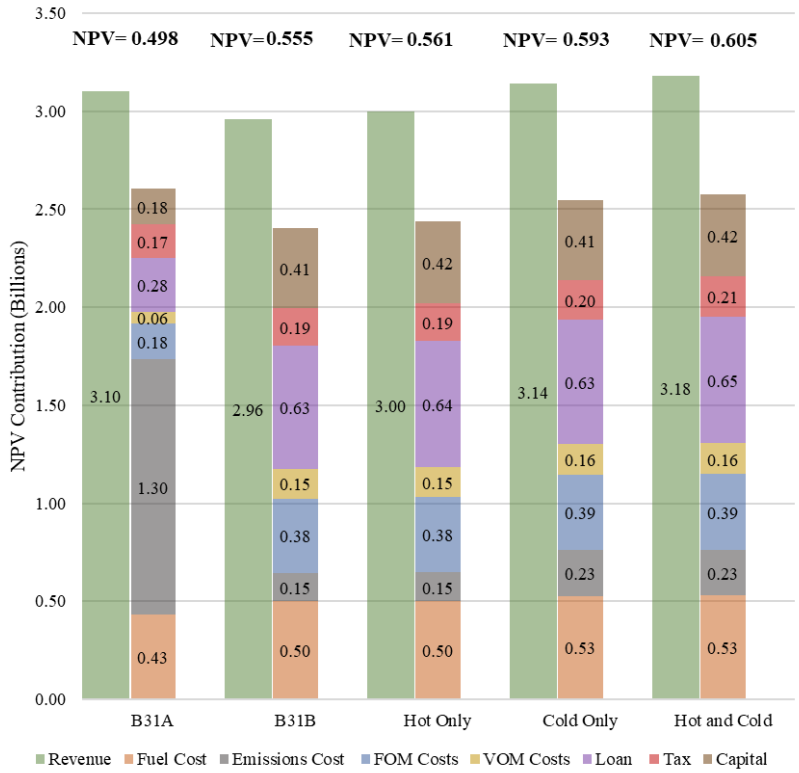

m) R100-PJM

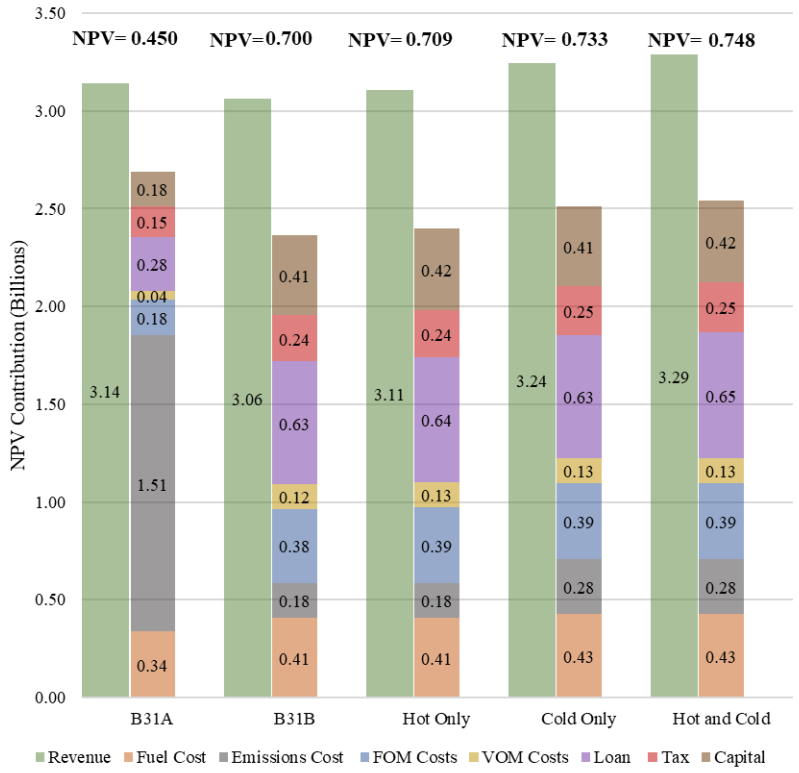

n) R150-PJM

Figure A- 10: Revenue and cost breakdowns for each market scenario